THE AMERICAN MINERALOGIST

JOURNAL OF THE MINERALOGICAL SOCIETY OF AMERICA

Vol. 32 MAY–JUNE, 1947 Nos. 5 and 6

APPLICATIONS OF THE NIGGLI-BECKE PROJECTION FOR ROCK ANALYSES

CHARLES S. BACON. JR.

CONTENTS

Illustrations

Figures

Tables

Abstract

Chemical and modal analyses of igneous, sedimentary, and metamorphic rocks are represented on ordinary graph paper as points in the Niggli-Becke quaternary chemical system of rock classification. The components of the system are al (alumina), fm (iron and magnesium oxides), c (lime), and alk (alkalies). Silica values (si) are plotted as ordinates against the quaternary system. Rules for calculating the points from chemical and modal rock analyses are given.

Graphically outstanding among the petrographic relationships are the different distribution fields of the igneous and sedimentary rocks, the four igneous areas in the si diagram (quartz-bearing rocks, quartz-free feldspathic rocks, feldspathoid bearing rocks, and ultra-femic and theralitic rocks), and the chemical transfers involved in metamorphic and weathering processes.

Introduction

Petrologic studies frequently involve the comparison, differentiation and relation of various rock types, either as regards chemical composition or mineral constituents. This may be done with diagrams or tables. Diagrams are preferable because they are more condensed, more readily comprehended and remembered than a series of numbers.

The tetrahedral system of Niggli (1923) as developed by Becke (1925) is the most comprehensive of all petro-chemical diagrams in that it enables a ready comparison of four major chemical units of rock analyses within a tetrahedrom, and by auxiliary diagrams gives the relation of silica and other constituents to the initial four. The system illustrates graphically the chemical variation of the igneous rocks, and of the sedimentary and metamorphic rocks as well. It is a chemical system but lends itself to the plotting of modal analyses, and thus permits chemico-modal comparisons. Genetic, metamorphic and weathering processes involving chemical change are demonstrated effectively.

The writer is grateful to Dr. A. O. Woodford of Pomona College for valuable suggestions and criticisms in the preparation of the manuscript and diagrams.

History

Graphical representation of rock analyses has been tried by numerous investigators (Iddings (1903), Adams (1914), Grout (1918, 1922, 1925), Von Wolff (1922), Hodge (1924), and Peacock (1931)), and several methods are still in use. The chief difficulty encountered has been the adequate representation of the 8 to 10 main oxides contained in most igneous and metamorphic rocks.

Iddings (1892) used a line diagram to express the relations between silica percentages, plotted as abscissas, and the other chemical constituents of rock analyses, plotted as ordinates. Niggli (1923) used diagrams of the same type to express relationships of silica to alumina, to alkalies, to lime, and to his fm value. At the present time, binary or two-component variation diagrams of this type are in common use.

Compositions of mixtures in a ternary or three-component system can be expressed graphically by a series of points in an equilateral triangle the corners of which represent the pure components. This type of diagram, introduced by Gibbs (1876), has come into general use in physical chemistry for illustrating the relations of ternary systems. In petrology this method was used quantitatively by Lang (1892) to express the CaO, Na_2O and K_2O ratios of the igneous rocks, and by Broegger (1895) to illustrate the relationship of monzonite to nepheline syenite, potash feldspar syenite and lime-rich diorite. Becke (1897) plotted K, Na and Ca in

a quantitative diagram illustrating the systematic chemical variation of the igneous rocks. This was followed by Osann's (1900) ACF system, subsequently improved by Becke (1912) by the addition of secondary triangles (SiUL) to express additional relationships.

In physical chemistry the relations of quaternary or four-component systems have been graphed frequently in top- and side-views of a tetrahedron, the four equidistant corners of which represent the pure components while mixtures of 2, 3 or 4 components are represented by points on the edges, faces and interior of the tetrahedron, respectively. Boeke and Eitel (1923) used this system to compare the chemistry of hornblende and augite. Niggli (1923) introduced the tetrahedron for classifying and comparing the chemical analyses of igneous, sedimentary, and metamorphic rocks (Fig. 1), the four corners representing essentially alumina (al), iron oxides and magnesia (fm), lime (c) and alkalies (alk). Niggli plotted al, fm, c and alk by dividing the tetrahedron into 10 slices each of which is a triangle having the corners al, alk and a definite c/fm ratio. Section I has a c/fm ratio of 5/95; section II of 15/85; section III of 25/75; etc. These triangles were plotted back to back along the al-alk edge, arranged so that sections I and X, II and IX, etc., went together. Five double triangles were required to represent the tetrahedron graphically, each analysis being represented by a point in one of the triangles. Points in the tetrahedron which do not fall in one of the section planes obviously cannot be placed accurately in the diagrams.

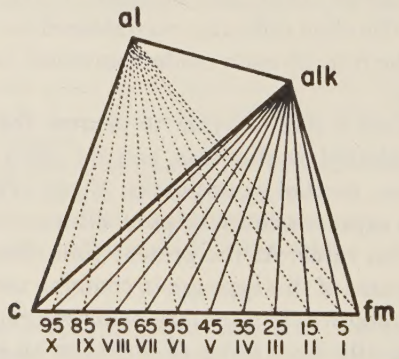

FIG. 1. Niggli tetrahedron showing the original 10 sections.

Becke (1925) rendered the system practicable by setting up the tetrahedron on one edge and viewing it from the top and one side.* In each of these two views the tetrahedron appears as a square cut by two diag-

* This is the crystallographic setup of a tetrahedron. The top and side views are therefore the cubic views 001 and 010, respectively.

onals. The side view is rotated 90° around one edge and placed in contact with the top view (Fig. 2). The analysis points were located in the tetrahedron by 3 coordinates, ξ and η in the top view, and ξ and ζ in the side view. ζ represents the height of the point in the tetrahedron. Becke plotted silica (si) as ordinates against the right side of the top view. He also developed the 6 triangular views of the tetrahedron obtained by sighting along its 6 edges, but made little use of them.*

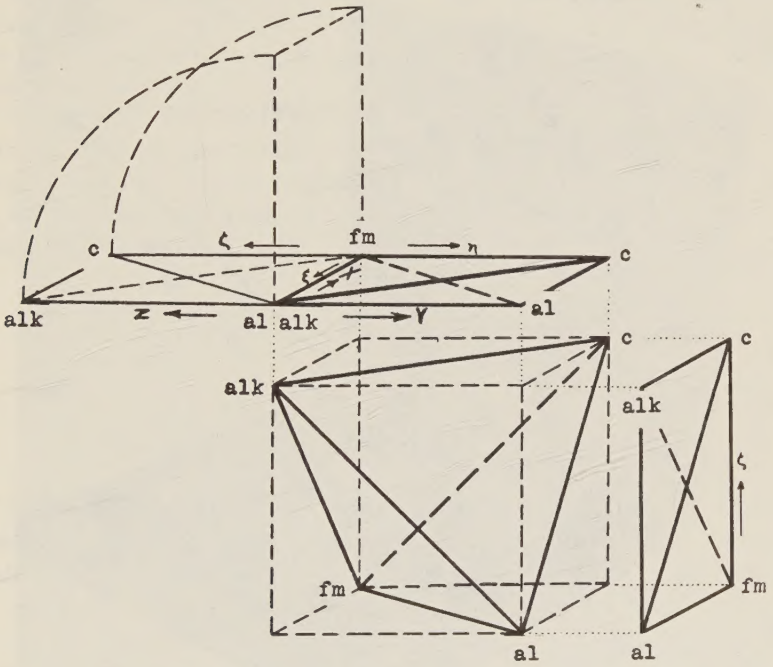

FIG. 2. Derivation of Becke's top and side view method of plotting rock analysis points in the Niggli tetrahedron. The right side view, which gives the elevations of analysis points above the base, is rotated into the horizontal plane and placed to the left of the top view. The newly introduced X, Y and Z coordinates are given in addition to those of Becke.

The photographed model (Fig. 3) of a tetrahedron shows the distribution of igneous rock analysis points. The coordinates X and Y (defined later) are plotted on the base for locating the wire pegs. The lengths of the pegs are equal to Z (defined later). Small wooden balls are slipped on the ends of the pegs to represent the analysis points. The side view is shown in an upright position.

* The triangular views of the tetrahedron are the dodecahedral views 110, $1\bar{1}0$, 011, $0\bar{1}1$, 101 and $\bar{1}01$, or their opposites.

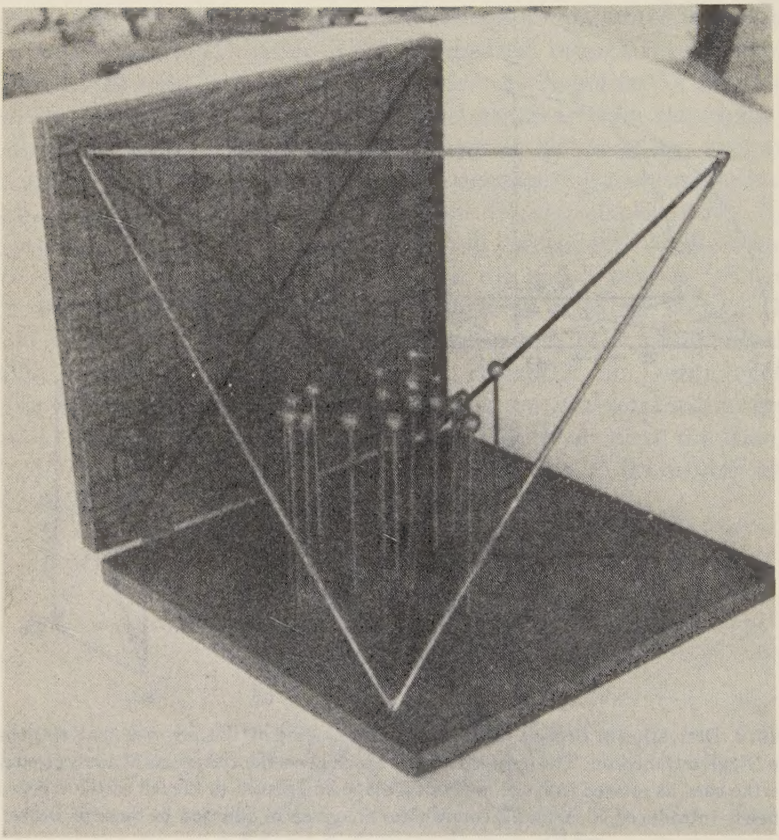

FIG. 3. Model of tetrahedron showing distribution of igneous rock analysis points.

Method of Calculation from the Chemical Analyses

1. Reduce the weight percentage of each oxide of the analysis to the molecular number.

$$\text{Molecular number} = \frac{\text{Weight percentage of the oxide}}{\text{Molecular weight of the oxide*}}.$$

2. If the molecular numbers have been calculated to four decimal places, multiply by 10,000 so as to avoid the use of decimal points in succeeding computations. Enter the figures in a column alongside the weight percentages.

3. Since one molecule of Fe_2O_3 contains twice as much Fe as a molecule of FeO, its molecular number must be multiplied by 2 for sake of proper comparison with the remaining molecular numbers.

4. The molecular numbers are grouped as shown below and then reduced to 100 per cent.

Al_2O_3 (plus any Cr_2O_3 and rare earths)	—al
$Fe_2O_3(\times 2)+FeO+MnO+MgO$ (plus NiO, CuO and other metallic oxides)	—fm
CaO (plus BaO and SrO)	—c
Na_2O+K_2O (plus Li_2O)	—alk
Total	100

5. The coordinate values X, Y and Z are obtained by simple addition and entered in the top and side views of the Becke diagram, hereafter called the *XYZ diagram.*

$$X = c + fm$$
$$Y = c + al$$
$$Z = c + alk.$$

These coordinates replace those of Becke† without change of diagram. From the focus (alk of top view, and al of side view) X increases verti-

* Washington (1917) used whole numbers for the molecular weights of the oxides and suggested that this practice be standardized because of slight changes which are made annually in the tables of atomic weights. The deviations involved are insignificant, and the values used by Washington are given below:

SiO_2	60	MgO	40	H_2O	18	MnO	71
Al_2O_3	102	CaO	56	CO_2	44	BaO	153.5
Fe_2O_3	160	Na_2O	62	TiO_2	80		
FeO	72	K_2O	94	P_2O_5	142		

† X is the reverse direction of ξ and is equal to $100-\xi$. Y corresponds to η and Z corresponds to ζ.

cally, Y increases to the right and Z to the left. The right half of the XYZ diagram will be called the *XY chart*, and the left half will be called the *XZ chart*.

The values al, fm, c and alk can be recalculated from the coordinate values as follows:

$$\text{al} = \frac{100 - X + Y - Z}{2}$$

$$\text{fm} = \frac{X - Y - Z + 100}{2}$$

$$\text{c} = \frac{X + Y + Z - 100}{2}$$

$$\text{alk} = \frac{100 - X - Y + Z}{2}.$$

6. Silica (si) is brought onto an equivalent basis with the Niggli tetrahedral values by the following equation:

$$\text{si} = \frac{\text{Molecular number of } SiO_2}{\text{Sum of the molecular numbers of al, fm, c and alk}}.$$

si is plotted as a variation diagram against X at the right of the XYZ chart using the c-al side as a base. This will be known as the *si chart*, and is the third unit of the diagram which is to be known hereafter as the *XYZ-si diagram*.

7. The values ti (TiO_2), p (P_2O_5), zr (ZrO_2), h (H_2O), co_2, so_3, so_4, cl_2, s, etc. are obtained in the same manner as si. They are not used often.

8. The values k and mg are obtained as follows:

$$\text{k} = \frac{\text{Molecular number of } K_2O}{\text{Molecular numbers of } K_2O + Na_2O \text{ (plus } Li_2O)}$$

$$\text{mg} = \frac{\text{Molecular number of MgO}}{\text{Molecular numbers of } Fe_2O_3\,(\times 2) + FeO + MnO + MgO}.$$

9. k and mg may be plotted as ordinates against X at the left of the XZ chart along the alk-c edge (Fig. 4), and become appendages to the XYZ-si diagram.

10. A salt such as NaCl in the analysis of a sedimentary rock is computed as the oxide of the metallic element. In this case the Na-portion of the molecular number of NaCl is divided by 2 so as to bring it to the same basis for calculation as Na_2O.

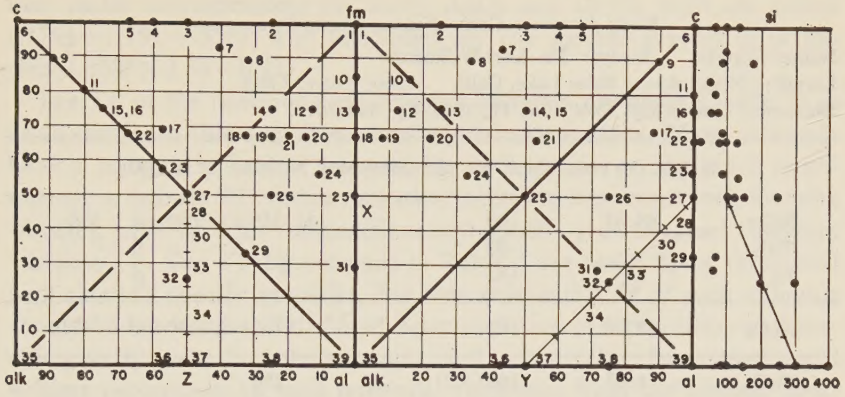

FIG. 4. Mineral distribution in the XYZ-si diagram.

KEY TO MINERALS PLOTTED IN THE XYZ-SI DIAGRAM

1 anthophyllite, antigorite, bronzite, brucite, chondrodite, enstatite, epsomite, goethite, hematite, hypersthene, ilmenite, limonite, magnetite, melanterite, olivine, periclase, pyrite, serpentine, siderite, talc, wolframite
2 actinolite, tremolite
3 diallage, diopside, dolomite, hedenbergite
4 andradite
5 akermannite
6 anhydrite, apatite, calcite, collophanite, fluorite, gypsum, perovskite, scheelite, titanite, wollastonite
7 augite
8 hornblende
9 apophyllite
10 chlorite
11 vesuvianite
12 phlogopite
13 almandite, beryl, chamosite, pyrope
14 pargasite
15 polyhalite
16 gehlenite, grossularite
17 allanite, epidote
18 acmite, aegirite, carnallite, riebeckite
19 arfvedsonite
20 biotite
21 xanthopyllite
22 prehnite
23 meionite, zoisite
24 glauconite
25 chromite, cordierite, spinel
26 montmorillonite
27 anorthite, scolecite
28 bytownite
29 margarite
30 labradorite
31 staurolite
32 chabazite, heulandite, phillipsite
33 andesine
34 oligoclase
35 halite, soda niter
36 marialite, sodalite
37 adular, albite, analcite, glaucophane, leucite, microcline, natrolite, nephelite, orthoclase, perthite, sanidine, spodumene
38 alunite, muscovite, paragonite, sericite
39 andalusite, bauxite, beidellite, corundum, diaspore, halloysite, hydrargillite, kaolinite, kyanite, pyrophyllite, sillimanite, topaz

The following example illustrates the method of calculation tabulated in a convenient form. Note the two subtotals ST which added to Al_2O_3 and CaO give the total T.

ROCK ANALYSIS CARD. NIGGLI-BECKE PROJECTION

Name: Granite Analyst: Dr. Karl Willmann
Locality: North side of Echo Lake, Calif. Spec. Grav. 2.663
Reference: *Univ. Calif. Publ.*, Vol. **17**, 1928. Pp. 360–361.

	Weight per cent ÷ Mol. Wt. of oxide = Mol. Number (×10,000)				
SiO_2	68.41	60	11,345 ÷ T 3690 = si		308
TiO_2		80	ti		
P_2O_5		142	p		
Al_2O_3	18.05	102	1766 ÷ T 3690 = al		47.9
Fe_2O_3	1.67	160 (×2)	210		
FeO	.71	72	99		
MnO					
MgO	.78	40	194		
			ST 503 ÷ T 3690 = fm		13.6
CaO	2.39	56	426 ÷ T 3690 = c		11.5
Na_2O	3.39	62	547		
K_2O	4.22	94	448		
			ST 995 ÷ T 3690 = alk		27.0
H_2O	.13		T 3690	Total	100.0
H_2O	.16				
Total	99.91				
$K_2O/ST = k$	.45		c + fm = X		25.1
$MgO/ST = mg$	.39		c + al = Y		59.4
			c + alk = Z		38.5

RULES FOR COMPUTING ROCK COORDINATES FROM THE MODES

1. Determine the *tetrahedral factor* TF of each mineral in the rock. From the formula or chemical analysis of the mineral find the weight percentages of the plottable oxides, i.e., those included in the al, fm, c and alk of the tetrahedron. Minerals such as quartz and rutile, lacking in tetrahedral components, are treated later. Divide the weight percentage of each plottable oxide by the molecular weight of the oxide to obtain the molecular number. The sum of the plottable molecular numbers multiplied by the specific gravity of the mineral is the TF of the mineral. Thus, orthoclase contains 64.8% SiO_2, 18.3% Al_2O_3 and 16.9% K_2O by weight. Only the Al_2O_3 and K_2O are plotted in the tetrahedron.* The molec-

* SiO_2 is plotted in the si-chart at the right of the XY chart.

ular ratios corresponding to 18.3% Al_2O_3 and 16.9% K_2O are added (.1794+.1791=.3585) and multiplied by the specific gravity of orthoclase (.3585×2.56=0.92).

The TF of the common rock forming minerals are given (Table 1) so as to eliminate this step from most modal calculations. Many minerals have a constant chemical composition and specific gravity, and consequently a definite TF. Other minerals, including important rock-forming silicates, have variable compositions and specific gravities, and therefore variable TF. The TF figures used in Table 1 are based upon the stated formulas and specific gravities. For best results the TF of such minerals should be based upon individual determinations of composition and specific gravity instead of the averages used in the table. In cases of small volume percentages of such minerals, variations from the average compositions will not displace the rock analysis points appreciably, but where larger percentages are involved accurate values of TF should be obtained.*

2. Multiply the volume percentage of each mineral by the appropriate TF to obtain the molecular number.

3. Reduce the molecular numbers of the minerals with plottable constituents to 100%.

4. Multiply the reduced molecular numbers of the minerals by the factors X, Y, Z and si listed in Table 1.

5. Make summations for X, Y, Z and si, respectively. The position of the rock in the XYZ diagram is given by the totals for X, Y, and Z.

6. Silica (si) is obtained by multiplying the volume percentage of free quartz by the factor 4.42 which is obtained in the same manner as the tetrahedral factors.† The molecular number thus obtained is divided by the sum of the plottable molecular numbers before reduction to 100%. The result is the si for quartz, to which must be added the si of all the other minerals. The si of a mineral such as zircon is obtained in the same manner as for quartz.

7. Other values such as ti, p, zr, h, etc., are obtained in the same manner as si.

The modal calculation of Johannsen's center point granite will serve as an example.

* The hornblende field is scattered between the aluminous pargasite and the ferruginous actinolite, and commonly includes some alkali. Johannsen's (1932) average of a number of analyses of various hornblendes from granites was selected as the center point for hornblende. Johannsen's average of dark mica from 34 granites was chosen for the center point of the biotites. Johannsen's average was used for the center point of augite. The chlorite point corresponds to Dana's (1932) formula of penninite and clinochlore, and falls half way between Becke's (1925) amesite molecule and serpentine.

† $\text{Si factor} = \frac{\text{Weight percentage}}{\text{Molecular weight}} \times \text{Spec. Grav.} = \frac{100}{60} \times 2.656 = 4.42.$

Mineral	Volume %		Tetrahedral Factor	Molecular Number	Plottable Mol. Numbers Reduced to 100%
Quartz	19.9	×	4.42*	88	
Orthoclase	38.1	×	.92	35.0	28.9
Plagioclase ($Ab_{70}An_{30}$)	14.5	×	1.30	18.9	15.6
Biotite	27.5	×	2.44	67.1	55.5
				ST 121.0	ST 100.0

* si factor.

Mineral	Reduced Mol. Nos.	Factors X	Y	Z	si	Rock Values X	Y	Z	si
Quartz	88/121								73
Orthoclase	28.9	0	50	50	300	0	14.5	14.5	87
Plagioclase	15.6	23	73	50	240	3.6	11.4	7.8	37
Biotite	55.5	67	22	15	74	37.2	12.2	8.3	41
	ST 100.0				Total	40.8	38.1	30.6	238

Checking the modal calculation

1. Multiply the volume percentages of all the minerals in the rock by their specific gravities and reduce to 100%. These are the weight percentages of the constituents.

2. Multiply the weight percentages by the oxide percentage composition of each mineral and enter the values in tabular form as in the example below. It may be difficult to obtain the correct weight percentages of the complex silicates, and the use of selected or average percentages introduces uncertainties.

3. Add the columns vertically to obtain the chemical composition of the rock.

4. From the chemical composition thus calculated determine X, Y, Z and si according to the method described earlier. These values should

correspond with those obtained from the mode by the regular method.*

Check of the Modal Calculation. (Johannsen's center point granite)

	Volume %	Vol. % ×Spec. Grav.	Wt. %	SiO_2	Al_2O_3	Fe_2O_3	FeO	MgO	CaO	Na_2O	K_2O
Quartz	19.9	52.7	19.4	19.4							
Orthoclase	38.1	97.5	36	23.3	6.6						6.1
Plagioclase ($Ab_{70}An_{30}$)	14.5	38.5	14.2	8.7	3.5				.8	1.2	
Biotite	27.5	82.5	30.4	11.2	5.2	2.3	4.4	2.8	.3	.3	2.5
Total	100.0	271.2	100.0	62.6	15.3	2.3	4.4	2.8	1.1	1.5	8.6
Mol. Nos. ×10,000				10381	1497	288 (×2)	613	694	196	242	913

al	=1497	33.7	X =40.3
fm = 288+613+694	=1595	35.9	Y =38.1
c	= 196	4.4	Z =30.4
alk =242+913	=1155	26.0	si =234

Mineral Distribution in the XYZ-si Diagram†

The mineral distribution in the XYZ-si diagram (Fig. 4) is the key to a thorough understanding of the rock positions and to chemico-modal relationships. Quartz is plotted only as si and has no place in the tetrahedron. The plagioclase feldspar line with its divisions marking the different members of the isomorphous series is the most important feature of Fig. 4. The division points were calculated from analyses given in Winchell (1927), and Tschermak, G. and Becke, F. (1920). The Z of all feldspars is 50. The si ranges from 300 in albite to 100 in anorthite. Located at the same point with the pure albite molecule is orthoclase, nepheline and leucite, but nepheline has an si of only 100 and leucite of 200. The biopyriboles are widely scattered toward the fm corner in both top and side views, with olivine and orthopyroxenes at fm.

Distinctively sedimentary minerals occur at all corners; calcite, gypsum and anhydrite at c, kaolinite and other clay minerals at al, rock salt and soda niter at alk, and the iron ores at fm. Dolomite lies between c and fm.

The minerals of the metamorphic rocks are widely distributed between fm and c, and between al and c.

* The calculated chemical composition of the rock should be compared with a chemical analysis, if available. Such a comparison frequently sheds light on the true compositions of complex silicates which cannot be determined optically. If average compositions of the complex silicates are assumed, the calculated weight percentages may differ notably from the actual analyzed values, and then the true nature of the silicates may be determined and the modal calculation adjusted.

† Printed forms of the XYZ-si diagram and the triangle charts on a single $8\frac{1}{2}\times11$ sheet are available at two dollars per 100 sheets. Sample on request. Address the author.

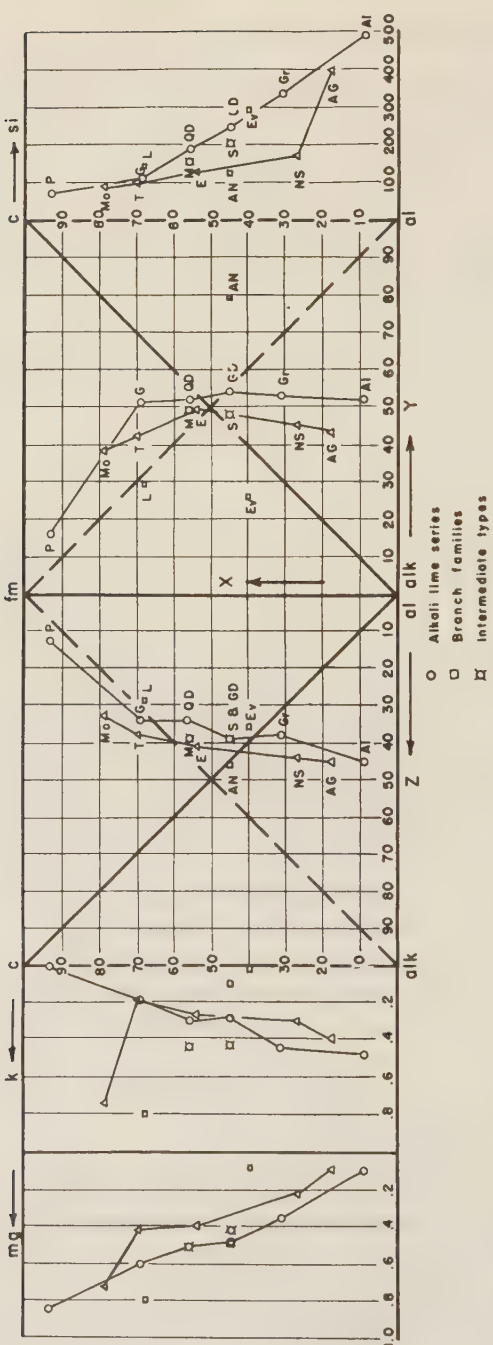

FIG. 5. Average composition of the igneous rocks in the XYZ-si-k-mg diagram.

Rock abbreviations: AG alkali granite, Al alaskite, AN anorthosite, E essexite, Ev evisite, G gabbro, GD granodiorite, Gr granite, L lamprolite, M monzonite, Mo missourite, NS nepheline syenite, P peridotite, QD quartz diorite, S syenite, T theralite.

Salient Features Illustrated in the XYZ-si Diagram

XY chart: Igneous rocks

The majority of igneous rocks fall into two main groups, the alkali-lime series and the alkali series.* These are distributed in a curved zone from alkali feldspar to the fm corner, the alkali-lime series with higher Y than the alkali series (Becke, 1925) (Fig. 5 and Table 2). The alkali-lime series includes alaskite, granite, granodiorite, quartz diorite, gabbro and peridotite. The alkali series includes alkali granite, nepheline syenite, essexite, theralite and missourite. Two intermediate families, syenite and monzonite, are included, as well as three branch families anorthosite, lamproite and evisite. The Daly (1910) averages are used with the exception of the following family types:

Essexite of Rongstock, Bohemia (preferred by Becke, 1925)
Theralite of Duppau, Bohemia (preferred by Becke, 1925)
Lamproite and evisite (Niggli, 1923)
Alkali granite (average of 13; Osann, 1900)

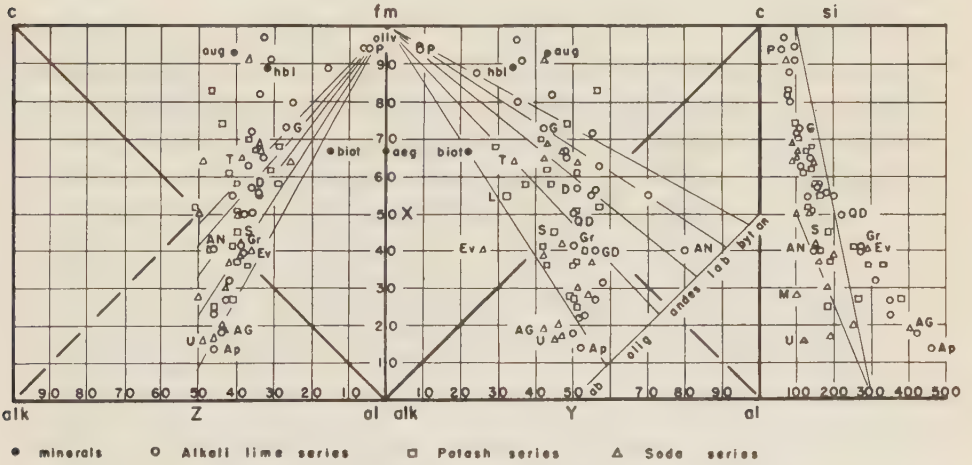

Fig. 6. Niggli's magma families in the XYZ-si diagram.

Minerals: aeg aegirine, aug augite, biot biotite, hbl hornblende, oliv olivine. The plagioclase feldspars are distributed along the line from X 0, Y 50 to X 50, Y 100. The lines converging at fm give the (OrAb)-An ratio of most rocks with X under 70.

Abbreviations of selected families: AG alkali granitic, AN anorthositic, Ap aplite granitic, D normal dioritic, Ev evistic, G normal gabbroid, GD granodioritic, Gr normal granitic, L lamproitic (Wyoming type), M monmouthitic, P peridotitic, QD quartz dioritic, S normal syenitic, T theralitic, U urtitic.

The projection for the anorthosite family lies between those for normal gabbro and for calcic plagioclase. Evisite, the soda-amphibole granite or

* Becke's (1925) Pacific and Atlantic suites respectively.

syenite family, known especially from Evisa, Corsica, is drawn strongly toward the riebeckite point. Lamproite, a family of potash and magnesia rich effusives of lamprophyric character which includes orendite, wyomingite, leucite phonolite and others, is drawn toward fm in consequence of the olivine (and phlogopite) in the rock.

Niggli (1923) grouped the magmas or igneous rock families in three series, the alkali lime series, the potash series, and the soda series (Fig. 6, Table 3). The separation of the two alkali series is not apparent in the XYZ-si diagram but can be demonstrated in a k chart (not shown).

Feldspars largely control the locations of rocks more alkalic than diorite, and the pyriboles predominantly determine the positions of the more femic igneous rocks. A line from fm through the rock analysis point to the feldspar line gives the approximate (OrAb) An (orthoclase-albite anorthite) or the AbAn ratio of the feldspars for rocks more salic than gabbro, the former when both types of feldspars are present, the latter when plagioclase is the only feldspar.* Rocks with soda-pyriboles have unusually low Y which gives the analysis points the appearance of having AbAn ratios in excess of the true values.

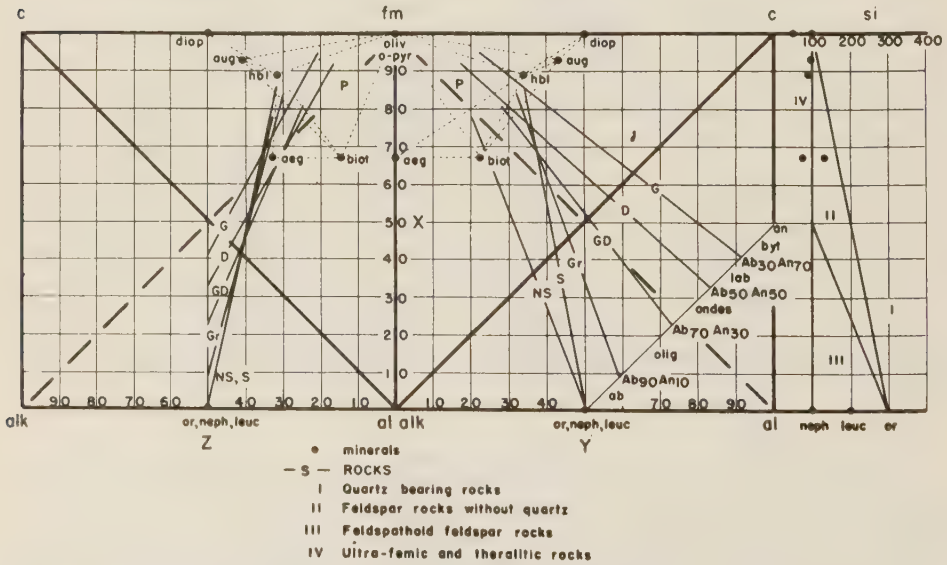

FIG. 7. Modal study of the igneous rocks in the XYZ-si diagram.

Mineral abbreviations: ab albite, aeg aegirite, an anorthite, andes andesine, aug augite, biot biotite, byt bytownite, diop diopside, hbl hornblende, lab labradorite, leuc leucite, neph nepheline, olig oligoclase, oliv olivine, o-pyr orthopyroxene, or orthoclase.

Rock abbreviations: D diorite, G gabbro, GD granodiorite, NS nepheline syenite, P peridotite, S syenite.

* Nepheline and leucite should be included with orthoclase and albite when present.

The families of Johannsen's (1920) quantitative mineralogical classification of the igneous rocks may be plotted like any other modes, but due to the chemical overlap of his families they are not reproduced here, as this would require numerous additional charts.

The distribution of the rocks as controlled by the leading mineral constituents is illustrated in Fig. 7. The average biopyriboles (biotite-pyroxene-amphibole) were calculated for 31 nepheline syenites, 10 syenites, 58 granites, 68 granodiorites, 16 diorites, and 42 gabbros (Johannsen, 1932, 1937, 1938). The XYZ-si of these average biopyriboles and the fields which the points represent are given below:

	X	Y	Z	si	Field
Nepheline syenite	78	20	33	107	aegirite, hornblende, biotite
Syenite	86	34	32	90	hornblende, biotite, augite, diopside
Granite	84	32	30	86	hornblende, biotite, augite
Granodiorite	81	28	25	82	biotite, hornblende
Diorite	92	17	17	92	hornblende, orthopyroxene, clinopyroxene, biotite
Gabbro	95	22	21	84	augite, orthopyroxene, hornblende, olivine

Lines from these points to the proper plagioclases give the linear distributions of the families, the leucocratic members near the feldspar line, the melanocratic members at the other end. Biotite granites are distributed between biotite and albite-oligoclase, whereas hornblende granites have higher Y and lie between hornblende and the same feldspar. The riebeckite granites have lower Y than the biotite granites. Granodiorites, diorites and gabbros lie between the biopyriboles and the plagioclases $Ab_{70}An_{30}$, $Ab_{50}An_{50}$ and $Ab_{30}An_{70}$ respectively. Olivine and orthorhombic pyroxene draw the points for olivine gabbros and norites toward the fm corner. Peridotites and related rocks lie in the triangular area defined by biotite, augite and the fm corner.

The field of the igneous rocks is limited by lines connecting fm, augite, anorthite, albite, aegirite and fm.

XY chart: Sedimentary rocks

The field of the sedimentary rocks in the Niggli tetrahedron has a shape very unlike that of the igneous rocks, due largely to the considerable quantities of lime and alumina in sedimentary rocks (Fig. 8, Table 4).

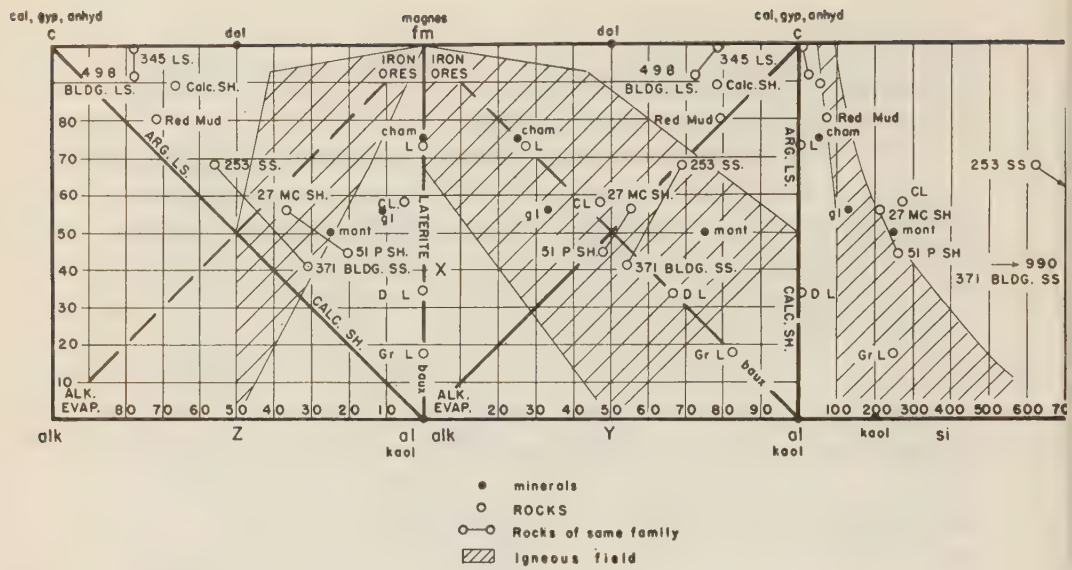

FIG. 8. Distribution of the sedimentary rocks in the XYZ-si diagram.

Mineral abbreviations: anhyd anhydrite, baux bauxite, cal calcite, cham chamosite, dol dolomite, gl glauconite gyp gypsum, kaol kaolinite, mont montmorillonite.

Rock abbreviations: ALK.EVAP. alkali evaporites, ARG.LS. argillaceous limestones, BLDG.LS. building lime stones, BLDG.SS. building sandstones, CALC.SH. calcareous shales, Calc.SH. calcareous shale, Mt. Diablo Calif., CL clay, D L diorite laterite, Gr L granite laterite, L laterite, LS limestones, MC SH Mesozoic and Cenozoi shales, P SH Paleozoic shales, SS sandstones.

Limestones, if pure, lie at the c corner. Most limestones are magnesian, with a little alumina present, and their positions in the diagram are almost, but not quite, on the calcite dolomite line.

Pure kaolin and other clay minerals lie at or near the al corner. Bauxite is usually somewhat ferruginous. Lateritic rocks may contain an fm-al ratio up to more than 2 to 1, occupying the igneous field. Shales lie in the igneous rock field, with an average near that of granodiorite and diorite. Calcareous shales and argillaceous limestones are likely to lie outside of the igneous field, nearer the al-c edge.

Sandstones are distinguished by higher c values than any igneous rocks except anorthosites.

Iron ores lie close to fm. Rock salt and other alkali evaporites lie near alk.

XY chart: Metamorphic rocks

Metamorphic rocks do not occupy an area distinguishable from those of igneous and sedimentary rocks. The mineral combinations in meta-

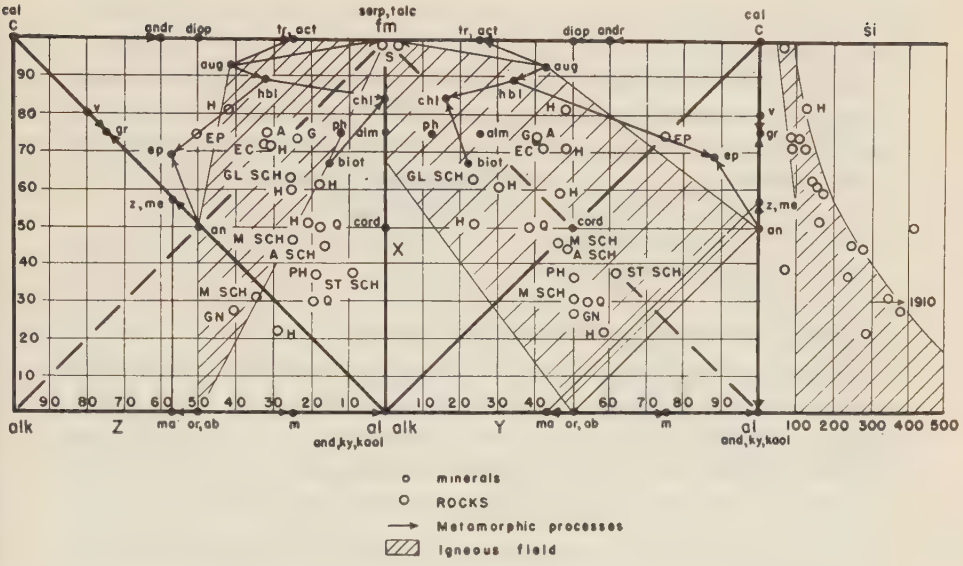

FIG. 9. Metamorphic rocks and processes, and weathering in the XYZ-si diagram.

Mineral abbreviations: ab albite, act actinolite, alm almandite, an anorthite, and andalusite, andr andradite, aug augite, biot biotite, cal calcite, chl chlorite, cord cordierite, diop dicpside, ep epidote, gr grossularite, kaol kaolinite, ky kyanite, m muscovite, ma marialite, me meionite, ph phlogopite, serp serpentine, talc talc, tr tremolite, v vesuvianite, z zoisite.

Rock abbreviations: A amphibolite, EC eclogite, EP epidosite, G greenstone, GL SCH glaucophane schist, GN gneiss, H hornfels, M SCH mica schist, PH phyllite, Q quartzite, ST SCH staurolite schist

morphic rocks are so varied and numerous so that it is possible to give only the general distribution of a few major rock types (Fig. 9, Table 5).

Slates and some schists differ only slightly from their parent shales and consequently have a similar distribution in the diagram.

Quartzites differ from their parent sandstones in several ways. The calcareous cements of the sandstones may have been replaced by silica. Contact metamorphism may have introduced minerals such as diopside, garnet and wollastonite. Such changes are evident in the diagram by a shift of the analysis points toward the contact minerals.

Contact metamorphosed marble will differ in composition from the parent limestone to the extent that reaction has occurred between the limestone and the magma, magmatic waters or pneumatolytic agents. The analysis points in the diagram will be drawn toward the newly developed minerals.

Gneisses derived from the igneous rocks generally possess the compositions of the parent plutonites, but changes in composition such as

those sometimes attending mylonitization or lit-par-lit injection result in shifts of the analysis points.

Schists differ widely in mineral content and are thus broadly scattered through the tetrahedron. Talc schists, chlorite schists, biotite schists, sericite schists, etc. focus around the dominant constituents but may be widely removed from the corresponding mineral positions if these minerals do not constitute a major portion of the rock.

If a metamorphic rock clearly lies beyond the limits of the igneous rock field, its sedimentary origin is reasonably certain.

XY chart: Metamorphic and weathering processes

A metamorphic change involving the development of new minerals but not attended by chemical transfer cannot be illustrated in the tetrahedron, but changes involving chemical transfers are frequently very prominent. The directions of shift of analysis points accompanying a number of major alteration processes are described below (Fig. 9):

Sericitization involves a loss of Na and generally an increase of K; this is expressed by a shift toward muscovite.

Kaolinization is expressed by a shift toward al due to loss of alk and c.

Alunitization involves loss of all plottable elements except K and Al.

Scapolitization is expressed by a shift from the plagioclase line toward alk and c, especially the latter, in accordance with the usual occurrence in limestone contact zones.

Zoisitization, which may be considered a change from anorthite to zoisite with loss of al, results in an increased X.

Epidotization may be considered a change from anorthite and hornblende towards epidote. The increase in c draws the projection of the rock analysis point toward the epidote point.

Grossularitization is represented as a reaction between plagioclase and limestone, and appears as a double shift from anorthite and c toward the grossularite point. Other types of garnetization may be illustrated in similar manner.

Chloritization may be considered a change from hornblende or biotite toward pennine or clinochlore. It generally involves a loss of alk and of c.

Uralitization is the alteration of pyroxene to amphibole, and its diagrammatic expression depends upon the nature of the particular pyriboles involved. Generally there is a gain in Mg and a loss of Ca which produces a shift toward the fm corner.

Actinolitization involves a change from augite to actinolite. Serpentinization is expressed by shifts from the pyriboles such as diopside, augite

and hornblende toward the fm corner. Olivine and orthorhombic pyroxene, which lie at fm, suffer no change in position when they are altered to serpentine.

Propylitization involves a moderate loss of alk, and a loss of Ca and Mg unless these enter into carbonates or epidote. Commonly propylitization is accompanied by sulfide enrichment (pyrite), and there is relatively little change in X and Y from the original rock.

XZ chart: Igneous rocks

The Z of unaltered igneous rocks is never above 50, and the distribution tapers from fm and the augite position toward the alkali feldspar point in a considerably restricted field (Fig. 5 and 6). The alkali lime series has a distinctly higher Z than the alkali series. Z is greatest for salic rocks with low X, and least for femic rocks with high X. Biotite rocks have lower Z than rocks of the same family containing hornblende or augite.

XZ chart: Sedimentary rocks

Most distinctively sedimentary rocks lie along the al-c edge so that Z increases with X, and the fm content causes the distribution to assume a curved field convex toward fm (Fig. 8). The field of the major sedimentary rocks thus crosses the igneous rock field at a high angle, and sedimentary analyses are rarely similar to igneous ones except at the intersection of the two fields. Bauxite, laterite and the iron ores are low in Z and fall below the igneous field. Many shales have lower Z than igneous rocks, but calcareous shales may lie in the igneous zone. Argillaceous limestones approach the c corner and lie above the igneous rock field.

The calcareous cementing materials of sandstones give to these rocks high c values, and place them above the igneous field. Arkoses and tuffs generally fall in the igneous field.

Rock salt and soda niter lie near the alk corner.

XZ chart: Metamorphic rocks and processes, and weathering

The sedimentary or igneous origin of a metamorphic rock can be recognized provided the projection point of the rock falls outside of the intersection of the two fields of distribution. Rocks above the igneous field (high Z) or below it (low Z) are very likely to have originated as sediments (Fig. 9). Rocks of fairly low X that lie within the igneous field are likely to be of igneous derivation. Sediments injected lit-par-lit or altered to migmatites are not likely to reveal their genesis by the analysis points.

If the origin of a rock is known, the shift in position of the altered rock with respect to its parent illustrates the nature of the chemical changes

that have taken place.

Metamorphic derivatives of the calcareous sediments occupy a field higher in the tetrahedron (greater Z) than the igneous derivatives, whereas aluminous derivatives occupy a lower field (smaller Z) close to the al-fm edge. The former are focused around the points of such minerals as grossularite, andradite, epidote, vesuvianite, gehlenite, etc., while the latter are drawn toward muscovite, kyanite, sillimanite, andalusite, cordierite, chlorite, and others.

The metamorphic processes described for the XY chart can be represented in this chart also.

si chart: Igneous rocks

A line from X 0, si 300 to X 100, si 100, connecting orthoclase and diopside, is the silica saturation or *quartz line* (Figs. 6 and 7). An analysis point with si above this line represents a rock supersaturated with silica and hence probably containing free quartz.

A line from X 0, si 300 to X 50, si 100 is the silica line of the plagioclase feldspars. The triangular field below the quartz line and above the plagioclase line and the si 100 line is that of the quartz-free feldspathic rocks, such as syenites, diorites and gabbros.

Rocks with si values below the plagioclase line have insufficient silica to combine with all of the alumina, lime and alkalies required to form feldspar, and consequently there is a development of feldspathoids. The field between the plagioclase line and the si 100 line is that of the nepheline and leucite syenite rocks.

There are no igneous rocks with si under 100 and X under 50. Those with X over 50 and si under 100 include the peridotites, pyroxenites, dunites, and a few gabbroic rocks with very basic plagioclase.

The si values of the igneous rocks are distributed through a curved zone the upper limit of which extends roughly from X 100, si 50–75 through X 50, si 200 where it crosses the quartz line, to X 10, si 400. When X lies between 0 and 10 the si values may rise much higher, as in the pegmatites. When the feldspar of pegmatites decreases to 0 the si approaches infinity and the rocks grade into quartz veins. The alkali lime rocks generally have distinctly higher si than rocks of the alkali series, and when X is under 50 they generally contain free quartz.

No igneous rocks are known which have high X and high si.

si chart: Sedimentary rocks

Sandstones have exceedingly high si (Fig. 8). The only igneous rocks with equally high si have X under 10, whereas most sandstones have X

well over 50. Shales have si values equal to or slightly higher than igneous rocks of the same X, and the si rises rapidly where the sediments grade into arenaceous and silicified rocks. Limestones, the alkali evaporites, bauxite and laterites have very low si.

si chart: Metamorphic rocks and processes

Silicification, whether hydrothermal or diagenetic, increases the si according to the degree of completion of the process. Silicified rocks are likely to have high si.

Metamorphic rocks differ as greatly in si as their parent rocks (Fig. 9). Metamorphic limestones, chlorite-, talc-, and biotite schists, amphibolites, eclogites, etc. may have very low si, but quartz mica schists, gneisses, quartzites, etc. have si ranging up to values far in excess of igneous rocks.

k chart

With the exception of lamproite and missourite, the k of igneous rocks decreases with increasing X (Fig. 5), and the potash series have higher k values than the soda series.

mg chart

The mg of igneous rocks increases with increasing X, and is generally higher in the alkali lime series than in the alkali series for any selected value of X (Fig. 5).

Triangle Views of the Tetrahedron

The ratios of any of the bases to one another can be shown graphically by viewing the tetrahedron from the following six positions (Figs. 10, 11, and 12):

c/fm chart: tetrahedron viewed parallel to the al-alk edge gives the c/fm ratio.

alk/al chart: tetrahedron viewed parallel to the c-fm edge gives the alk/al ratio

alk/c chart: tetrahedron viewed parallel to the al-fm edge gives the alk/c ratio

al/c chart: tetrahedron viewed parallel to the alk-fm edge gives the al/c ratio

al/fm chart: tetrahedron viewed parallel to the alk-c edge gives the al/fm ratio

fm/alk chart: tetrahedron viewed parallel to the c-al edge gives the fm/alk ratio

These views are isosceles triangles of altitude equal to the side of the square top view, and of base equal to the diagonal. To obtain the projection point of a rock analysis in one of the triangles follow the line of given ratio until it intersects the altitude line, the latter representing the sum of the other two components. The intersection is the desired point.

As an example, the triangle positions of Becke's granite are calculated from the X 31, Y 53 and Z 38 coordinates.

$$al = \frac{100 - 31 + 53 - 38}{2} = 42$$

$$fm = \frac{31 - 53 - 38 + 100}{2} = 20$$

$$c = \frac{31 + 53 + 38 - 100}{2} = 11$$

$$alk = \frac{100 - 31 - 53 + 38}{2} = 27.$$

The positions of the granite point in the triangles lie at the intersections of the following ratio and altitude lines:

Chart	Ratio	Altitude
c/fm	c:fm =35:65	100−X=69
alk/al	alk:al =39:61	X=31
alk/c	alk:c =71:29	100−Z=62
al/c	al:c =79:21	100−Y=47
al/fm	al:fm =68:32	Z=38
fm/alk	fm:alk=43:57	Y=53

The alternate triangles are turned upside down for illustrative convenience. The altitude is always measured from the base or long side of the triangle toward the peak with the two components.

The triangle views are readily constructed and demonstrate certain rock relationships that are not expressed in the XYZ diagram.

c/fm chart (Fig. 10)

Igneous Rocks.—The field of the igneous rocks is bounded by the al-alk/fm edge and lines connecting anorthite with augite and fm. The c-fm ratio of .35 plus or minus .10 is characteristic for the major portion of both series of igneous rocks. Exceptions are anorthosite, the high c-fm ratio of which is due to abundant plagioclase feldspar; peridotite, the low c-fm ratio of which is due to the abundance of ferromagnesian constituents such as olivine, orthorhombic pyroxene and magnetite; and alkali granite with a low c-fm ratio owing to the scarcity and low lime

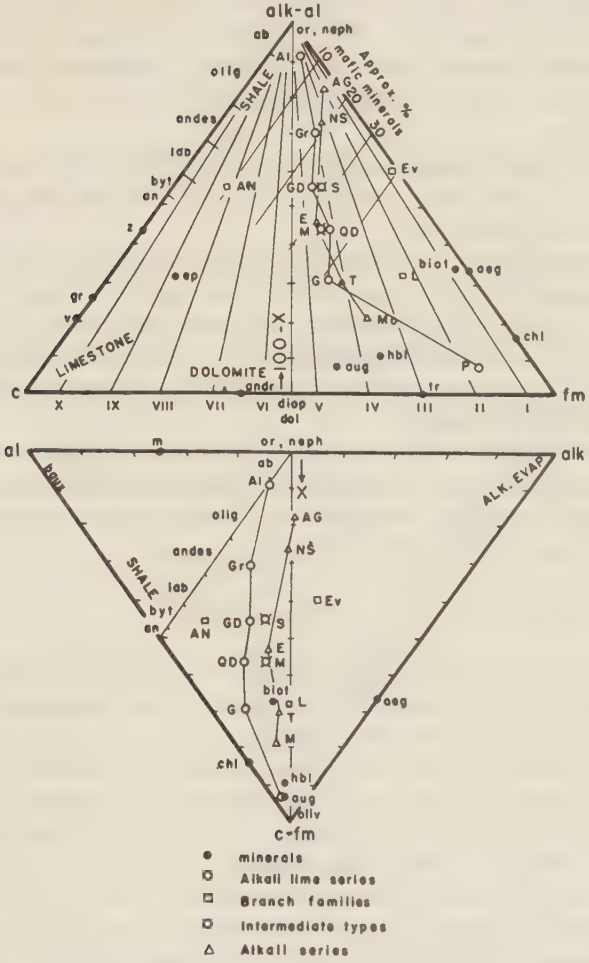

FIG. 10. Triangle views of the tetrahedron: c/fm and alk/al charts.

Mineral abbreviations: ab albite, aeg aegirite, an anorthite, andes andesine, andr andradite, aug augite, baux bauxite, biot biotite, byt bytownite, chl chlorite, diop diopside, dol dolomite, ep epidote, gr grossularite, hbl hornblende, lab labradorite, m muscovite, neph nepheline, olig oligoclase, oliv olivine, or orthoclase, tr tremolite, v vesuvianite, z zoisite.

Rock abbreviations: AG alkali granite, Al alaskite, AN anorthosite, E essexite, Ev evisite, G gabbro, GD granodiorite, Gr granite, L lamproite, M monzonite, Mo missourite, NS nepheline syenite, P peridotite, QD quartz diorite, S syenite, T theralite.

content of the plagioclase. The extremely alkaline nature of evisite is indicated by its low c-fm ratio. Lamproite has a low c-fm ratio.

From alkali feldspar rocks to diorite the approximate AbAn ratios of the plagioclase feldspars can be determined by dropping lines from fm through the rock analysis points to the plagioclase line. This is true also for anorthosite.

The percentage of mafic constituents can be estimated satisfactorily up to 40% by determining the altitude of the analysis point relative to the c/alk-al edge as a base.

This chart illustrates the planes along which Niggli cut the tetrahedron.

Sedimentary Rocks.—The sediments lie along the c/alk-al edge, limestone and gypsum at c, and the clays and shales nearer alk-al. The alkali evaporites also lie at alk-al. Dolomite is on the middle of the c-fm edge. Except for the iron ores, the distribution field of the sediments overlaps the igneous field very little.

Metamorphic Rocks and Processes.—Epidotization exhibits an increase of lime. Serpentinization involves a shift toward fm due to a loss of all but iron and magnesia. Chloritization, zoisitization and garnetization can also be demonstrated with this chart.

alk/al chart (Fig. 10)

Igneous Rocks.—The field of the igneous rocks is in the central portion of the triangle between the feldspar line and a line joining aegirite with orthoclase. The alkali lime series has an alk-al ratio under .40 (with the exception of alaskite), and the alkali series has an alk-al ratio over .40 (with the exception of missourite). The relation of lamproite and evisite to the alkali series is expressed by an alk-al ratio above normal for the series. The relation of anorthosite to gabbro is shown by the fact that it has the same alk-al ratio, but the higher plagioclase content draws the point toward basic plagioclase. The intermediate positions of monzonite and syenite are indicated by their analysis points.

Bowen's reaction series finds expression in the nearly vertical line from olivine through augite, hornblende and biotite to orthoclase, and by the plagioclase line from anorthite to albite, the two lines converging in the middle of the alk-al edge.

Sedimentary Rocks.—Most sediments have low alk-al ratios and lie close to the al/c-fm edge, but they coincide in part with the igneous field. Alkali evaporites lie at the alk corner.

Metamorphic Rocks and Processes, and Weathering.—Sericitization and kaolinization are expressed by shifts towards the muscovite point and al respectively.

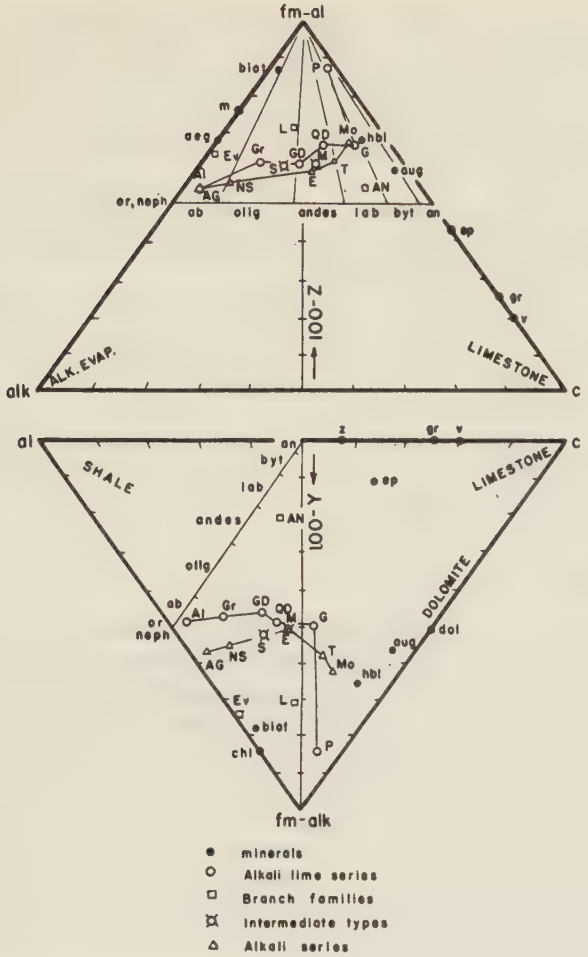

FIG. 11. Triangle views of the tetrahedron: alk/c and al/c charts.

Mineral abbreviations: ab albite, aeg aegirite, an anorthite, andes andesine, andr andradite, aug augite, baux bauxite, biot biotite, byt bytownite, cal calcite, dol dolomite, ep epidote, gr grossularite, hbl hornblende, lab labradorite, m muscovite, neph nepheline, olig oligoclase, or orthoclase, v vesuvianite, z zoisite.

Rock abbreviations: AG alkali granite, Al alaskite, AN anorthosite, E essexite, Ev evisite, G gabbro, GD granodiorite, Gr granite, L lamproite, M monzonite, Mo missourite, NS nepheline syenite, P peridotite, QD quartz diorite, S syenite, T theralite.

alk/c chart (Fig. 11)

Igneous Rocks.—The field of the igneous rocks lies between the feldspar line and the fm-al corner. Prevalence of alkali feldspar is marked by a high alk-c ratio. Increasing amounts of soda-lime feldspar cause a reduc-

tion of the alk-c ratio down to gabbro. At the gabbro point the igneous rock curve bends sharply toward fm as it approaches peridotite. Evisite lies between the soda amphiboles (aegirite and riebeckite) and alkali feldspar. Anorthosite lies between normal gabbro and labradorite. Olivine (and phlogopite) cause lamproite to have higher fm-al than normal phonolites or trachytes.

The chart gives the best estimates of the AbAn ratios of the plagioclase feldspars in the igneous rocks. In the case of orthoclase- and plagioclase bearing rocks the ratio is (OrAb)An.

Sedimentary Rocks.—Most sedimentary rocks have a low alk-c ratio and lie close to the fm-al/c line. The clays, laterites and iron ores lie at fm-al, dolomite at the anorthite point, and pure limestone at c. Rock salt and other alkali evaporites lie at alk.

Metamorphic Rocks and Processes, and Weathering.—Epidotization appears as a process involving an increase of lime, because epidote has a higher c than either anorthite or pyribole. Since the alk-c ratio of epidote is zero, there is also a slight loss of alk.

al/c chart (Fig. 11)

Igneous Rocks.—Prevalence of alkali feldspar is marked by a high al-c ratio, while increasing amounts of soda-lime feldspar accompanied by a reduction of alkali feldspar lower the ratio until in gabbro there is more lime than alumina. With the exception of peridotite, the alkali series is separated from the alkali lime series by higher fm-alk values. Anorthosite lies between normal gabbro and basic plagioclase. Evisite and lamproite show their relation to the alkali series by their high fm-alk values. The alkali lime series makes a sharp bend at the gabbro point due to the rapid decrease in plagioclase as the peridotite point is approached.

The igneous rock field is roughly diamond shaped, between fm-alk, orthoclase, anorthite and augite.

Sedimentary Rocks.—The major sediments lie along the al-c edge and are very effectively separated from the igneous rock field. Alkali evaporites and iron ores overlap the igneous field in the vicinity of the fm-alk corner.

Metamorphic Rocks and Processes.—Uralitization involves a loss of lime and gain in Mg which is indicated by the shift from augite to hornblende. Serpentinization, epidotization, garnetization and chloritization are also readily shown on this chart.

ol/fm chart (Fig. 12)

Igneous Rocks.—The field of the igneous rocks is defined by a triangle connecting the feldspars, fm and augite. The alkali lime series is distinctly separated from the alkali series by its lower Z, and syenite and mon-

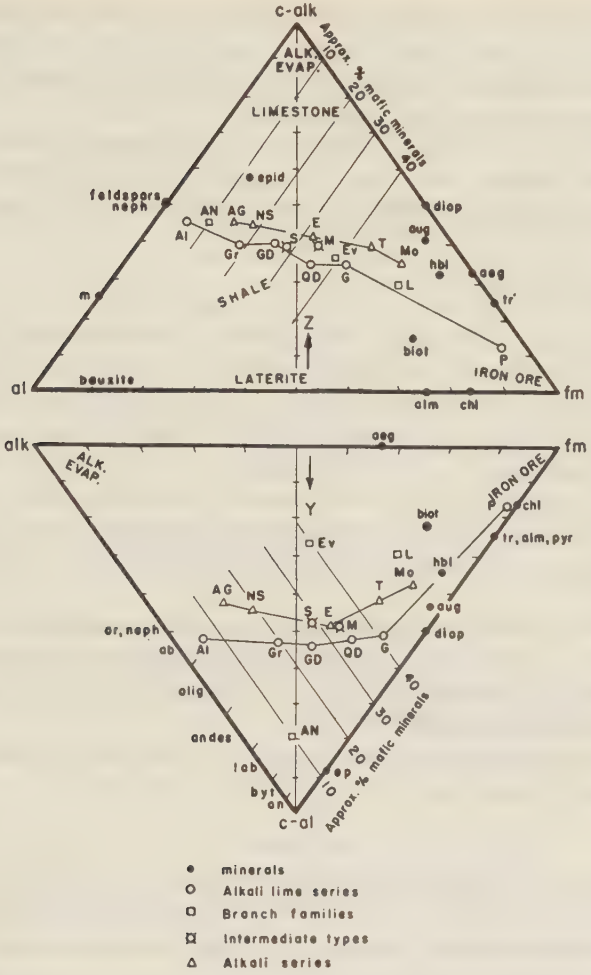

FIG. 12. Triangle views of the tetrahedron: al/fm and fm/alk charts.

Mineral abbreviations: ab albite, aeg aegirite, alm almandite, an anorthite, andes andesine, aug augite, biot biotite, byt bytownite, chl chlorite, diop diopside, ep epidote, hbl hornblende, lab labradorite, m muscovite, neph nepheline, olig oligoclase, or orthoclase, pyr pyrite, tr tremolite.

Rock abbreviations: AG alkali granite, Al alaskite, AN anorthosite, E essexite, Ev evisite, G gabbro, GD granodiorite, Gr granite, L lamproite, M monzonite, Mo missourite, NS nepheline syenite, P peridotite, QD quartz diorite, S syenite, T theralite.

zonite occupy intermediate positions.

The percentage of mafic constituents can be estimated up to 40% by determining the altitude of the analysis point relative to the al/c-alk edge as a base.

Sedimentary Rocks.—Except for the iron ores which lie near fm, the sediments range themselves between al and c-alk. There is only a slight overlap of the igneous field. Clays lie at al, pure limestones and alkali evaporites at c-alk, and the shales between.

Metamorphic Rocks and Processes, and Weathering.—The chart is adapted to illustrate the chemical changes involved in epidotization, sericitization, kaolinization, lateritization, chloritization and scapolitization.

fm/alk chart (Fig. 12)

Igneous Rocks.—The field of the igneous rocks lies between the fm/c-al edge and a line joining orthoclase and aegirite. The alkali series has Y under 50 and the alkali lime series has Y over 50 with the exception of peridotite. The relation of lamproite and evisite to the alkali series is shown by the high alk and low Y compared to the normal for the series. The anorthosite point lies between normal gabbro and basic plagioclase.

The percentage of mafic constituents can be estimated up to 40% by determining the altitude of the analysis point relative to the alk/c-al edge as a base.

Sedimentary Rocks.—The sediments occur bunched up at each of the corners. The most important corner is c-al where all gradations from limestone through calcareous shales to pure kaolin are located. Alkali evaporites lie at alk, and the iron ores at fm.

Metamorphic Rocks and Processes.—This chart may be used to illustrate chloritization, uralitization and serpentinization.

Conclusions

Any minerals or rocks containing one or more components of the quaternary chemical system al, fm, c and alk may be plotted as points in the Niggli-Becke tetrahedral system. The diagrams are suited for plotting chemical and modal analyses of all classes of rocks. The graphic nature and the broad adaptability of the projection for illustrating extremely varied petrochemical studies merits the recognition of all petrologists and students.

References Cited

Adams, F. D. (1914), Chemical relations of a petrographic province: *Jour. Geol.*, **22**, 689–693.

Becke, F. (1897), Gesteine der Columbrates: *Tschermak's miner. u. petrog. Mitt.*, **16**, 319.

——— (1912), Chemische Analysen von krystallinen Gesteinen aus der Zentralkette der Ostalpen: *Denkschriften d. math. naturwiss. Klasse d. k. Akad. d. Wissensch.*, Wien, **75**, 153.

——— (1925), Graphische Darstellung von Gesteinsanalysen: *Tschermak's miner. u. petrog. Mitt.*, **37**, 27–46.

BOEKE, H. E., AND EITEL, W. (**1923**), *Grundlagen der physikalisch-chemischen Petrographie*, 2nd ed., Berlin.

BROEGGER, W. C. (1895), Die Eruptionsfolge der triadischen Eruptivgestine bei Predazzo in Südtirol: *Videnskabs Selskabets Skrifter*, Kristiania, No. **7**, 55.

CLARKE, F. W. (1924), Data of Geochemistry: *U. S. Geol. Survey*, Bull. **770.**

DALY, R. A. (1910), Average chemical composition of igneous rocks: *Proc. Am. Acad. of Arts and Sci.*, vol. **45.**

DANA, E. S., AND FORD, W. E. (**1932**), *Textbook of Mineralogy*, New York.

GIBBS, J. W. (1876), Equilibrium of heterogeneous substances: *Trans. Conn. Acad.*, **3**, 176.

GROUT, F. F. (1918), A form of multiple rock diagrams: *Jour. Geol.*, **26**, 622–625.

——— (1922), Graphic study of igneous rock series: *Geol. Soc. Am., Bull.*, **33**, 617–638.

——— (1925), The Vermillion batholith of Minnesota: *Jour. Geol.*, **33**, 484–485.

GRUBENMANN, U., AND NIGGLI, P. (1924), *Die Gesteinsmetamorphose*, vol. **1**, Berlin.

HODGE, E. T. (1924), A proposed classification of igneous rocks. *Univ. of Oregon Publ.*, **2**, no. 7. Also in Johannsen (1932).

IDDINGS, J. P. (1892), Origin of igneous rocks: *Bull. Phil. Soc. Washington*, vol. **12.**

IDDINGS, J. P. (1903), Chemical composition of igneous rocks expressed by means of diagrams, with reference to rock classification on a quantitative chemico-mineralogical basis: *U. S. Geol. Survey*, Prof. Paper **18.**

JOHANNSEN, A. (1920), A quantitative mineralogical classification of igneous rocks, revised: *Jour. Geol.*, **28**, 38–60; 159–177; 210–232.

——— (1932, 1937, 1938), *A Descriptive Petrography of the Igneous Rocks*, Chicago, vols. **1, 2, 3,** and **4.**

LANG, H. O. (1892), Beiträge zur Systematik der Eruptivgesteine: *Tschermak's miner. u. petrog. Mitt.*, **13**, 160.

NIGGLI, P., AND BEGER, P. J. (1923), *Gesteins und Mineralprovinzen*, Berlin, vol. **1.**

OSANN, A. (1900), Versuch einer chemischen Classifikation der Eruptivgesteine: *Tschermak's miner. u. petrog. Mitt.*, **19**, 351–469.

PEACOCK, M. A. (1931), Classification of igneous rock series: *Jour. Geol.*, **39**, 54–67.

SCHUSTER, M. (1881), Ueber die optische Orientierung der Plagioklase: *Tschermak's miner. u. petrog. Mitt.*, vol. **3.**

TSCHERMAK, G., AND BECKE, F. (1920), *Lehrbuch der Mineralogie*, Wien.

VON WOLFF, F. (1922), Die Prinzipien einer quantitativen Klassifikation der Eruptivgesteine, insbesondere der jungen Ergussgesteine: *Geol. Rundschau*, **13**, 9–17. Also in Johannsen (1932).

WASHINGTON, H. S. (1917), Chemical analyses of igneous rocks: *U. S. Geol. Survey*, Prof. Paper **99.**

WINCHELL, A. N. (1933), *Elements of Optical Mineralogy*, Pt. **2**, p. 320.

TABLE 1. TABLE OF MINERALS GIVING SPECIFIC GRAVITIES, CHEMICAL FORMULAS, TETRAHEDRAL FACTORS, AND THE X, Y, Z AND si FACTORS WHICH REPRESENT THE MINERAL POSITIONS IN THE XYZ-si DIAGRAM

Mineral	Spec. Grav.	Chemical Formula	Tetr. Fact.	X	Y	Z	si
acmite	3.53	$Na_2O \cdot Fe_2O_3 \cdot 4SiO_2$	2.28	67	0	33	133
actinolite	3.1	$CaO \cdot 3(Mg, Fe)O \cdot 4SiO_2$	2.84	100	25	25	100
aegirite (acmite)			2.28	67	0	33	133
akermannite	3.18	$2CaO \cdot MgO \cdot 2SiO_2$	2.33	100	67	67	67
allanite (orthite: see epidote)			2.77	69	88	57	86
almandite	4.25	$3FeO \cdot Al_2O_3 \cdot 3SiO_2$	3.41	75	25	0	75
alunite	2.66	$K_2O \cdot 3Al_2O_3 \cdot 4SO_3 \cdot 6H_2O$	1.28	0	75	25	0
analcite	2.25	$Na_2O \cdot Al_2O_3 \cdot 4SiO_2 \cdot 2H_2O$	1.02	0	50	50	200
andalusite	3.18	$Al_2O_3 \cdot SiO_2$	1.97	0	100	0	100
andradite (melanite)	3.75	$3CaO \cdot Fe_2O_3 \cdot 3SiO_2$	3.68	100	60	60	60
anhydrite	2.95	$CaSO_4$	2.17	100	100	100	0
anthophyllite	3.03	$(Mg, Fe)O \cdot SiO_2$	2.81	100	0	0	100
antigorite (see serpentine)			2.78	100	0	0	67
apatite	3.2	$CaF_2 \cdot 3Ca_3(PO_4)_2$	3.1	100	100	100	0
apophyllite	2.35	$KF \cdot 4CaO \cdot 8SiO_2 \cdot 8H_2O$	1.31	89	89	89	178
arfvedsonite	3.45	$3Na_2O \cdot 8FeO \cdot Al_2O_3 \cdot 16SiO_2 \cdot 2H_2O$	2.22	67	8	25	133
augite (Average. Johannsen (1932))			2.92	93	43	41	98
bauxite	2.55	$Al_2O_3 \cdot 2H_2O$	1.85	0	100	0	0
beidellite	2.6	$Al_2O_3 \cdot 3SiO_2 \cdot 4H_2O$	0.73	0	100	0	300
beryl	2.7	$3BeO \cdot Al_2O_3 \cdot 6SiO_2$	2.01	75	25	0	150
biotite (Average. Johannsen (1932))			2.44	67	22	15	74
bronzite	3.25	$(Mg, Fe)O \cdot SiO_2$	2.88	100	0	0	100
calcite	2.71	$CaCO_3$	2.71	100	100	100	0
carnallite	1.60	$KCl \cdot MgCl_2 \cdot 6H_2O$	1.15	67	0	33	0
chabazite	2.12	$(Ca, Na_2)O \cdot Al_2O_3 \cdot 4SiO_2 \cdot 6H_2O$	0.82	25	75	50	200
chamosite	3.2	$15(Mg, Fe)O \cdot 5Al_2O_3 \cdot 11SiO_2 \cdot 16H_2O$	2.72	72	25	0	55
chondrodite	3.15	$Mg_2SiO_4 \cdot F_2Mg_2SiO_4$	4.15	100	0	0	40
chlorite	2.71	$4H_2O \cdot 5(Mg, Fe)O \cdot Al_2O_3 \cdot 3SiO_2$	2.94	84	16	0	50
chromite	4.5	$FeO \cdot Cr_2O_3$	4.01	50	50	0	0
collophanite	2.75	$Ca_3(PO_4)_2 \cdot H_2O$	2.75	100	100	100	0
cordierite	2.63	$2MgO \cdot 2Al_2O_3 \cdot 5SiO_2$	1.44	50	50	0	125
corundum	4.0	Al_2O_3	3.92	0	100	0	0
diallage (diopside)			3.04	100	50	50	100
diaspore	3.4	$Al_2O_3 \cdot H_2O$	2.83	0	100	0	0
diopside	3.29	$CaO \cdot MgO \cdot 2SiO_2$	3.04	100	50	50	100

TABLE 1—(*continued*)

Mineral	Spec. Grav.	Chemical Formula	Tetr. Fact.	X	Y	Z	si
dolomite	2.85	$CaCO_3 \cdot MgCO_3$	3.10	100	50	50	0
enstatite	3.15	$MgO \cdot SiO_2$	3.15	100	0	0	100
epidote	3.4	$H_2O \cdot 4CaO \cdot 3(Al, Fe)_2O_3 \cdot 6SiO_2$ (Al:Fe=73:27)	2.77	69	88	57	86
epsomite	1.75	$MgSO_4 \cdot 7H_2O$	0.71	100	0	0	0
fluorite	3.18	CaF_2	4.07	100	100	100	0
gehlenite (melilite)	2.98	$3CaO \cdot Al_2O_3 \cdot 3SiO_2$	3.06	75	100	75	50
glauconite	2.5	$K_2O \cdot 2MgO \cdot 3(Fe,Al)_2O_3 \cdot 12SiO_2 \cdot 6H_2O$	1.34	56	33	11	133
glaucophane	3.07	$Na_2O \cdot Al_2O_3 \cdot 4SiO_2$	1.52	0	50	50	200
goethite	4.28	$Fe_2O_3 \cdot H_2O$	4.81	100	0	0	0
grossularite	3.53	$3CaO \cdot Al_2O_3 \cdot 3SiO_2$	3.13	75	100	75	75
gypsum	2.32	$CaSO_4 \cdot 2H_2O$	1.35	100	100	100	0
halite	2.16	NaCl	3.70	0	0	100	0
halloysite	2.1	$Al_2O_3 \cdot 2SiO_2 \cdot nH_2O$ (20%H_2O)	0.75	0	100	0	200
hedenbergite	3.55	$CaO \cdot FeO \cdot 2SiO_2$	2.86	100	50	50	100
hematite	5.2	Fe_2O_3	6.5	100	0	0	0
heulandite	2.2	$(Ca, Na_2)O \cdot Al_2O_3 \cdot 6SiO_2 \cdot 5H_2O$	0.73	25	75	50	300
hornblende (Average. Johannsen (1932))			2.92	89	34	32	91
hydrargillite (gibbsite)	2.35	$Al_2O_3 \cdot 3H_2O$	1.51	0	100	0	0
hypersthene	3.45	$(Fe, Mg)O \cdot SiO_2$	3.73	100	0	0	100
ilmenite	4.75	$FeO \cdot TiO_2$	3.13	100	0	0	0
kaolinite	2.61	$2H_2O \cdot Al_2O_3 \cdot 2SiO_2$	1.01	0	100	0	200
kyanite	3.61	$Al_2O_3 \cdot SiO_2$	2.23	0	100	0	100
leucite	2.48	$K_2O \cdot Al_2O_3 \cdot 4SiO_2$	1.14	0	50	50	200
limonite	3.8	$2Fe_2O_3 \cdot 3H_2O$	4.04	100	0	0	0
magnetite	5.17	$FeO \cdot Fe_2O_3$	7.22	100	0	0	0
margarite (Ca-mica)	3.04	$H_2O \cdot CaO_2 \cdot 2Al_2O_3 \cdot 2SiO_2$	2.28	33	100	33	67
marialite (scapolite)	2.62	$2NaCl \cdot 3(Na_2O \cdot Al_2O_3 \cdot 6SiO_2)$	0.99	0	43	57	257
meionite (scapolite)	2.77	$CaCO_3 \cdot 3(CaO \cdot Al_2O_3 \cdot 2SiO_2)$	2.21	57	100	57	86
melanterite	1.90	$FeSO_4 \cdot 7H_2O$	0.68	100	0	0	0
melilite (see gehlenite or akermannite)							
microcline and anorthoclase	2.55	$K_2O \cdot Al_2O_3 \cdot 6SiO_2$	0.92	0	50	50	300
montmorillonite	2.25	$MgO \cdot Al_2O_3 \cdot 5SiO_2 \cdot 6H_2O$	2.25	50	75	25	250
muscovite and sericite	2.88	$2H_2O \cdot K_2O \cdot 3Al_2O_3 \cdot 6SiO_2$	1.45	0	75	25	150
natrolite	2.23	$Na_2O \cdot Al_2O_3 \cdot 3SiO_2 \cdot 2H_2O$	1.17	0	50	50	150
nepheline	2.60	$Na_2O \cdot Al_2O_3 \cdot 2SiO_2$	1.82	0	50	50	100

TABLE 1—(*continued*)

Mineral	Spec. Grav.	Chemical Formula	Tetr. Fact.	X	Y	Z	si
olivine	3.32	$2(Mg, Fe)O \cdot SiO_2$	4.58	100	0	0	50
orthoclase and sanidine	2.55	$K_2O \cdot Al_2O_3 \cdot 6SiO_2$	0.92	0	50	50	300
paragonite (Na-mica)	2.84	$Na_2O \cdot 3Al_2O_3 \cdot 6SiO_2 \cdot 2H_2O$	1.49	0	75	25	150
pargasite (hornblende)	3.05	$CaO \cdot 2MgO \cdot Al_2O_3 \cdot 3SiO_2$	2.92	75	50	25	75
periclase	3.8	MgO	9.5	100	0	0	0
perovskite	4.0	$CaO \cdot TiO_2$	2.93	100	100	100	0
perthite (same as orthoclase or albite)							
phillipsite	2.2	$(K_2, Ca)O \cdot Al_2O_3 \cdot 4SiO_2 \cdot 4\frac{1}{2}H_2O$	0.90	25	75	50	200
phlogopite	2.81	$2H_2O \cdot K_2O \cdot 6MgO \cdot Al_2O_3 \cdot 6SiO_2$	2.70	75	13	13	75
plagioclase albite							
$Ab_{100}An_0$	2.62	$Na_2O \cdot Al_2O_3 \cdot 6SiO_2$	1.00*	0	50	50	300
$Ab_{95}An_5$	2.63		1.05	5	55	50	282
oligoclase $Ab_{90}An_{10}$	2.64		1.10	9	59	50	265
$Ab_{85}An_{15}$	2.65		1.15	13	63	50	248
$Ab_{80}An_{20}$	2.65		1.20	17	67	50	233
$Ab_{75}An_{25}$	2.66		1.25	20	70	50	222
andesine $Ab_{70}An_{30}$	2.67		1.30	23	73	50	208
$Ab_{65}An_{35}$	2.67		1.35	26	76	50	197
$Ab_{60}An_{40}$	2.68		1.40	29	79	50	186
$Ab_{55}An_{45}$	2.69		1.45	31	81	50	176
labradorite $Ab_{50}An_{50}$	2.69		1.50	33	83	50	166
$Ab_{45}An_{55}$	2.70		1.55	36	86	50	158
$Ab_{40}An_{60}$	2.71		1.60	38	88	50	149
$Ab_{35}An_{65}$	2.72		1.65	39	89	50	142
bytownite $Ab_{30}An_{70}$	2.72		1.70	41	91	50	136
$Ab_{25}An_{75}$	2.73		1.75	43	93	50	129
$Ab_{20}An_{80}$	2.73		1.80	44	94	50	122
$Ab_{15}An_{85}$	2.74		1.85	46	96	50	116
anorthite $Ab_{10}An_{90}$	2.75		1.90	47	97	50	111
Ab_5An_{95}	2.75		1.94	49	99	50	106
Ab_0An_{100}	2.76	$CaO \cdot Al_2O_3 \cdot 2SiO_2$	1.98	50	100	50	100
polyhalite	2.78	$2CaSO_4 \cdot MgSO_4 \cdot K_2SO_4 \cdot 2H_2O$	1.90	75	50	75	0
prehnite	2.88	$H_2O \cdot 2CaO \cdot Al_2O_3 \cdot 3SiO_2$	2.09	67	100	67	100
pyrite	5.03	FeS_2	4.20	100	0	0	0
pyrope	3.51	$3MgO \cdot Al_2O_3 \cdot 3SiO_2$	3.48	75	25	0	75
pyrophyllite	2.85	$H_2O \cdot Al_2O_3 \cdot 4SiO_2$	0.79	0	100	0	400

TABLE 1—(*continued*)

Mineral	Spec. Grav.	Chemical Formula	Tetr. Fact.	X	Y	Z	si
quartz and opal	2.66	SiO_2 (and $SiO_2 \cdot nH_2O$)	4.42**	not plotted			
riebeckite	3.44	$Na_2O \cdot Fe_2O_3 \cdot 4SiO_2$	2.23	67	0	33	133
sanidine (see orthoclase)			0.92	0	50	50	300
scapolite (see marialite and meionite)							
scheelite	6.0	$CaWO_4$	2.08	100	100	100	0
scolecite	2.28	$CaO \cdot Al_2O_3 \cdot 3SiO_2 \cdot 3H_2O$	1.16	50	100	50	100
sericite (see muscovite)			1.45	0	75	25	150
serpentine	2.58	$3MgO \cdot 2SiO_2 \cdot 2H_2O$	2.78	100	0	0	67
siderite	3.86	$FeCO_3$	3.32	100	0	0	0
sillimanite	3.24	$Al_2O_3 \cdot SiO_2$	2.00	0	100	0	100
sodalite	2.22	$2NaCl \cdot 3(Na_2O \cdot Al_2O_3 \cdot 2SiO_2)$	1.61	0	43	57	86
soda niter	2.27	$NaNO_3$	1.33	0	0	100	0
spinel	3.8	$MgO \cdot Al_2O_3$	5.35	50	50	0	0
spodumene	3.17	$Li_2O \cdot Al_2O_3 \cdot 4SiO_2$	1.69	100	50	50	200
staurolite	3.71	$H_2O \cdot 2FeO \cdot 5Al_2O_3 \cdot 4SiO_2$	2.84	29	72	0	57
talc	2.75	$3MgO \cdot 4SiO_2 \cdot H_2O$	2.18	100	0	0	133
titanite	3.48	$CaO \cdot TiO_2 \cdot SiO_2$	1.78	100	100	100	100
topaz	3.5	$Al_2F_2O_2 \cdot SiO_2$	1.90	0	100	0	100
tremolite	3.05	$CaO \cdot 3MgO \cdot 4SiO_2$	2.94	100	25	25	100
vesuvianite	3.4	$2H_2O \cdot 12CaO \cdot 3Al_2O_3 \cdot 10SiO_2$	3.16	80	100	80	67
wolframite	7.3	$(Fe, Mn)WO_4$	2.40	100	0	0	0
wollastonite	2.85	$CaO \cdot SiO_2$	2.46	100	100	100	100
xanthophyllite	3.05	$H_2O \cdot CaO \cdot 4MgO \cdot 3SiO_2$—45% $H_2O \cdot CaO \cdot MgO \cdot 3Al_2O_3$—55%	3.64	67	53	20	27
zircon	4.5	$ZrO_2 \cdot SiO_2$	2.46**	not plotted			
zoisite	3.31	$4CaO \cdot 3Al_2O_3 \cdot 6SiO_2 \cdot H_2O$	2.54	57	100	57	86

* Note: The tetrahedral factor increases by 0.01 for each per cent increase of An, except for anorthite.

** These are si factors equivalent to the tetrahedral factors but not plotted in the tetrahedron. Zircon also has a zr factor of 2.46.

TABLE 2. AVERAGE COMPOSITIONS OF THE IGNEOUS ROCKS PLOTTED IN THE XYZ-si DIAGRAM

Rock Family	X	Y	Z	si	k	mg
ALKALI LIME SERIES						
Alaskite	9	52	45	487	48	9
Granite	31	53	38	335	44	35
Granodiorite	45	54	39	248	28	48
Quartz diorite	56	52	34	188	30	51
Gabbro	69	51	34	107	19	60
Peridotite	93	16	13	70	0	84
BRANCH FAMILIES						
Anorthosite	45	79	46	124	12	52
Lamproite	68	29	29	140	80	80
Evisite (pantellerite)	40	26	36	290	3	8
INTERMEDIATE TYPES						
Syenite	45	48	39	204	43	43
Monzonite	56	49	39	154	44	52
ALKALI SERIES						
Alkali granite	18	43	45	398	40	9
Nepheline syenite	27	45	44	171	30	22
Essexite	54	49	41	131	27	40
Theralite	70	42	38	96	19	42
Missourite	79	38	33	89	74	72

TABLE 3. NIGGLI'S MAGMA FAMILIES IN THE XYZ-si DIAGRAM

Series	Magma Group	Magma Types or Rock Families	X	Y	Z	si
Alkali lime series	Granitic	aplite granitic	13	52	46	460
		engadinitic, e. granitic	18	50	44	420
		yosemititic, y. granitic	17	56	43	350
		normal granitic	41	50	39	270
		granodioritic	40	56	38	270
		opdalitic (quartz monzonitic)	50	50	36	215
	Dioritic	trondhjemitic	23	53	46	350
		plagioclase granitic, oligoclasitic	32	58	42	310
		quartz dioritic	50	50	38	220
		tonalitic	55	55	34	200
		peleeitic	56	56	34	180
		normal dioritic	57	51	36	155
		gabbro-dioritic	65	48	33	135

TABLE 3—(*continued*)

Series	Magma Group	Magma Types or Rock Families	X	Y	Z	si
Alkali lime series	Gabbroid & Anorthositic	normal gabbroid	73	42	27	108
		pyroxenite-hornblende gabbroid	72	55	36	100
		ossipitic, o. gabbroid	63	57	37	110
		anorthosite gabbroid	55	70	41	130
		andesine-labradorite-felsic and anorthositic	40	80	46	145
	Ultra femic	issitic, ostraitic	82	44	34	75
		pyroxenitic	91	36	31	95
		koswitic	97	35	33	65
		hornblenditic	80	35	25	80
		hornblendite-pyroxenite-peridotitic	88	24	16	80
		orthaugitic	95	9	6	95
		peridotitic	94	9	5	60
Soda series	Alk. granitic pulaskitic	alkali granitic (soda granitic)	19	42	43	400
		nordmarkite-pulaskitic	20	46	44	250
		soda-quartz-syenitic, soda syenitic	39	42	39	200
		soda-lamprosyenitic	64	34	26	145
		evisitic	40	26	36	290
	Foyaitic	larvikitic and monzonite foyaitic	30	51	43	180
		normal foyaitic	17	47	46	190
		urtitic	16	45	49	116
		monmouthitic	28	54	50	100
		nosykombitic	42	47	39	150
		ijolitic	50	50	50	100
		melteigitic (theralitic-ijolitic)	64	51	49	90
		lujavritic, agpaitic	33	34	43	160
	Essexitic	toensbergitic or essexite-dioritic	37	55	42	180
		essexitic (normal essexitic)	50	50	40	130
	Theralitic or Alk. gabbroid	theralitic	65	42	39	100
		theralite gabbroid	69	43	34	90
		essexite gabbroid	67	47	34	105
		jacupirangitic	91	42	37	70
Potash series	Quartz-syenitic or Granite-syenitic	rapakiwitic	27	49	41	380
		granosyenitic	27	50	43	260
		adamellitic	36	50	40	330
		tasnagranitic	36	43	37	290
		syenite granitic	41	42	41	250

TABLE 3—(*continued*)

Series	Magma Group	Magma Types or Rock Families	X	Y	Z	si
Potash series	Syenitic	juvitic or leuco-syenitic	25	51	46	178
		vesuvitic	40	53	47	160
		monzonite syenitic	37	51	40	190
		normal syenitic	45	45	40	185
		lamprosyenitic-lampromonzonite syenitic	58	37	29	160
		lamprosommaitic	62	43	31	140
		lamproitic (Wyoming type)	55	32	41	165
		lamproitic (Murcia type)	68	29	29	140
		borolanitic	52	57	51	130
	Monzonitic	normal monzonitic	51	51	40	140
		sommaitic	61	51	42	115
		sommaitic dioritic	67	48	35	130
		yogoitic, y. monzonitic	58	44	40	145
	Shonkinitic	normal shonkinitic	70	41	37	105
		missouritic	74	48	44	95
		pyroxenolitic	83	56	47	80

TABLE 4. SEDIMENTARY ROCKS PLOTTED IN THE XYZ-si DIAGRAM

Name of rock or sediment	X	Y	Z	si
Composite analysis of 345 limestones (Clarke 1924; p. 564)	99	79	78	9
Composite analysis of 498 limestones used for building purposes (Clarke 1924; p. 564)	91	73	78	23
Composite of 51 Paleozoic shales (Clarke 1924; p. 552)	45	48	20	257
Composite of 27 Mesozoic and Cenozoic shales (Clarke 1924; p. 552)	56	55	37	210
Cretaceous shale (highly calcareous), Mt. Diablo, Calif. (Clarke 1924; p. 552)	89	78	67	56
Composite analysis of 253 sandstones (Clarke 1924; p. 547)	68	68	56	618
Composite analysis of 371 sandstones used for building purposes (Clarke 1924; p. 547)	41	54	31	990
Granite laterite (Clarke 1924; p. 498)	17	83	0	248
Diorite laterite (Clarke 1924; p. 498)	34	66	0	4
Laterite F. India (Clarke 1924; p. 498)	73	27	0	tr
Marine red clay (23 analyses) (Clarke 1924; p. 516)	58	47	5	276
Marine red mud (Clarke 1924; p. 517)	80	79	72	75

TABLE 5. METAMORPHIC ROCKS PLOTTED IN THE XYZ-si DIAGRAM

Name of rock	X	Y	Z	si
Serpentine A (Clarke 1924; p. 617)	98	3	1	66
Lime silicate hornfels (Grubenmann and Niggli 1924; p. 260)	81	48	42	120
Epidosite (Clarke 1924; p. 610)	74	74	51	92
Amphibolite (Grubenmann and Niggli 1924; p. 496)	74	40	32	90
Greenstone with hornblende, albite and chlorite (Grubenmann and Niggli 1924; p. 488)	73	40	24	104
Plagioclase diopside hypersthene hornfels (Grubenmann and Niggli 1924; p. 486)	71	42	31	118
Eclogite, Tirol (Grubenmann and Niggli 1924; p. 405)	71	48	33	92
Glaucophane schist (Grubenmann and Niggli 1924; p. 497)	63	23	26	139
Lime silicate hornfels (Grubenmann and Niggli 1924; p. 260)	61	30	18	151
Plagioclase hypersthene hornfels (Grubenmann and Niggli 1924; p. 486)	59	46	26	162
Lime silicate hornfels (Grubenmann and Niggli 1924; p. 260)	51	23	21	157
Quartzite A (Clarke 1924; p. 619)	50	38	18	410
Quartz, two mica garnet schist; average of 6 analyses (Grubenmann and Niggli 1924; p. 485)	46	47	26	244
Andalusite schist A (Clarke 1924; p. 625)	45	49	17	275
Staurolite biotite schist (Grubenmann and Niggli 1924; p. 495)	38	61	9	72
Quartz-muscovite-chlorite-phyllite; average of 8 analyses (Grubenmann and Niggli 1924; p. 485)	37	50	19	231
Feldspathic mica schist (Clarke 1924; p. 626)	31	50	35	342
Quartzite C (Clarke 1924; p. 619)	30	53	20	1910
Biotite orthoclase gneiss (Grubenmann and Niggli 1924; p. 391)	27	50	41	376
Andalusite-cordierite-hornfels (Grubenmann and Niggli 1924; p. 486)	22	58	29	291

METAMORPHISM OF MINERALS[1]

M. J. Buerger and Edward Washken,
Massachusetts Institute of Technology, Cambridge, Mass.

Abstract

The sources of the energy which drives metamorphism are discussed. It is pointed out that an important source of energy which is almost universally overlooked by the geologist is the strain energy which arises from plastic deformation of crystals. Theoretically, this energy ought to be capable of causing metamorphism when released either by annealing or by contact with solvent fluids. The remainder of the paper is devoted to demonstrating experimentally that metamorphism can be caused by this means, and to deriving the laws governing the process. An important feature is that no recrystallization occurs unless a critical temperature, which is characteristic of the particular crystal species, and which varies with the intensity of plastic deformation, is exceeded. Experiments are also cited in which recrystallization following plastic deformation is caused to occur with the aid of solvent fluids.

Theoretical Background

The fact that something changes to something else in any kind of metamorphism shows that the new system has lower energy than the old. For the present discussion, let us exclude the kinds of metamorphism which are concerned with a change of over-all composition of the metamorphosed material. Then the energy drop which drives the metamorphic process must come from a difference in the free energy of the old set of crystals and the free energy of a new set. This energy drop can be realized in an obvious way for polymineralic aggregates. For such instances, metamorphism implies that under the conditions of the metamorphic environment a new set of minerals, $U, V, W, \cdots$ has a lower net energy than the old set of minerals, $A, B, C, \cdots$.

But metamorphism also takes place in monomineralic aggregates. In this case, the new collection of minerals is the same as the old collection. What drives the metamorphic process in such instances? At least two forms of energy are available to differentiate the beginning from the end aggregates: surface energy and strain energy. Thus, a fine-grained aggregate could be metamorphosed into a coarse-grained one, with a reduction of the net surface energy of the aggregate. Or, a strained aggregate could be metamorphosed into an unstrained one, with a net reduction in the strain energy of the aggregate.

The latter scheme is of particular importance because strain is an inevitable consequence of plastic deformation. This has been known since some of the earliest work on the plastic deformation of single crystals. For example, Johnson customarily determined the planes along which

[1] Read at the annual meeting of The Mineralogical Society, Pittsburgh, December 27, 1945.

translation-gilding took place in the transparent crystals he investigated, by observing the strain-anisotropism which arose from the deformation.[2] The strain is localized in the immediate neighborhood of the functional planes along which the gliding takes place. As early as 1930 one of us suggested that these strains were part of the cause of the recrystallization which accompanies metamorphism.[3]

It is thus evident that a plastically deformed mineral aggregate contains strain energy. The strain has the form of bending and other kinds of distortion of the crystal structure, especially in the neighborhood of the functional gliding planes. If a mineral which is so deformed is subjected to conditions under which a transfer of its matter is possible, it will distill, or dissolve, so that its matter comes to be added to a strain-free crystal or crystals. To have this transfer take place, it is only neceessary to heat the strained mineral until its vapor pressure gives rise to an appreciable transfer of material from strained to unstrained crystals. Alternatively, the transfer may be accomplished by placing the strained mineral in a fluid in which it is slightly soluble. Either means provides the vehicle for transfer of matter from strained to unstrained crystal, and hence induces recrystallization.

Experimental Material

Guided by this reasoning, extensive experimental work has been undertaken in artificially metamorphosing monomineralic aggregates. For the first trials, minerals were selected which were known to be rather plastic, and whose subsequent heating would not be complicated by chemical decomposition to any appreciable extent. The minerals fluorite, periclase, and anhydrite appeared well suited in these properties. (Lists of the plastic characteristics of minerals are available.)[4] Thus fluorite has 3 planes and 6 directions of translation-gliding; periclase has 6 planes and 6 directions; while anhydrite has 3 planes and 2 directions. The planes of anhydrite are known to visibly crinkle when the mineral is plastically deformed.

General Experimental Procedure

Since it is easier to plastically deform small crystals than large ones, deformation is readily accomplished with powders. For this purpose,

[2] Johsen, A., Biegungen und Translationen: *Neues Jahrb. f. Min., Geol., u. Pal.*, II, 148–150 (1902).

[3] Buerger, M. J., Translation-gliding in crystals: *Am. Mineral.*, **15**, 46 (1930).

[4] Characteristics of crystals which undergo translation-gliding are given in: M. J. Buerger, Translation-gliding in crystals. *Am. Mineral.*, **15**, 61–64 (1930).

A compilation of the characteristics of crystals which undergo twin gliding was also prepared by M. J. Buerger, and was published by Bell: Handbook of Physical Constants, *G. S. A. Special paper* No. **36**, pp. 120–121 (1942).

powders finer than 170 mesh proved to be suitable. When compressed in a piston and cylinder device at pressures which can easily be obtained by commercial presses (about 5000 atmospheres) plastic deformation is induced throughout the smallest grains and is also induced in at least the corners and edges of the larger grains.

The aggregate so treated now possesses strain energy. To release this energy it is merely necessary to raise the temperature to such a level that atoms or groups of atoms can migrate from one crystal to another. This permits differential migration in the direction of unstrained crystals. A few hours proved sufficient to make the migration appreciable.

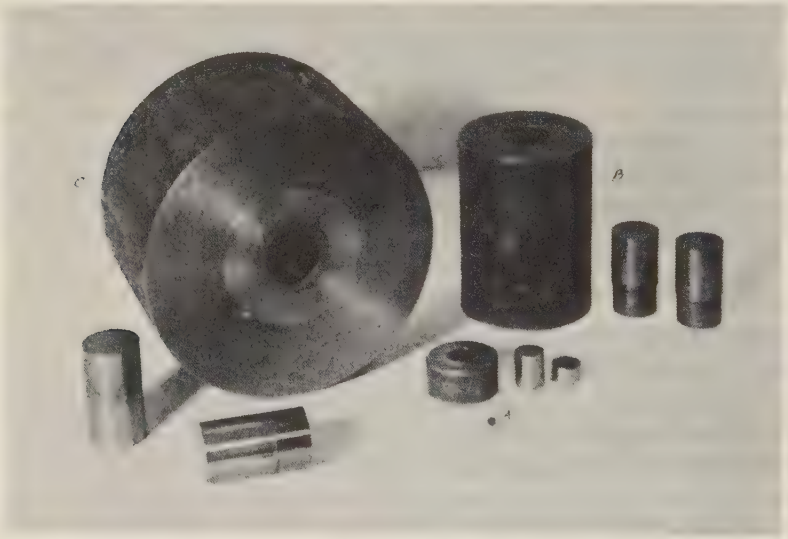

FIG. 1

EXPERIMENTAL EQUIPMENT

Experimental metamorphism can be produced with the aid of rather simple laboratory equipment. To produce the plastic deformation of the original powder, simple piston and cylinder sets are used, Fig. 1. Ordinary high chrome, high carbon steel cylinders, 5/8 inch I. D., Fig. 1*A*, are satisfactory for deforming rather plastic materials such as anhydrite, fluorite and periclase. When the material is to be deformed at elevated temperatures, nitrided steel cylinders, Fig. 1*B*, are required, since the surface of this material retains its hardness at elevated temperatures. For plastically deforming powders of hard minerals such as corundum, it was found necessary to use dies made of tungsten carbide, Fig. 1*C*. All surfaces of the dies which come in contact with the material to be deformed are lapped and polished to nearly a mirror finish.

The required pressures using the 5/8 inch diameter die are easily obtained with a simple hydraulic press of 20 tons capacity, equipped with a gauge indicating the total pressure on the piston, Fig. 2. The platens of the press can be protected from damage by the die by means of two surface-hardened steel plates about three inches square.

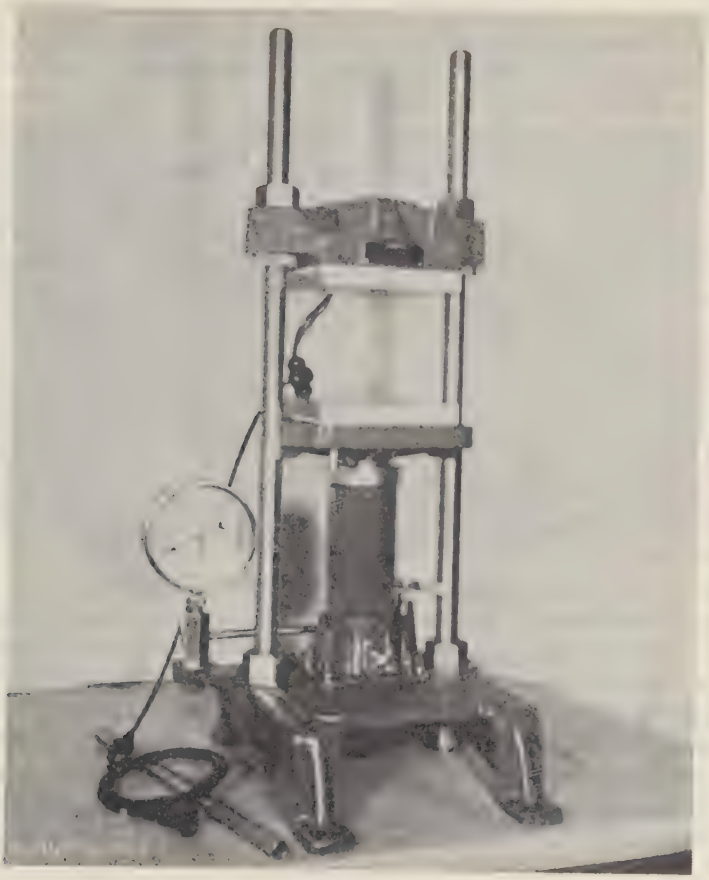

Fig. 2

The annealing is conveniently carried out in an ordinary muffle furnace. In our experiments a globar muffle furnace was used, with temperature indicated by a platinum-13% rhodium thermocouple.

Preliminary Experiments

It has already been pointed out that anhydrite is plastic. Furthermore some earlier work by one of us had indicated that anhydrite had an ap-

preciable vapor pressure in the neighborhood of 1200° C. Thus anhydrite was known to have characteristics favorable to a preliminary experiment in artificial metamorphism, and accordingly the first experiments were carried out with anhydrite.

Some finely powdered anhydrite was plastically deformed by compressing it at 40 tons per square inch. When ejected from the die the compressed powder was in the form of a coherent slug. This was annealed at 1200° C. for two hours. Ordinary visual examination of the slug then revealed that it had undergone a thorough recrystallization, and this observation was abundantly confirmed by an examination of a thin section.

We do not labor the details of this preliminary experiment. It is easy to duplicate simple thermal metamorphism experimentally.

The qualitative success of this preliminary experiment, which was based strictly on the ratiocination outlined in the first section, suggested a further investigation of the process of recrystallization, with emphasis on some of the quantitative aspects of the phenomenon.

For the next set of experiments, fluorite was selected as the appropriate crystal material. The reasons for this change of material were as follows: Anhydrite had shown a tendency to decompose on annealing. It might be expected to decompose to a greater extent at higher temperatures and longer annealing times. To avoid any complications imposed by possible decomposition while annealing, another mineral was selected which was known not to decompose. The selection of the particular material was further guided by the knowledge that isometric substances, if plastic, are very plastic because of the large number of symmetrically equivalent planes and directions of gliding. Among the several plastic isometric substances,[4] fluorite was known to be reasonably stable at temperatures approaching the melting point, so it appeared to be a natural choice for the experiments. It is true that fluorite deposits of metamorphic origin are apparently not known, but this was not regarded as a drawback for the material since we were seeking to find some of the general laws of this kind of metamorphism, and not trying merely to produce something to artificially duplicate a natural occurrence.

Fluorite

Preliminary Investigation.—Preliminary experiments, following the lines of the original experiment with anhydrite, made it clear that fluorite could be caused to recrystallize in the same way, Fig. 3. In these and subsequent experiments hand-picked fluorite from Rosiclare, Illinois, was used. This was reduced to pass 170 mesh.

We first wished to get some quantitative idea of the rate at which the

recrystallization takes place with change of annealing temperature. To this end we plastically deformed a number of slugs of fluorite powder by pressing them all at 40 tons per square inch. These were all heated for the same time, namely 10 hours, but each was annealed at a different temperature. The temperature range from 1600° F. to 2200° F. was covered in steps of approximately 100° F. In a general way it was visually evident that increasing temperature of annealing brought about increasing grain size in the recrystallized product. We now sought to measure this grain size.

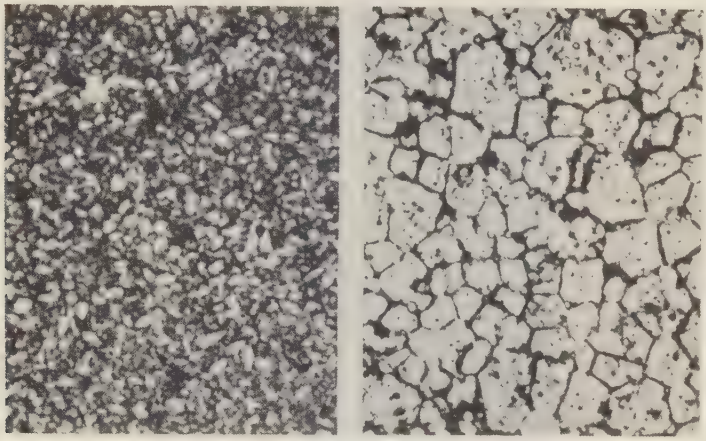

FIG. 3. The recrystallization of fluorite. Left: thin section of specimen made by pressing powder at 40 tons per square inch. Right: thin section of similar material after recrystallization caused by annealing (both ×25).

We first thought that thin sections would permit us to measure the dimensions of the grains. It turned out that, while thin sections were of some aid in studying specimens annealed at 2000° F. and higher, they were not very helpful for specimens annealed at lower temperatures. This was because the unrecrystallized material constituted a dust-like interstitial cement between the recrystallized grains, and such fine material is not easy to study in thin section.

We then turned to polished sections and sought an appropriate etch to reveal the grain boundaries. After considerable experimentation it was found that the grain boundaries could be brought out by immersing the polished section for 5 seconds in hot concentrated sulfuric acid. In Fig. 4 is shown a series of photographs of typical sections etched in this way. The course of recrystallization is made apparent by this series. The low-

est temperature sections are characterized by the angular grains of the original plastically deformed slug with fine interstitial flour. At increasing temperatures the angularity decreases and the flour vanishes until the section shows a mosaic texture of equant grains.

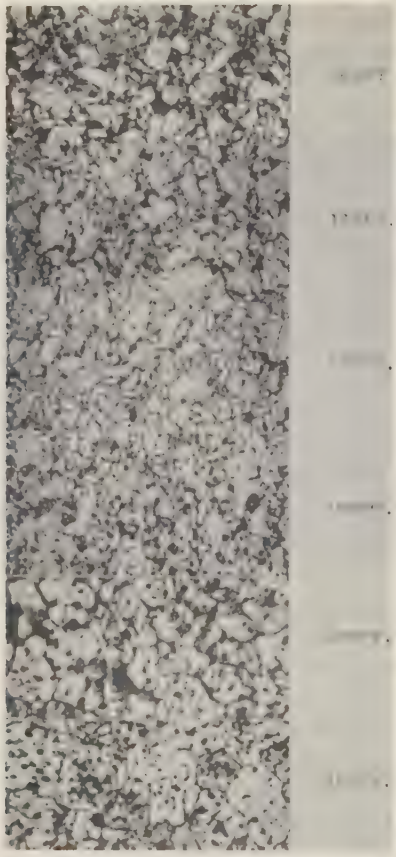

FIG. 4. The effect of temperature on recrystallization. Polished sections of fluorite etched with hot concentrated sulfuric acid to bring out grains. All samples were deformed at 40 tons per square inch and subsequently annealed 10 hours at the temperatures indicated (×50).

It is not an easy matter to make grain-size measurements in mixtures of angular grains and interstitial flour. For this reason we do not regard our measurements as very accurate, but they do give an indication of the trend of recrystallization. They are shown in graphical form in Fig. 5.

Determination of the Onset of Recrystallization.—A neat way was developed for investigating certain aspects of grain growth. This consisted in studying the x-ray powder photograph of the recrystallized aggregate

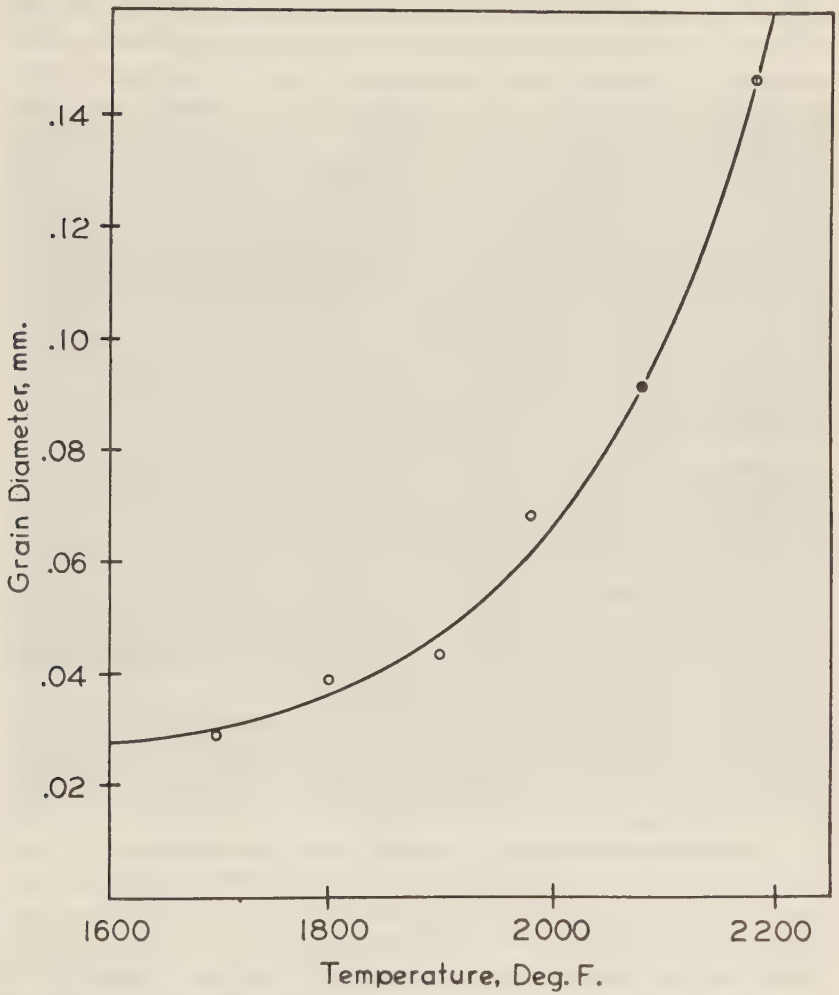

FIG. 5. Grain diameter as a function of annealing temperature. (Fluorite powder pressed at 40 tons per square inch; annealing time, 10 hours.)

according to the features discussed in the next paragraph. For this purpose the entire sample was made in the form of a small pin of such dimensions as to constitute a suitable sample for direct insertion into a standard x-ray powder camera.

The white component of the characteristic x-radiation produces Laue spots in the ordinary powder photograph provided that the specimen is not rotated.[5] If the crystals are strained, Laue spots are known to display asterism,[6] i.e., they are elongated into streaks. This is due to a bending of the Bragg reflecting planes, which is a manifestation of the strain in the crystal. When the strain is relieved, the asterism disappears from the spots and they assume normal appearance. Thus, by heating the specimen to various temperatures and watching the Laue-spot aspect of the powder photograph of the resulting sample, the temperature at which the strain becomes relieved can be determined.

The monochromatic component of the x-radiation produces the ordinary Debye lines. As the crystal grains of the sample grow by recrystallization, the number of crystals in the sample decreases. This causes the lines to become discontinuous and to break up into a series of beads. Each bead represents the reflection of a single crystal. As recrystallization continues, these beads increase in size, but decrease in number, indicating that the crystal size of the aggregate is increasing.

A part of such a sequence for fluorite powder pressed at 40 tons per square inch and annealed at various temperatures for three hours is shown in Fig. 6. It will be observed that the specimen annealed at 1600° F. shows asterism of the Laue spots near the center of the photograph, while for specimens annealed at temperatures higher than 1700° F. the asterism has disappeared. Furthermore, grain growth, as indicated by the disappearance of continuous Debye lines, is marked in specimens annealed above temperatures of 1800° F. in this series. This information is consistent with that shown in Figs 4 and 5.

Effect of Time on Recrystallization.—From the experiments just described one concludes that there is a definite temperature above which a deformed mineral aggregate must be heated before its strain begins to be relieved. The question naturally arises whether a longer time of annealing at a lower temperature would not bring about the same result. To test this question, specimens were deformed by the same amount and annealed at different times for each of a series of temperatures. It was found that annealing below 1700° F. for as long as 24 hours produced no apparent recrystallization of fluorite deformed at 40 tons per square inch.

These experiments confirm the conclusion that for a given amount of plastic deformation there is a critical temperature above which the material must be heated for any recrystallization to take place. To antic-

[5] Buerger, M. J., The design of x-ray powder cameras: *Jour. Appl. Phys.*, **16,** 508, Fig. 6C (1945).

[6] Schiebold, E., Die Verfestigungsfrage vom Standpunkt der Röntgenforschung: *Zeit. Metallk.*, **16,** 417–425 (1924).

ipate, it has been found that this temperature differs from mineral to to mineral and is characteristic of a species. It is easy to rationalize this. The critical temperature is that which just supplies the energy to move material from one crystal to another over the potential barrier provided by its attachment to the crystal structure. It is therefore characteristic of the structure.

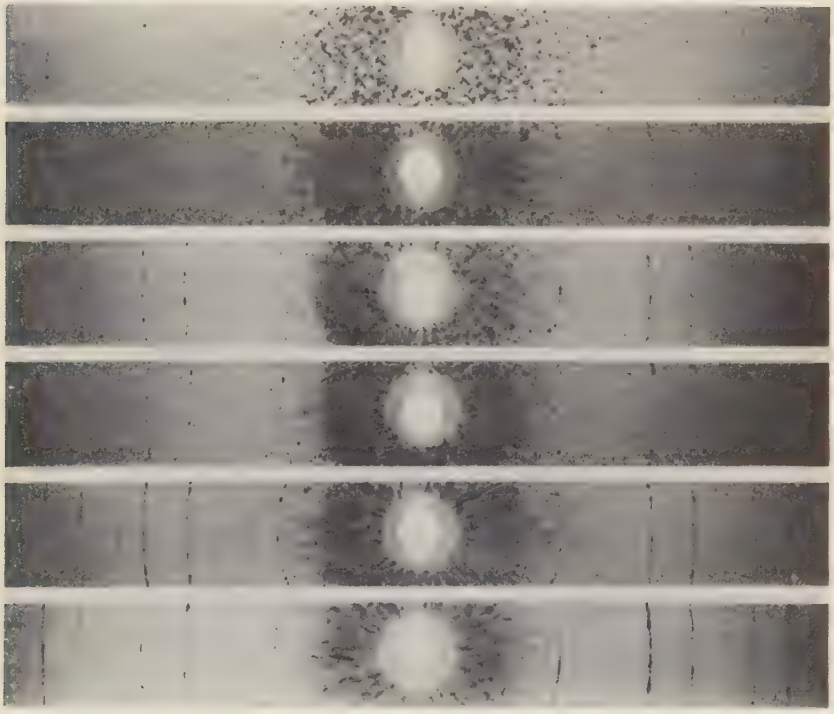

FIG. 6. Series of x-ray powder photographs of fluorite samples annealed at 1500°, 1600°, 1700°, 1800°, 1900°, and 2000° F. (from bottom to top).

Effect of Intensity of Plastic Deformation.—The above discussion suggests that the critical temperature might be varied with the severity of plastic deformation because the barrier energy is a function of the crystal structure energy. The latter should be lower for severely deformed structure.

That this is indeed the case is evident from Fig. 7, which graphically shows the results of a series of experiments designed to investigate the change of the strain relief point with intensity of deformation. It will be observed that the higher the pressure of deformation (and therefore the

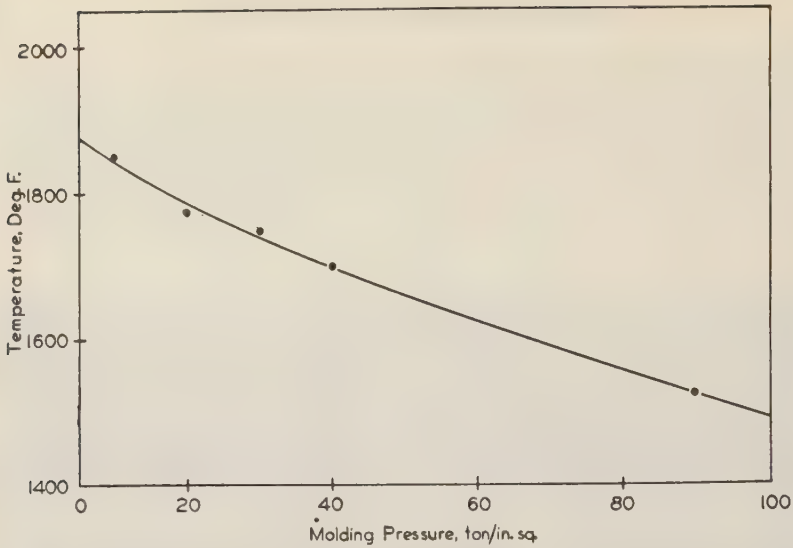

FIG. 7. The reduction of the critical temperature with the intensity of plastic deformation for fluorite.

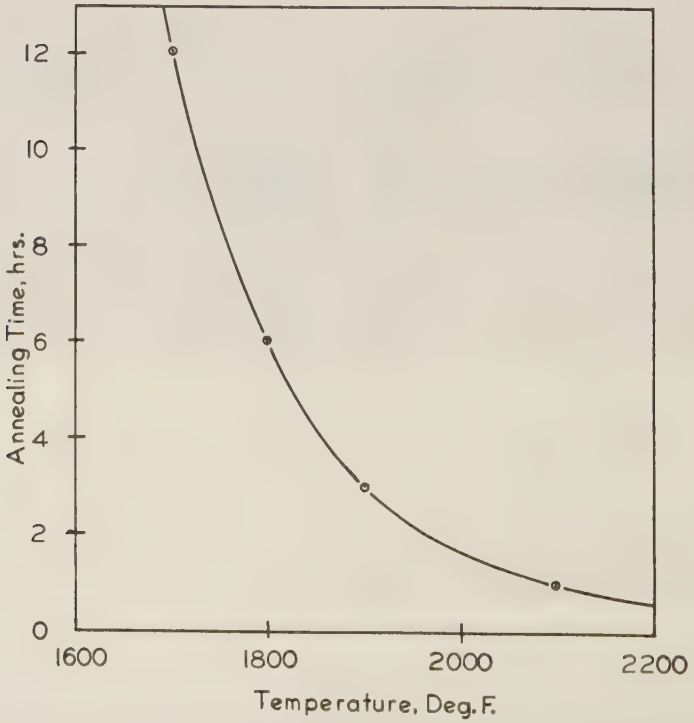

FIG. 8. The time necessary to relieve all traces of strain caused by plastic deformation. (Fluorite powder pressed at 40 tons per square inch.)

more severe the plastic deformation), the lower the critical temperature.

Time Necessary to Relieve Strain.—It is interesting to inquire into the time of annealing necessary to remove all traces of strain from the deformed specimen. This can be judged by the vanishing of the last traces of asterism of the Laue spots on the powder photograph of the specimen. Data obtained from fluorite powder pressed at 40 tons per square inch is plotted in Fig. 8. It will be noted that the curve of time of complete relief of stress trends more or less asymptotically toward about 1650° F. This is consistent to the finding that approximately 1700° F. is the critical temperature for this pressure.

Periclase

Periclase is another isometric mineral which is known to be plastic.[4] Since it is harder than fluorite it was expected that it would be more

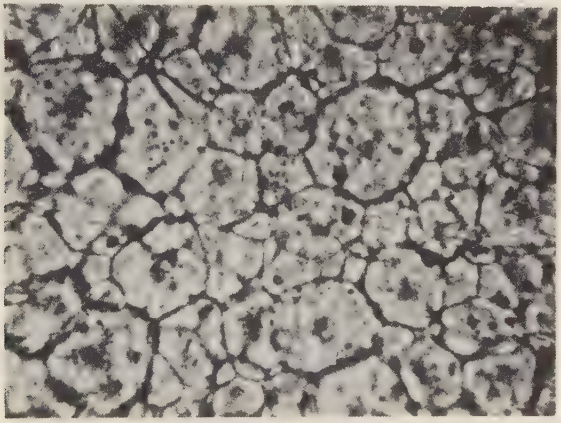

Fig. 9. Thin section of recrystallized periclase (×260). The plastic deformation was furnished by pressing powder at 40 tons per square inch; the recrystallization occurred on annealing for 6 hours at 1500° C.

difficult to deform than fluorite and this proved to be the case. It was not found possible to obtain a large supply of natural periclase so artificial material made by the Norton Company in Worcester, Massachusetts, was used. The material used was a powder which passed 170 mesh.

The experimentation on periclase was not so extensive as that on fluorite, but followed the same general lines. It will suffice here to state that the critical temperature was determined to lie in the neighborhood of 2200° F. for deformations resulting from pressures of 40 tons per square inch. Figure 9 is a photograph of a thin section of recrystallized MgO.

Other Materials and Experimental Variations

In addition to the minerals anhydrite, fluorite, and periclase, above discussed, we have also successfully recrystallized corundum, BeO, and certain other materials. Corundum, though very hard, was known to be plastic.[4] Because of the abrasive quality of such hard material, tungsten carbide dies are used.

We have also performed the plastic deformation part of the metamorphic scheme at temperatures up to 500° C. using nitrided dies. The resistance to deformation falls off very quickly with increasing temperature. Furthermore we have performed the recrystallization part of metamorphism with the aid of solvent fluids at greatly reduced temperatures. In later contributions we plan to give further information on the experimental results.

Conclusions

The following general conclusions can be drawn from the experimental work on artificial metamorphism:

(1) A mineral will not recrystallize in the absence of solvents unless it is heated to at least a critical temperature.

(2) For the same initial conditions, this critical temperature varies with the mineral, and is characteristic of it.

(3) The critical temperature of recrystallization decreases for increasing initial deformation.

(4) Time does not affect the critical temperature of recrystallization within the limits studied.

(5) Time does affect the extent of crystal growth, the crystal dimensions increasing with time provided that the critical temperature is exceeded.

(6) Provided that the critical temperature is exceeded, rapidity of crystal growth increases with temperature, other factors being equal.

THE STRUCTURE OF EPIDOTE ($HCa_2(Al, Fe)Al_2Si_3O_{13}$)

T. Ito, *The Mineralogical Institute, Imperial University of Tokyo.*

Material

The crystals used in the present investigation came from the Prince of Wales Island, Alaska, and were given to the present writer by Dr. Edward P. Henderson of the U. S. National Museum in 1938. They are dark green crystals, ranging up to several cm. in length, out of which for the x-ray experiments comparatively small specimens were chosen. According to a chemical analysis made in this laboratory this epidote contains 15.53% of Fe_2O_3 and may be roughly expressed by the formula $HCa_2FeAl_2Si_3O_{13}$.

Unit Cell and Space Group

The unit cell and space group of epidote were already determined by H. Strunz. The results of our experiments in which Weissenberg-Buerger photographs were taken, confirm his results. The unit cell was found to be $a=8.96$Å, $b=5.63$Å, $c=10.20$Å, $\beta=115°\ 24'$, giving the axial ratio: $a:b:c=1.591:1:1.812$, in agreement with that given by N. von Koksharov. There are two molecules of $HCa_2(Al, Fe)Al_2Si_3O_{13}$ in the cell. The only possible space group for epidote is $C_{2h}^2-P2_1/m$, the reflections $(0k0)$ being absent when k is odd.

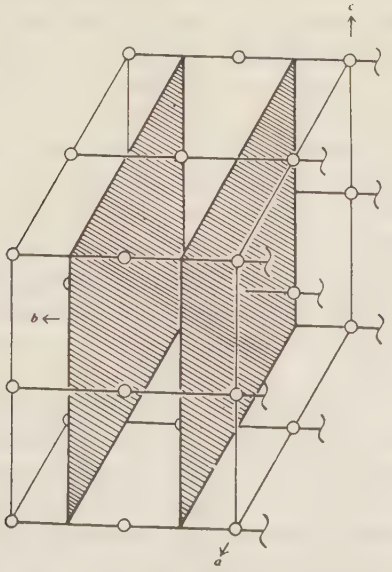

Fig. 1. Symmetry elements of the space group $C_{2h}^2-P2_1/m$. Small circles represent centers of symmetry. Shaded planes represent reflection planes. Orientation set up as in epidote.

Figure 1 shows the essential symmetry elements of the space group. There is one set of four digonal screw-axes and four sets of two symmetry centers. An atom in the general position has four equivalent positions, the intensity of reflection (hkl) being proportional to the square of $F=\Sigma 4f \cos 2\pi\,(hx+k/4+lz) \cos 2\pi\,(ky-k/4)$, where f is the atomic scattering factor appropriate to each atom.

We have to determine altogether thirty nine parameters, if no atom (except those required by the space group) lie on the reflection planes or on the centers of symmetry.

Determination of the Position of the Atoms

In determining the parameters of atoms, the present writer first took into consideration the intensity of reflection measured by means of an ionization spectrometer, using Mo K_α radiation and rock salt as standard (Tables 1 and 4).

The intensity of reflection $(0k0)$ is very strong when $k/2=2n$, while it is not strong when $k/2=2n+1$. (Compare the reflections (040), (080), (0120) with the reflections (020), (060), (0100).) This suggests at once that the y-parameters of the atoms should be ones of 0, 0.25, 0.50 and 0.75 and no other values.

This can also be deduced from the geometry of the lattice and the ionic size of atoms. The b-length of the unit cell is just twice the ionic diameter of oxygen atoms. Since in the assigned space group $(010)\frac{1}{4}$ and $(010)\frac{3}{4}$ are reflection planes, oxygen atoms either lie on these reflection planes, i.e. $y=0.25$, 0.75, or just touch them, i.e., $y=0$, 0.50. As for the other atoms, they must be placed, as usual, in the centers of polyhedra formed of oxygen atoms. On the other hand, the tetrahedra of oxygen atoms around silicon atoms must also be in a position symmetrical to the reflection planes (as projected on (100) or (001), they must appear as regular or bilateral triangles), the vertices of which lie on the reflection planes or in the middle between them. It is, therefore, scarcely possible to place the silicon and other metallic atoms, which should lie in the centres of oxygen polyhedra, in positions other than $y=0$, 0.25, 0.50, 0.75.

In epidote, as in other silicates, it is reasonable to assume that the coordination of oxygen around Ca (and Fe) is eight or six, around Al six or four, while around Si is four. There are several ways to accommodate the necessary number of such ionic polyhdera in the unit cell of epidote, bearing fully in mind the restriction imposed by the space group and dimensions of the cell. The intensity of $(h0l)$ spectra may profitably be taken into consideration at this stage of analysis. The intensity of reflections $(40\bar{6})$ and $(60\bar{4})$, for example, is so strong that we can safely

regard all the atoms contributing waves in the same phase. Although, according as we take the signs of $(40\bar{6})$ and $(60\bar{4})$ reflections the same or opposite, the permissible domains of atoms are different. This helped to discard some geometrically possible atomic arrangements.

A Patterson-Harker synthesis, further, was of assistance to decide between still remaining plausible atomic arrangements. Since the y-parameters of the atoms in epidote are, as above deduced, ones of 0.00, 0.25, 0.50, 0.75 the synthesis is extremely simple.

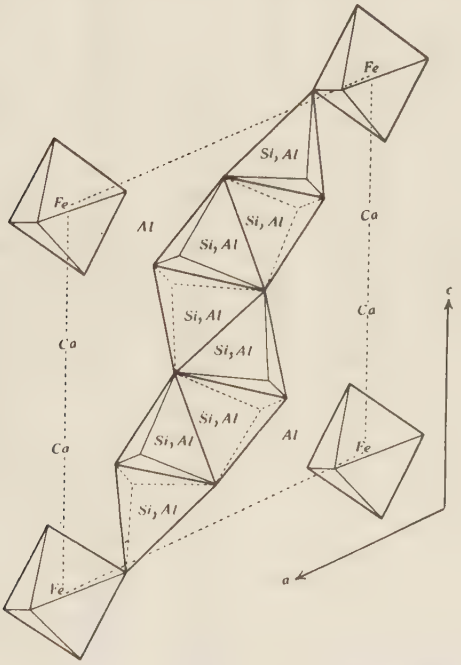

FIG. 2. The ideal structural scheme for epidote, diagrammatically shown as linked polyhedra of O and OH around metals. Projection on (010).

The structural scheme finally adopted for epidote is shown diagrammatically in Fig. 2, which is a projection on (010) of ionic polyhedra linked to each other by oxygen atoms and OH groups. Fourier synthesis was then carried out, using the F-values experimentally determined (Tables 1 and 4). The signs of the F-values are fixed provisionally by the approximate positions of atoms. We repeated this procedure several times, making necessary adjustment of the positions of atoms, assigning a renewed set of signs to the experimental F-values and improving step by step the parametral values of atoms.

TABLE 1. INTENSITY OF REFLECTIONS ($h0l$), WITH THE FINAL SET OF SIGNS AS USED IN FOURIER ANALYSIS. MEASUREMENT WITH IONIZATION SPECTROMETER (Mo K_α, $\lambda = 0.707$Å)

Indices	$\sin\theta$	$\rho' \times 10^6$	F′	Sign	Indices	$\sin\theta$	$\rho' \times 10^6$	F′	Sign
101	.0704	25.50	45.2	+	601	.2854	0.86	24.2	+
102	.1042	55.00	82.2	+	602	.3089	2.52	35.8	−
103	.1401	3.90	28.2	+	603	.3350	4.36	48.9	+
104	.1785	14.00	57.6	+	604	.3621	2.08	36.0	+
105	.2160	8.30	40.0	+	605	.3909	0.76	22.3	−
106	.2550	3.91	37.0	+					
107	.2920	6.50	56.5	−	701	.3275	3.73	45.2	+
108	.3305	4.65	53.4	+	702	.3501	1.68	35.4	−
109	.3690	2.26	38.4	−	703	.3759	5.03	56.0	+
1.0.10	.4077	1.84	37.3	+					
					$10\bar{1}$	.0437	17.30	28.6	+
201	.1110	7.40	33.1	+	$10\bar{2}$	.0690	67.10	73.1	+
202	.1408	44.80	95.6	+	$10\bar{3}$	.1050	5.20	25.2	+
203	.1745	20.30	74.6	+	$10\bar{4}$	.1400	14.30	55.0	+
204	.2090	9.60	52.4	−	$10\bar{5}$	.1775	10.80	44.1	+
205	.2455	1.92	27.5	−	$10\bar{6}$	.2140	44.50	116.2	+
206	.2802	3.10	40.0	+	$10\bar{7}$	.2530	6.75	44.3	−
207	.3180	5.72	55.1	−	$10\bar{8}$	.2910	1.25	24.1	+
208	.3570	1.60	30.9	+	$10\bar{9}$	.3290	2.15	33.8	−
					$1.0.\bar{1}0$	.3675	4.80	55.9	−
301	.1540	0.85	16.0	+					
302	.1800	4.45	33.2	+	$20\bar{1}$	.0789	1.70	14.2	−
303	.2112	6.15	42.9	+	$20\bar{2}$	.0874	15.50	38.3	+
304	.2445	11.50	64.9	+	$20\bar{3}$	.1101	9.20	38.2	+
305	.2785	14.60	83.2	+	$20\bar{4}$	.1392	4.20	24.2	−
306	.3135	2.06	33.2	+	$20\bar{5}$	.1723	11.70	56.5	+
307	.3500	0.88	22.8	−	$20\bar{6}$	.2100	6.20	40.1	+
					$20\bar{7}$	.2435	3.92	20.0	−
401	.1901	3.90	32.8	+	$20\bar{8}$	.2800	9.87	68.5	+
402	.2221	3.29	31.9	−	$20\bar{9}$	.3100	8.15	65.5	−
403	.2510	7.15	51.8	+	$2.0.\bar{1}0$	.3550	7.90	68.5	+
404	.2817	10.60	71.0	+					
405	.3150	2.14	33.6	−	$30\bar{1}$	.1195	1.30	16.0	−
406	.3490	2.50	38.5	+	$30\bar{2}$	.1204	28.25	63.3	+
					$30\bar{3}$	.1311	1.86	13.9	+
501	.2415	0.86	14.2	+	$30\bar{4}$	.1521	0.80	15.2	−
502	.2651	13.70	78.4	+	$30\bar{5}$	.1780	3.70	30.8	+
503	.2925	1.90	31.9	+	$30\bar{6}$	.2088	26.80	89.5	+
504	.3210	0.49	16.4	+	$30\bar{7}$	.2420	3.65	36.5	+
505	.3521	6.45	62.1	−	$30\bar{8}$	.2760	24.00	107.0	+
506	.3850	2.90	43.9	−	$30\bar{9}$	.3150	2.60	37.3	+
					$3.0.\bar{1}0$	.3460	1.52	30.8	+

TABLE 1—(*continued*)

Indices	sin θ	$\rho' \times 10^6$	F′	Sign	Indices	sin θ	$\rho' \times 10^6$	F′	Sign
$40\bar{1}$	.1635	41.10	99.6	−	$70\bar{1}$	.2951	3.63	43.1	−
$40\bar{2}$	.1580	1.70	23.0	+	$70\bar{2}$	.2830	0.41	14.4	+
$40\bar{3}$	.1628	12.90	55.9	+	$70\bar{3}$	.2785	2.42	20.3	−
$40\bar{4}$	.1748	1.68	18.7	+	$70\bar{4}$	.2782	3.21	39.2	+
$40\bar{5}$	.1982	1.96	24.0	+	$70\bar{5}$	.2825	1.42	20.6	+
$40\bar{6}$	.2205	46.00	119.0	−	$70\bar{6}$	.2915	0.60	14.1	−
$40\bar{7}$	.2480	0.76	14.0	+	$70\bar{7}$	.3058	1.22	21.3	−
$40\bar{8}$	.2616	3.25	40.5	+	$70\bar{8}$	.3241	6.51	59.8	+
$40\bar{9}$	.3112	3.20	41.1	−	$70\bar{9}$	.3459	2.10	35.4	−
$4.0.\bar{1}0$	.3459	1.60	30.8	+	$7.0.\bar{1}0$	.3715	11.80	89.6	−
$50\bar{1}$	.2075	0.37	10.2	−	$80\bar{1}$	.3401	5.70	57.0	−
$50\bar{2}$	.1992	25.20	85.5	+	$80\bar{2}$	.3269	9.30	71.5	+
$50\bar{3}$	.1990	2.20	27.0	−	$80\bar{3}$	.3211	11.60	79.6	−
$50\bar{4}$	.2061	2.08	24.5	−	$80\bar{4}$	.3167	2.97	40.5	+
$50\bar{5}$	.2185	1.27	17.2	+	$80\bar{5}$	.3210	2.86	39.6	+
$50\bar{6}$	.2359	11.10	59.2	−	$80\bar{6}$	.3255	1.48	28.5	−
$50\bar{7}$	.2630	0.46	14.0	−	$80\bar{7}$	.3359	1.90	32.9	+
$50\bar{8}$	.2891	0.15	10.1	−	$80\bar{8}$	.3495	1.12	22.0	−
$50\bar{9}$	.3182	0.25	11.7	−	$80\bar{9}$	.3691	0.81	22.4	−
$5.0.\bar{1}0$	.3486	3.47	47.0	+	$8.0.\bar{1}0$	.3863	0.33	14.8	+
$60\bar{1}$	.2509	3.51	36.4	+					
$60\bar{2}$	.2391	3.63	33.2	+					
$60\bar{3}$	.2368	11.00	62.5	−					
$60\bar{4}$	.2409	53.60	127.0	+					
$60\bar{5}$	.2490	5.92	47.0	+					
$60\bar{6}$	.2622	1.22	19.1	−					
$60\bar{7}$	.2810	1.04	23.3	+					
$60\bar{8}$	.3042	1.01	22.6	+					
$60\bar{9}$	.3298	2.70	38.4	−					
$6.0.\bar{1}0$	.3580	0.30	13.8	+					

FIG. 3. The two-dimensional Fourier representation of the electron density of epidote projected on (010). An $AlSi_3O_9$ group (cf. below) can be traced in the projection (dotted straight lines).

TABLE 2. COORDINATES OF ATOMS IN DECIMAL FRACTIONS OF THE AXIAL LENGTH: THE ORIGIN IS PLACED AT A CENTER OF SYMMETRY

Kind of Atom	Number in the Cell	x/a	y/b	z/c
O_I	4	.042	.000	.843
O_{II}	4	.301	.000	.742
O_{III}	4	.783	.000	.694
O_{IV}	2	.535	.250	.821
O_V	2	.535	.750	.821
O_{VI}	2	.420	.250	.582
O_{VII}	2	.420	.750	.582
O_{VIII}	2	.000	.000	.500
O_{IX}	2	.179	.750	.033
OH	2	.179	.250	.033
$(Si, Al)_I$	2	.394	.250	.711
$(Si, Al)_{II}$	2	.604	.750	.695
$(Si, Al)_{III}$	2	.582	.250	.553
$(Si, Al)_{IV}$	2	.375	.750	.940
Al	2	.789	.250	.814
Al, Fe	2	.000	.000	.000
Ca_I	2	.963	.250	.641
Ca_{II}	2	.963	.750	.641

The final result of analysis is graphically represented in Fig. 3. The positions of atoms obtained are given in Table 2 and the interatomic distances calculated in Table 3. The values give a fair agreement between the theoretical and experimental F-values as shown in Table 4.

TABLE 3. INTERATOMIC DISTANCES IN EPIDOTE

Atom	Neighbour	Distance in A	Atom	Neighbour	Distance in A
O_I	O_{II}	3.5	$(Si, Al)_{III}$	O_{III}	2.3
	OH	2.8		O_{III}'	2.3
	O_{VIII}	3.2		O_{VII}	2.4
				O_{VI}'	1.4
O_{II}	O_{IV}	2.5			
	O_{VI}	2.4	$(Si, Al)_{IV}$	O_{II}	2.3
	OH	3.7		O_{II}'	2.3
				O_V	2.3
O_{III}	O_{IV}	3.2		O_{IX}	2.3
	O_{VI}	3.2			
	O_{VI}'	2.7	Al	O_I	2.7
				O_I'	2.7
O_{IV}	O_{VI}	2.5		O_{IV}	2.6
	O_{IX}	2.4		O_{IX}'	1.5
	OH	4.3		O_{II}'	2.0*
				O_{II}'	2.0*
$(Si, Al)_I$	O_{II}	1.8			
	O_{II}'	1.8	(Al, Fe)	(O_I, O_I')	1.7
	O_{IV}	1.4		O_{IX}, O_{IX}'	2.2
	O_{VI}	1.5		(OH), (OH)′	2.2
$(Si, Al)_{II}$	O_{III}	2.1	Ca	O_I, O_I'	2.3
	O_{III}'	2.1		O_{II}, O_{II}'	3.2
	O_V	1.4		O_{III}, O_{III}'	2.6
	O_{VII}	1.8		O_{VIII}, O_{VIII}'	2.5

* With no valency residue.
Prime denotes atoms in the adjoining cell.

STRUCTURAL DETAILS

The positions of atoms in the structure of epidote are shown in Fig. 4, which is a projection of the unit cell on (010). Figure 5 visualizes the structural scheme with a frame-work of linked polyhedra of oxygen atoms and the OH groups around metal atoms. We see here that some of the polyhedra are more or less deformed in contrast to those in Fig. 2, from which we started the Fourier analysis.

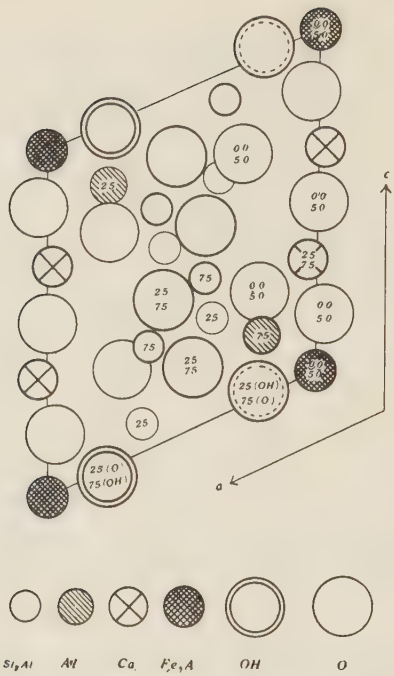

FIG. 4. The structure of epidote projected on (010). Numbers give in decimal fractions of the *b*-axis the height of atoms in the unit cell.

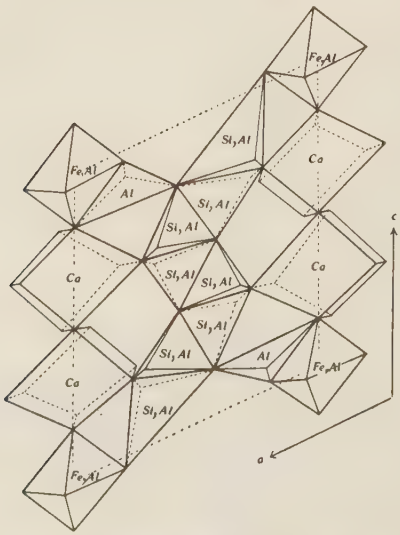

FIG. 5. The structure of epidote shown as linked polyhedra of O and OH around (Si, Al), Al, (Al, Fe) and Ca. Projection on (010). Some of the corners of polyhedra are somewhat displaced from their true positions in order to make their shape show.

TABLE 4. INTENSITY OF REFLECTIONS

(1) Measurements with ionization spectrometer
(Mo K_α radiation 0.707Å)

Indices	Sin θ	$\rho' \times 10^6$	F obs.	F calc.	Indices	Sin θ	$\rho' \times 10^6$	F obs.	F calc.
100	.0438	22.10	32.2	+ 48.1	101	.0704	25.50	45.2	+ 44.1
200	.0876	82.80	88.6	+114.2	202	.1408	44.80	95.6	+124.5
300	.1314	55.00	84.6	+109.2	303	.2112	6.15	32.9	+ 23.2
400	.1752	27.50	75.6	+ 52.4					
500	.2190	4.46	31.8	+ 19.3	$10\bar{1}$	.0437	17.30	28.6	+ 41.0
600	.2628	6.50	40.5	− 39.5	$20\bar{2}$	.0874	15.50	38.3	+ 37.4
700	.3066	1.35	22.4	− 3.0	$30\bar{3}$	.1311	5.86	23.9	+ 40.8
800	.3504	1.24	23.2	− 33.4	$40\bar{4}$	.1748	1.68	18.7	+ 26.0
900	.3942	1.24	25.4	− 15.8					
10.0.0	.4380	4.50	51.0	− 43.7	201	.1110	7.10	33.0	− 28.0
11.0.0	.4818	0.93	25.4	− 15.6	402	.2221	3.29	31.9	+ 50.5
					$20\bar{1}$	.0789	16.40	37.1	+ 54.5
020	.1257	138.70	130.0	−116.3	$40\bar{2}$	.1580	1.80	23.0	− 42.0
040	.2514	117.60	181.8	+213.6	$60\bar{3}$	.2368	11.00	62.5	− 57.7
060	.3771	18.40	93.1	− 61.8					
080	.5028	16.96	112.2	+ 98.0	203	.1745	20.30	74.6	+ 90.6
0.10.0	.6285	2.00	43.6	− 30.4					
0.12.0	.7542	3.76	62.5	+ 64.4	$20\bar{3}$	.1101	9.20	38.2	+ 50.0
					$40\bar{6}$	.2203	46.00	119.5	+ 81.8
001	.0385	1.16	6.4	+ 20.0					
002	.0770	4.62	17.9	+ 30.1	301	.1540	1.20	16.6	− 7.8
003	.1155	8.49	30.5	+ 60.3	602	.3080	2.52	35.8	+ 48.3
004	.1540	1.98	18.5	− 19.8					
005	.1925	2.22	21.5	+ 30.2	$30\bar{1}$	.1185	5.00	16.0	+ 23.1
006	.2310	4.92	35.0	+ 45.5	$60\bar{2}$	.2370	3.63	33.2	− 34.5
007	.2695	2.63	28.0	− 18.1					
008	.3080	1.45	22.8	+ 10.9	302	.1800	4.45	33.0	+ 56.6
009	.3465	1.02	20.6	− 28.3					
0.0.10	.3850	0.85	20.0	− 30.5	$30\bar{2}$	.1204	14.10	43.6	− 34.9
0.0.11	.4235	5.15	54.6	+ 43.0	$60\bar{4}$	.2409	53.60	127.0	+ 90.3

TABLE 4—(*continued*)

(2) Intensity estimated in the Weissenberg photographs
(Co K_α $\lambda = 1.79$Å)

Indices	Sin θ	Intensity	F calc.	Indices	Sin θ	Intensity	F calc.
110	.1936	—	+ 7.5	311	.4149	—	+11.4
210	.2760	w	+11.8	612	.7814	—	+ 2.2
310	.3680	w	+15.4				
410	.4682	w	+12.1	31$\bar{1}$	.3364	m	+33.4
				61$\bar{2}$	.6300	—	− 5.4
011	.1863	—	+ 5.1				
012	.2511	—	− 2.2	312	.4773	m	+ or −56.0
013	.3315	m	−43.5				
014	.4210	w	−32.8	31$\bar{2}$	.3424	m	+42.0
				61$\bar{4}$	.6285	w	− 8.9
111	.2362	—	+ 2.0				
212	.3859	w	−31.2	121	.3633	w	+28.0
313	.6774	w	−10.3	222	.4734	w	+33.1
				323	.6148	—	− 4.9
11$\bar{1}$	.1939	w	+36.6				
21$\bar{2}$	.2766	w	+37.4	12$\bar{1}$	.3362	—	−13.0
31$\bar{3}$	.3701	m	+43.4	222	.3880	s	+59.9
41$\bar{4}$	.4755	w	−24.0	32$\bar{3}$	.4613	w	+ 4.9
				42$\bar{4}$	.5498	s	+67.1
211	.3195	w	+ 5.6				
412	.5760	w	−26.2	221	.4212	m	+45.7
				422	.6310	w	+12.5
21$\bar{1}$	.2555	w	−31.0				
41$\bar{2}$	.4298	w	−10.0	42$\bar{2}$	.5188	m	+48.3
61$\bar{3}$	.6202	w	− 8.0	62$\bar{3}$	.6780	m	+15.4
213	.4808	—	+ 5.5	223	.5392	w	−37.4
21$\bar{3}$	.3718	w	+31.5	22$\bar{3}$	.4242	s	−121.2
41$\bar{6}$	.5850	w	+15.5	42$\bar{6}$	.6421	m	−19.8

The structure in its main feature is composed of complex chains of linked Si tetrahedra stretched in the direction of the b-axis. The SiO_3-chains, which can be traced in the structure, are,though in linkage similar to, in form different from those found in pyroxenes. While in pyroxenes one tetrahedron of the chain is so related to the next as if rotated ca. 109° about the chain direction (Fig. 6), in epidote this angle amounts to only ca. 71° (Fig. 7). In both minerals the chains consist of two layers of

oxygen atoms. Whereas in pyroxenes two thirds of oxygen atoms of the chain lie on one layer and the remaining one third on the other, in epidote oxygen atoms are equally distributed between the two layers of the chain. In epidote four of the latter SiO_3-chains are bound with one another, holding bordering oxygen atoms in common, and build up a composite chain or band having the composition Si_4O_9, thus

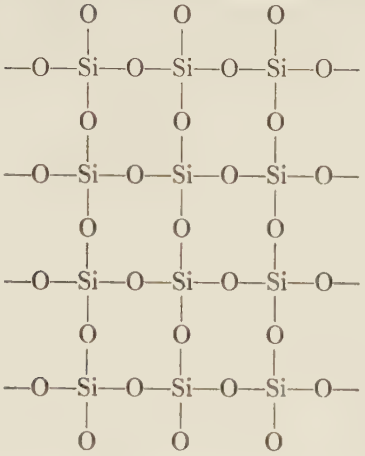

In the actual structure of epidote one of four silicon atoms of the group Si_4O_9 is statistically replaced by the Al atom.

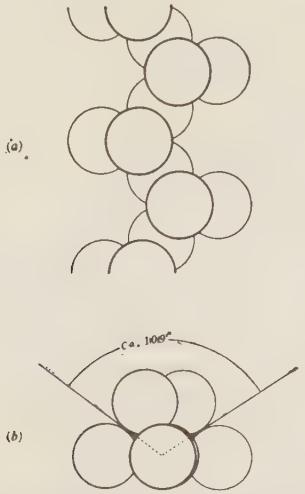

FIG. 6. The SiO_3 chain in pyroxenes. The Si atoms are omitted (*a*) plan; (*b*) viewed end on.

The composite chains or band of this type are bound together laterally by the Ca, Al(Fe) and Al atoms. The Ca atoms occupy the centers of distorted cubes formed of oxygen atoms of the chains and ones outside the chains. The Al(Fe) atoms, lying on the centers of inversion, occupy the centers of more or less regular octahedra formed of oxygen atoms and OH groups. The remaining Al atoms which cannot be replaced either by Fe or by Si atoms, occupy the centers of oxygen tetrahedra

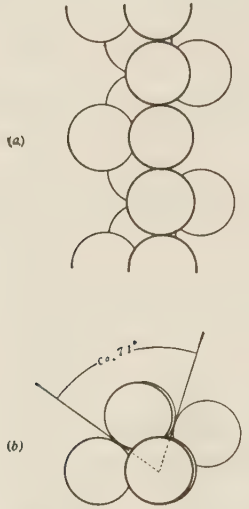

FIG. 7. The SiO_3 chain which can be traced in epidote. The Si atoms are omitted (*a*) plan; (*b*) viewed end on.

(counting only surrounding oxygen atoms with residual bonds), which share an edge with the Al(Fe) octahedra and a corner with the Si(Al) tetrahedra and another with the Ca cube.

In the structure thus formed the oxygen atoms are between two Si(Al) atoms, or one Si(Al), one Al and two Al(Fe) atoms, or two Ca and two Si(Al) atoms, or two Ca, one Al and one Al(Fe) atoms, while the OH groups are always between two Al(Fe) atoms.

The structural aspect of epidote can be represented by the formula $Ca_2O \cdot (Al, Fe)O_2OH \cdot Al \cdot AlSi_3O_9$ or, in the extreme case as in epidote used in the present investigation, since Fe replaces Al to the fullest degree, by the formula $Ca_2O \cdot FeO_2OH \cdot Al \cdot AlSi_3O_9$.

Cleavages of epidote, being perfect after (001) and less so after (100), are parallel to the direction of the chains.

Twinning of Epidote; the Structural Relation of Epidote to Zoisite

The twinning of epidote takes place on (100). If we consider in the structure a reflection across $(100)_0$ with a glide $b/2$, the occurrence of the twin may easily be accounted for. The relative positions as well as coordination of atoms, then, in the simple and twinned structures are almost exactly the same. The only difference between them is that while in the former the shared edges of the Al(Fe) octahedron with neighbour-

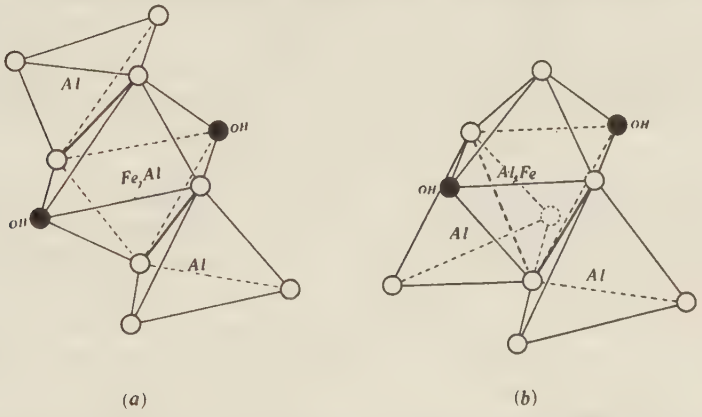

Fig. 8. Polyhedral arrangement of oxygen atoms and OH groups around Al(Fe) in epidote (*a*) and in twinned epidote (or zoisite) (*b*). Open circles represent oxygen atoms.

ing Al tetrahedra are *parallel* (Fig. 8*a*), in the latter they are *inclined*, meeting in a vertex (Fig. 8*b*). The Al(Fe) octahedra, further, are more symmetrical in shape in the twinned position.

Zoisite may be regarded as intimately twinned epidote (or rather clinozoisite) as pointed out by several investigators. Zoisite is almost always poor in iron. The substitution of Al by Fe therefore seems to render the occurrence of twinning more haphazard and less regular. This may be due to the difference of ionic radii of the Al and Fe atoms. The (Al, Fe) octahedra are namely, though more symmetrical, less spacious in the structure in the twinned position than in the normal position to accommodate the larger Fe atoms.

THE SPECTROSCOPE IN DETERMINATIVE MINERALOGY[1]

MAURICE J. PETERSON,[2] ALBERT J. KAUFFMAN, JR.[3]
AND HOWARD W. JAFFE[4]

ABSTRACT

The applications of the spectroscope in determinative mineralogy are discussed. It can be used advantageously as a replacement for chemical and blowpipe tests in the identification of most metallic elements. By means of a direct-current arc the mineral sample is volatilized from a graphite electrode and the metallic constituents are determined objectively by visual observation of their spectral lines. Small amounts of either valuable or undesirable metal constituents in certain minerals may be detected. Elements normally difficult to differentiate chemically often are identified easily. The method is limited to the visible region of the spectrum and does not serve to detect most anionic constituents. A laboratory set-up of the instrument, its calibration and its operation are described.

INTRODUCTION

Minerals are identified on the basis of their chemical and physical properties. Fundamentally, an identification depends upon the determination of a sufficient number of properties to differentiate the mineral from all others through a process of elimination. The constants obtained through the use of the microscope often are sufficient to identify the mineral, but recourse frequently must be made to the determination of its chemical composition and x-ray diffraction pattern.

Qualitative chemical tests either by use of the blowpipe or wet methods may be inconclusive unless the unknown is carried through an entire qualitative scheme of analysis. In the latter case the procedure is time-consuming.

As a rapid and satisfactory approach to the problem of the determination of metallic ions in minerals, the Bureau of Mines laboratory, Metallurgical Branch, at College Park, Maryland, for the past ten years has been using the spectroscope and spectrograph as routine analytical tools.

Lee and Wright (6) have discussed the usefulness of the spectrograph in mineral analysis, and numerous other papers have been published on the spectrographic determination of elements present in various minerals. The use of the *spectroscope* as a routine tool in determinative mineralogy apparently has not been emphasized.

[1] Published by permission of the Director, Bureau of Mines, U. S. Department of the Interior.

[2] Spectrographer, Bureau of Mines, College Park Division, Metallurgical Branch, College Park, Maryland.

[3] Chemist-Petrographer, Bureau of Mines, College Park Division, Metallurgical Branch, College Park, Maryland.

[4] Chemist-Petrographer, Bureau of Mines, College Park Division, Metallurgical Branch, College Park, Maryland.

As shown in Fig. 1, over half the elements yield spectra in the visible range when subjected to arc excitation. Thus most of the common and many of the rarer metallic elements occurring in any appreciable concentration in minerals can be rapidly determined.

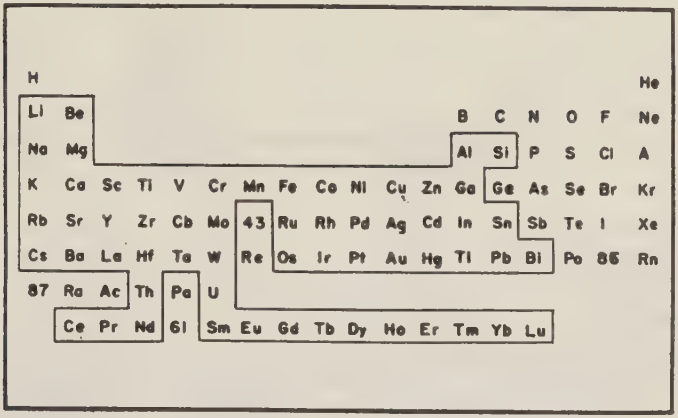

FIG. 1

A—The elements enclosed within the boundary lines yield spectral lines in the visible region.

B—Fluorine may be detected by adding calcium to the sample (if it does not already contain that element) and observing the CaF_2 band (8).

C—Boron may be detected by the green color appearing on the test screen due to the BO molecule (10).

THE SPECTROSCOPE AND ACCESSORIES

The set-up of the apparatus used in this laboratory is shown in Fig. 2. The light source (A) consists of a direct-current arc produced between two graphite electrodes. Power at 220 volts is supplied by a motor-generator set. On the wiring diagram for the arc, shown in Fig. 3, (R) is a variable rheostat used to control the power input to the arc and is capable of dissipating approximately 2500 watts. A carbon compression type of rheostat is recommended, since it will give stepless control of the current within the working range of 3 to 15 amperes. The ammeter (A) has a total range of 25 amperes with subdivisions of $\frac{1}{2}$ ampere. The gap (G) between the graphite electrodes is 3 mm.

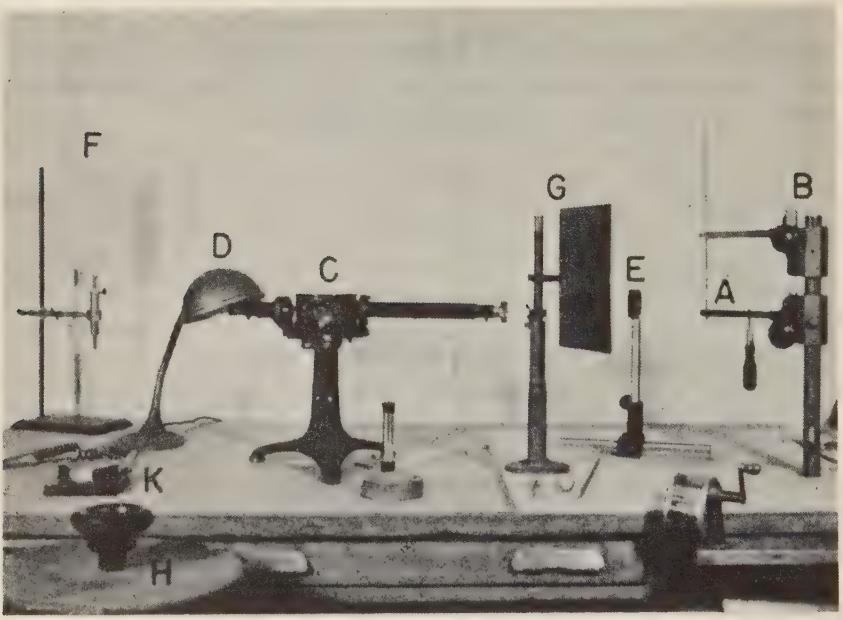

FIG. 2. Arrangement of the apparatus.

A. Arc
B. Arc stand
C. Spectroscope
D. Light for illuminating the scale
E. Double convex lens
F. Electrode positioning screen
G. Metal shield to protect operator from direct radiation of the burning arc
H. Rheostat
K. Ammeter

The arc stand (B in Fig. 2) consists of an upright bakelite post with two steel spring clip arms attached in a horizontal position. These hold the graphite electrodes. Each electrode clamp is connected to a rack and pinion assembly mounted on the bakelite post and actuated by insulated knobs so that the electrodes can be spaced vertically by mechanical

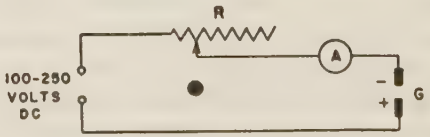

FIG. 3

manipulation while the arc is burning. A permanently mounted clip spreader is used to spread the clip arms when the lower electrode is being changed. This tool is made from a screw driver by cutting off the steel portion approximately 2 inches above the handle. Two flat parallel surfaces are machined on the metal to allow the spreader to fit between the clips of the electrode clamp. Arc stands of various designs are offered for sale by manufacturers of spectrographic equipment.

The graphite electrodes used in this laboratory are 3/16″ diameter for the lower and 1/8″ or 3/16″ diameter for the upper. The lower electrode is cut to a length of $1\frac{1}{2}$″, and one end is drilled approximately 7 mm. deep to provide a conical cavity for holding the sample. The upper electrode is pointed by means of the pencil sharpener. "Ordinary-grade" spectroscopic carbons are suitable for most mineral identification work, although traces of several elements present as impurities may be detected in them with the spectroscope.

The spectroscope* (C) shown is a conventional three-arm Bunsen type constructed with a dispersing system consisting of two 60° flint-glass prisms. The telescope arm can be swung through an arc to enable the observer to view any portion of the visible spectrum. By means of a hair line in the eyepiece the exact position of the spectral lines are determined relative to the illuminated scale which is imaged directly above the spectrum. A shielded incandescent light (D) is used to illuminate the scale.

A double convex lens (E) of approximately 5 inches focal length is used to project an image of the light source upon an electrode positioning screen (F) located about 4 feet from the electrodes. The screen is marked to outline the exact position of the electrode image when the center of the arc and the slit are at the same vertical height. The correct vertical height and electrode gap are maintained during arcing by manipulation of the insulated knobs of the arc stand so that the electrode image is kept within the marked boundaries on the screen.

A small hood, not shown in Fig. 2, is mounted above the arc stand to carry away the gases produced by the burning arc.

The cost of the instrument and accessories is not prohibitive. A satisfactory assembly costs no more than a fully equipped petrographic microscope.

Technically trained persons can easily acquire proficiency in the use of the spectroscope in a short time.

* The spectroscope described above is one of several types available on the market. The reader is referred to the general textbooks listed in the bibliography for specific designs and details on the optics of the instruments (1) (2) (3) (11).

Operation

The general procedure for an unknown sample is as follows: (1) Place the powdered sample or fragment into the cavity of a previously prepared 3/16″ diameter graphite electrode; (2) fit the electrode into the lower electrode clamp; (3) insert a 1/8″ or 3/16″ diameter graphite rod which has been pointed by means of the pencil sharpener into the upper electrode clamp. The upper electrode clips may be spread apart with a short screw driver or other similar tool; (4) the vertical height of the arc is adjusted to be the same as the spectroscope slit, leaving a gap of 3 to 5mm. between the electrodes; after the master switch is thrown, an arc is struck by making momentary contact between the electrodes with a graphite rod provided with an insulated handle (when striking the arc the free hand of the operator should be kept away from contact with any metallic surface as a safety precaution against possible electrical shock); (6) the current is adjusted to the desired value by means of the rheostat. The current used will depend to a large extent upon the composition of the particular sample. Materials with a high iron content, for example, must be arced at 3 to 5 amperes to prevent loss of the sample due to sputtering. If small amounts of easily volatilized elements are being sought it is best to operate at low current in order that the sample will be consumed less rapidly. Since many mineral samples contain both low-boiling and high-boiling constituents, the arc is usually started at about 3 amperes, operated at 3 to 5 amperes for the first two minutes, then increased to 12 amperes in order to volatilize the more refractory elements. The more volatile elements include the alkalis, Cd, Zn, Bi, Pb, and Tl. Intermediate and more persistent are Au, Ag, Sn, Mn, Ca, Cu, Fe, Ni, V, Cr, Si, Ti and Ba. The most refractory are the rare earths, the platinum group, Al, Be, Mo, Zr, Cb, Ta, W, Th and U. There is, however, in some cases an overlapping between the groups. The individual members of each group are not necessarily arranged according to their volatility. When the more volatile constituents are suspected of being present, the usual procedure is to set the telescope in a position to observe the lines of the particular element in question before striking the arc.

Radiation from an arc source composed of all wave lengths of light in the visible spectral range produces a continuous spectrum. The emission from individual elements volatilizing in the arc produces line spectra which appear as colored images of the slit. With the set-up shown in Fig. 2, the lines are superimposed upon the continuous spectrum background, since no provision is made to prevent the light from the glowing elec-

trodes from entering the slit of the spectroscope. Band spectra resulting from molecular excitation, also may appear superimposed upon the continuous background. The bands consist of a large number of lines lying close together with a crowding toward a limiting line or head. Oftentimes the band heads only are observed, since the remaining portion may be too weak to be detected visually.

Metals in concentrations as low as 0.5 to 1.0 per cent can be readily identified in most cases. With further decreases in concentration, the spectral lines become correspondingly less persistent and may result in a flash or fugitive spectrum not easily detected. However, in a few cases, such as Na and Li, owing to their extremely sensitive lines, concentrations down to at least 0.001 per cent may be detected.

Calibration

The visible portion of the spectrum lies approximately between 3900 and 7800 angstroms. It can be arbitrarily divided into the following groups:

Red	7800–6470 angstroms
Orange	6470–5850 angstroms
Yellow	5850–5750 angstroms
Green	5750–4912 angstroms
Blue	4912–4240 angstroms
Violet	4240–3900 angstroms

A convenient method of calibrating the instrument is to arc metals and metallic salts of high purity and record the scale readings corresponding to their strongest spectral lines. A working curve can then be constructed by plotting wave lengths in angstrom units with respect to scale readings. The parabolic curve obtained demonstrates the nonlinear dispersion of a spectroscope fitted with prisms. With the instrument used in this laboratory, two lines in the red portion of the spectrum differing in wave length by five angstroms can be differentiated only with difficulty, whereas lines appearing in the violet which differ by only two angstrom units are easily distinguished.

The scale of the instrument used in this laboratory is divided and numbered into 17 equal parts, and each part is subdivided into tenths. The D lines of Na at 5896 and 5890 angstroms correspond to 3.0 on the scale and serve as reference points for aligning the instrument. Ca, Fe, Sr, K, Rb, and Cs may be selected in preparing the curve, since they yield spectral lines in the visible range which are easily identified.

TABLE 1

Element	*Element*	*Element*
Aluminum	4572.3	5153.3
3961.5	4562.4	5105.6
3944.0	4528.5	Gold
Barium	4186.6	4792.0
5777.7	4165.6	Hafnium
5535.5	4040.8	5552.1
5519.1	4012.4	4800.5
5424.6	Cesium	4620.8
4934.1	6983.4	4336.7
4554.0	6973.3	4232.4
Beryllium	6723.3	4093.2
4572.7	6586.5	Iron
Bismuth	4603.8	5615.7
5552.2	4593.2	5586.7
4722.2	4555.5	5371.5
Cadmium	Chromium	5328.4
5085.8	5791.0	5269.5
4678.5	5409.8	5266.6
Calcium	5348.3 5345.8	5232.9
5270.3	5328.4	5227.2
5265.6	5298.3	5167.5
5264.2	5208.4	4957.6
5262.2	5206.0	4951.3
5261.7	4289.7	4919.0
5260.4	4274.8	4891.5
4878.2	4254.3	4878.2
4585.8	Cobalt	4415.1
4581.5	4867.9	4404.8
4578.6	4840.3	4383.5
4456.6	4813.5	4337.1
4455.9	4792.9	4315.1
4454.7	Columbium	4282.4
4434.9	5344.2	Lanthanum
4425.4	5276.2	6249.9
3968.5	5095.3	5930.6
3933.7	5079.0	5455.1
Calcium fluoride	4137.1	5302.0
5291.0	4123.9	5183.4
(band head)	4079.7	4921.8 4921.0
Cerium	4058.9	4899.9
5512.1	Copper	4860.9
4678.2	5220.1 5218.2	4824.1
4593.9		

TABLE 1—(*continued*)

Element	*Element*	*Element*
Lead	5805.2	5031.0
5201.0	5476.9	4670.4
Lithium	5146.5	Silicon
6707.9	5142.8	3905.5
6103.6	5099.9	Silver
4971.9	5035.4	5465.4
{4603.0	{4715.8	5209.0
{4602.0	{4714.4	Sodium
Magnesium	Platinum	5895.9
5183.6	6710.4	5889.9
5172.9	6326.6	Strontium
5167.3	5478.5	6878.4
4705.0	5475.8	4962.3
Manganese	5368.9	{4876.3
4823.5	5301.0	{4876.1
4783.4	5227.6	4872.5
4766.4	5059.5	4855.1
4762.4	4552.4	4832.1
4754.1	4520.9	4811.9
Molybdenum	4498.8	4607.4
5570.5	4442.6	4215.5
5533.0	Potassium	4077.7
5506.5	7699.0	Tantalum
4830.5	7664.9	5402.5
4819.3	6939.0	4819.5
4760.2	6911.3	4691.9
4731.5	4047.2	{4574.3
4707.3	4044.2	{4573.3
4434.9	Praseodymium	4530.8
4411.7	5381.3	{4511.5
4381.6	5322.8	{4510.9
Neodymium	5220.1	Thallium
5319.8	{5110.8	5350.5
5293.2	{5110.4	Thorium
5249.5	Rubidium	5049.8
5192.6	6298.6	5017.2
4859.0	6206.5	4919.8
4825.5	4244.4	4863.2
4811.3	4215.6	Tin
4706.5	4201.8	4524.7
4303.6	Scandium	Titanium
4177.3	5526.8	5014.3
Nickel	5239.8	5007.0
5857.8		

TABLE 1—(*continued*)

Element	*Element*	*Element*
4999.5	5492.9	4900.1
4991.1	Vanadium	4883.7
4981.7	5627.7	4854.9
Tungsten	4881.5	4674.8
5514.7	4875.5	4643.7
5224.7	4864.8	Zinc
5053.3	4851.5	4810.5
5015.3	4807.6	4722.2
5006.2	4594.1	4680.1
4843.8	4460.3	Zirconium
4680.5	Yttrium	4815.6
Uranium	5662.9	4772.3
6449.2	5205.7	4739.5
5915.4	5200.4	4710.0
5527.8	5087.4	4687.8

The K doublet at 6939 and 6911 angstroms and the Cs lines at 6983 and 6973 angstroms serve as points to calibrate the red portion of the scale. Ca produces suitable lines in the orange and yellow and Fe gives many lines in the green. A Sr line at 4216 angstroms and a Rb line at 4202 angstroms are near the violet end of the scale.

Several important lines lie beyond the limits of our scale, but within the observed spectral field. They can be detected and identified after a little practice. For example, in the red region the strongest lines of K occur at 7699 and 7665 angstroms, and in the violet a characteristic group of four lines is emitted by Ca at 3968 and 3934 angstroms, and Al at 3962 and 3944 angstroms. Several lines and groups of lines resulting solely from the burning of the electrodes are visible in the spectroscope. At 5165 angstroms is a band head resulting from the C_2 molecule. A band resulting from the CN molecule appears as a group of lines with its head at 4216 angstroms.

DETERMINATIVE TABLES

The wave lengths of the spectral lines that can be used for identification purposes are listed in Table 1. No attempt has been made to list all the lines of each element. Only those most characteristic (in the spectroscope) have been recorded.

Many of the elements commonly found in minerals have some of their

spectral lines arranged in characteristic groups. After a little practice the observer will recognize these characteristic groups and be able to identify rapidly the respective constituents.

These characteristic groups are listed in the following table.

TABLE 2

Element	*Characteristic groups*
Aluminum	A group of two lines (3961.5 and 3944.0) beyond the scale in the violet. Strong lines of Ca (3968.5 and 3933.7) form a group of four with the Al.
Calcium	A group of three lines in the green (5270.3—[5265.6–5264.2]—[5262.2–5261.7–5260.4]). Also a group of four lines in the blue (4456.6—[4455.9–4454.7]—4434.9–4425.4).
Calcium fluoride	A band head in the green (5291.0) fading toward the red.
Chromium	A group of three in the green ([5348.3–5345.8]—5328.4–5298.3).
Copper	A group of three lines in the green ([5220.1–5218.2])—5153.3–5105.6).
Iron	A group of five lines in the green (5371.5–5328.4—[5269.5–5266.6]—5232.9–5227.2).
Lithium	Two lines in the red (6707.9 and 6103.6).
Magnesium	A group of three lines in the green (5183.6–5172.9–5167.3).
Manganese	A group of five lines in the blue (4823.5–4783.4–4766.4–4762.4–4754.1).
Molybdenum	A group of three lines in the green (5570.5–5533.0–5506.5) also a group of three in the blue (4760.2–4731.5–4707.3).
Potassium	Two doublets—one off the scale in the red (7699.0 and 7664.9) and (6939.0 and 6911.3).
Sodium	The D lines in the yellow (5895.9 and 5889.9).
Titanium	A group of five lines in the green (5014.3–5007.0–4999.5–4991.1–4981.7).
Vanadium	A group of five lines in the blue (4881.5–4875.5–4864.8–4851.5–4807.6).
Zinc	A group of three lines in the blue (4810.5–4722.2–4680.1).

Lines enclosed in brackets are considered as single lines, because in most cases they are not readily resolved.

Many elements when present in major amounts can be quickly identified without a spectroscope through recognition of the colors they impart to the arc. They will be imaged on the test screen in the form of a halo surrounding the center portion of the arc.

The following characteristics will aid in identifying major constituents:

TABLE 3

Element	*Color on positioning screen or other characteristics*
Al	Greenish blue
Sb	White fumes
As	Garlic odor
Ba	Green
Be	Greenish blue
B	Green
Ca	Orange
CaF_2	Canary yellow
Cb	Blue with red fringe—pitted lower electrode and white oxide coating
Cr	Green
Cs	Bluish white
Cu	Green
Fe	Blue with yellowish-white fringe—sparks and popping bead
Li	Red
Mg	Green
Mo	Blue—metallic coating on lower electrode
Nd	Light orange-red
K	Bluish-white
Pr	Greenish-gray
Sc	Light orange
Sm	Red
Ag	Green
Na	Yellow
Sr	Red
Ta	Blue with a red fringe—pitting on lower electrode and white oxide coating
Tl	Green (very intense)
Ti	White
U	Bluish white
W	Blue when current is reduced—pitting of lower electrode and yellow oxide coating
Y	Red
Zr	White flashes

N. B. The various greens and reds can be distinguished with practice. For a detailed study similar to the above the reader is referred to a publication by Wm. Roy Mott (7).

APPLICATION

As a replacement for blowpipe and chemical tests in determinative mineralogy the spectroscopic method offers the following applications:

1. All the common and most of the rare metallic elements may be rapidly identified.

2. Spectroscopic analysis permits the use of a very small sample. In many instances, single mineral grains have been analyzed in order to avoid contamination by associated minerals.

3. The possible interference of one element or a combination of elements with the determination of another depends only upon the complexity of the observed spectra. Elements normally difficult to differentiate chemically are no more difficult than any other spectroscopic determination, e.g., Ce from La and Y.

4. Minor amounts of either valuable or undesirable metals associated with certain minerals or commercial ores may be readily determined.

Applications supplementing petrographic examinations may be summarized as follows:

1. Two or more minerals having similar optical properties may be readily distinguished on the basis of their principal metallic components, e.g., individual members of certain isomorphous mineral groups are more readily distinguished than solely by optical means.

2. The identification of the opaque minerals and minerals having refractive indices lying above the usual range of index oils is considerably simplified and accelerated.

3. Finely divided inclusions in minerals may be more readily identified.

The limitations of the spectroscope may be stated as follows:

1. Most of the anionic constituents of minerals cannot be detected spectroscopically.

2. Spectroscopic examinations are limited to the visible region of the spectrum. If it is desired to determine elements whose principle lines lie in the infra-red or ultra-violet regions, recourse to the spectrograph is necessary.

3. The lines of minor constituents may be obscured if the major constituents have complex spectra, e.g., a small amount of Ni in pyrrhotite.

Specific examples of the application of the spectroscope in mineral identification are numerous. For example, pairs or groups of minerals often confused on the basis of their physical or optical properties can be readily differentiated spectroscopically by the presence or absence of one or two distinguishing elements. The following minerals, arranged in groups of two to four, are typical of those that are difficult to differentiate. These, however, can be identified readily by spectroscopic means.

Mineral	*Composition*
Fluorite	CaF_2
Opaline silica	SiO_2
Talc	$3MgO \cdot 4SiO_2 \cdot H_2O$
Pyrophyllite	$Al_2O_3 \cdot 4SiO_2 \cdot H_2O$
Chlorite	$9MgO \cdot 3Al_2O_3 \cdot 5SiO_2 \cdot 8H_2O$
Sericite	$(K, Na)_2O \cdot 3Al_2O_3 \cdot 6SiO_2 \cdot 2H_2O$
Barite	$BaSO_4$
Celestite	$SrSO_4$
Chalcopyrite	$CuFeS_2$
Pyrite	FeS_2
Quartz	SiO_2
Beryl	$3BeO \cdot Al_2O_3 \cdot 6SiO_2$
Nephelite	$Na_2O \cdot Al_2O_3 \cdot 2SiO_2$
Chromite	$(Fe, Mg)O \cdot Cr_2O_3$
Franklinite	$(Zn, Fe, Mn)O \cdot (Fe, Mn)_2O_3$
Sphene	$CaO \cdot TiO_2 \cdot SiO_2$
Zircon	$ZrO_2 \cdot SiO_2$
Pleonaste	$(Mg, Fe)O \cdot Al_2O_3$
Gahnite	$ZnO \cdot Al_2O_3$
Uvarovite	$3CaO \cdot Cr_2O_3 \cdot 3SiO_2$
Arizonite	$Fe_2O_3 \cdot 3TiO_2$
Euxenite	Columbate and titanate of Y, Er, Ce, U, etc.
Fergusonite	$(Y, Er, Ce)_2O_3 \cdot (Cb, Ta)_2O_5U$
Molybdenite	MoS_2
Pyrolusite	MnO_2
Sooty Chalcocite	Cu_2S
Carbonaceous material	C
Witherite	$BaO \cdot CO_2$
Aragonite	$CaO \cdot CO_2$
Rutile	TiO_2
Cassiterite	SnO_2
Epidote	$4CaO \cdot 3Al_2O_3 \cdot 6SiO_2 \cdot H_2O$
Allanite	$4(Ca, Fe)O \cdot 3(Al, Ce, Fe, Di)_2O_3 \cdot 6SiO_2 \cdot H_2O$
Greenockite	CdS
Carnotite	$K_2O \cdot 2UO_3 \cdot V_2O_5 \cdot 8H_2O$

Minor amounts of impurities in minerals that may be detected spectroscopically include:

Ti, V in magnetite	Sn in tantalite
Mo in scheelite	Ni in pyrrhotite
Zn in goethite	Cr, Li, V in mica
Cb in rutile	Ag in galena
Li, Na in beryl	Ag in sphalerite
Cr in clay	V in carbonaceous rocks
Zn, Mn in calcite	Fe in quartz and feldspar
Pb, Y in uraninite	Mn in calamine

Frequently, the petrographic laboratory is called upon to furnish rapid spectroscopic examinations of furnace slags, chemical precipitates, metals and alloys and various miscellaneous products other than minerals. While these do not properly fall within the scope of this paper, such application may be of interest to a person engaged in any phase of economic petrography.

Acknowledgments

This investigation was conducted under the general direction of J. B. Zadra, Chief, College Park Division and the immediate supervision of Alton Gabriel to whom the writers are indebted for valuable criticism and advice.

The writers also wish to thank Elizabeth Hechmer and D. A. Falck for preparing the diagrams, Myron Ritter for making the photograph (Fig. 2) and Morris Slavin for reading and criticizing the manuscript.

References

1. Brode, W. R., *Chemical Spectroscopy*, John Wiley and Sons, Inc., N. Y., Chapman and Hall, Limited, London (**1943**).
2. Baly, E. C. C., *Spectroscopy* (3 volumes), Longmans, Green and Co., N. Y. (**1924, 1927**).
3. Gibb, R. P., *Optical Methods of Chemical Analysis*, McGraw-Hill Book Co., Inc., N. Y. and London (**1942**).
4. *Handbook of Chemistry and Physics*, Chemical Rubber Publishing Co., Cleveland, Ohio.
5. *M. I. T. Wavelength Tables*, The Technology Press, Massachusetts Institute of Technology, John Wiley and Sons, Inc., N. Y., Chapman and Hall, Limited, London (**1939**).
6. Lee, O. I., and Wright, T. A., On identifying minerals with the aid of the spectrograph: *Proceedings of the 6th Summer Conference on Spectroscopy and its Application*, The Technology Press, M. I. T., John Wiley and Sons, Inc., N. Y., Chapman and Hall, Limited, London (**1939**).
7. Mott, Wm. R., Arc images in chemical analysis: *Trans. Am. Electrochemical Soc.*, **37**, (1920).
8. Papish, J., Hoag, L. E., and Snee, W. E., Spectroscopic detection of fluorine: *Ind. and Eng. Chem.*, Anal. Ed., 2, 263–264 (**1930**).
9. Papish, J., and Holt, D. A., Arc spectrographic detection and estimation of gallium: *Jour. Physical Chem.*, **32**, 142–147 (1928).
10. Pearse, R. W. B., and Gaydon, A. G., *The Identification of Molecular Spectra*, John Wiley and Sons, Inc., N. Y. (**1941**).
11. Sawyer, R. A., *Experimental Spectroscopy*, Prentice-Hall, Inc., N. Y. (**1944**).

BIREFRINGENCE-DISPERSION RATIO AS A DIAGNOSTIC[1]

A. N. Winchell, *Stamford Research Laboratories, American Cyanamid Company, Stamford, Connecticut,*
and
Ward B. Meek, *University of Wisconsin, Madison, Wisconsin.*

Abstract

The ratio between the birefringence (B_D) and the dispersion of the birefringence ($B_F - B_C$) is an optical property which is almost unknown, but it is useful in certain cases. For example, a three- (or four-) component system may have physical properties such that "contour" lines for the commonly used physical characters, such as refringence, birefringence, and specific gravity, are all nearly parallel, but the birefringence-dispersion ratio lines are far from parallel with the other lines in some cases. Some examples are given.

In the case of a simple variation in chemical composition of any mineral, like the variation in olivine from Mg_2SiO_4 to Fe_2SiO_4, a simple diagram showing the relation between variations in composition and variations in physical characters makes it possible to learn the composition by measuring any one of the physical characters included in the diagram. But when the variation in chemical composition is more complex, leading to three (or four) end-members, no diagram can be made which will give the composition by means of measuring one physical property, since any physical property is necessarily the same along some line (or plane) of the diagram. In order to determine the composition by measuring the physical characters in such a case it is necessary to make use of at least two characters which are represented in the diagram by lines which are not parallel; indeed such lines should be (approximately) at right angles to give satisfactory results. In some cases the lines showing the commonly measured physical characters, such as refringence, birefringence, and specific gravity are parallel (or nearly so) in such diagrams. For such cases it is important to find a physical property which varies in such a way as to be represented by lines (nearly) normal to those for one or more of the other physical characters. It seems probable that such a physical character has been found at least for some ternary systems of the carbonates of the divalent metals commonly known as the calcite group. This group has at least six end-members, namely, $CaCO_3$, $MgCO_3$, $FeCO_3$, $MnCO_3$, $ZnCO_3$, and $CoCO_3$ but so little is known about the properties of $CoCO_3$ that it will not be considered further.

Calcite is found so often in very pure well-formed crystals that its properties have been measured with unusual accuracy. They may be

[1] This article in its present form was written by the senior author, but it is based in large part upon an unpublished article written by the junior author when he was a graduate student at the University of Wisconsin in 1937.

summarized as follows:[2] G = 2.71(5)

	λ=656(C)	589(D)	486(F)
N_O	1.65440	1.65835	1.66783
N_E	1.48457	1.48639	1.49074
$N_O - N_E$ =	.16983	.17196	.17709

Accordingly, the birefringence for the Na line (or B_{Na}) is 0.17196 and the dispersion of the birefringence, that is, the difference between the birefringence for the F line and that for the C lines, is: $B_F - F_C = .00726$. The ratio between these values {that is $B_{Na} \div (B_F - B_C)$} is 23.7. Since $B_F - B_C$ is the dispersion (D), $B_{Na} \div (B_F - B_C)$ may be shortened to B/D for convenience. This ratio between the birefringence and the dispersion of the birefringence is the physical property which seems to be useful in some cases.

From other excellent measurements[2a] of the refringence of calcite it is reasonable to conclude that B/D varies from 23.3 to 24.7, doubtless because of small variations in the composition, such as the presence of small amounts of Mg, Fe, or Mn, proxying for Ca.

Dolomite, $CaMgC_2O_6$, nearly always contains more or less Fe, Mn, and excess Ca, which proxy for Mg, therefore its properties vary considerably. According to recent data[3] believed to be accurate the magnesian end-member has the following properties: G = 2.869.

	λ=656(C)	589(D)	486(F)
N_O	1.67610	1.68005	1.68901
N_E	1.49950	1.50125	1.50550
$N_O - N_E$ =	.17660	.17880	.18351

Therefore $B_F - B_C = 0.00691$ and B/D = 27.3

A careful study of siderite from Cornwall[4] containing 97.5 mol. per cent of $FeCO_3$ and only 1.8% $MnCO_3$, 0.5 $MgCO_3$, and 0.2 $CaCO_3$ gave the following results for Li, Na, and Tl light: G = 3.937.

For prism 1

	λ=671(Li)	589(D)	535(Tl)
N_O	1.8649	1.8734	1.8809
N_E	1.6297	1.6333	1.6373

For prism 1a

	λ=671(Li)	589(D)	535(Tl)
N_O	1.8655	1.8733	1.8812
N_E	1.6306	1.6342	1.6377

For prism 2

	λ=671(Li)	589(D)	535(Tl)
N_O	1.8643	1.8724	1.8799
N_E	1.6299	1.6338	1.6371

For prism 3

	λ=671(Li)	589(D)	535(Tl)
N_O	1.8642	1.8722	1.8798
N_E	1.6278	1.6310	1.6344

[2] Gifford, J. W., *Proc. Roy. Soc. London*, **70**, 336 (1902).

[2a] See those of Sarasin: *Zeit. Kryst.*, **9**, 605 (1883); Schrauf: *Zeit. Kryst.*, **11**, 20, 674 (1885); Mülheims: *Zeit. Kryst.*, **14**, 224 (1888) and Martens: *Ann. Phys.*, (4) **6**, 603 (1901).

[3] Gübelin, E.: *Schw. Min. Pet. Mit.*, **19**, 325 (1940).

[4] Hutchinson, A.: *Mineral. Mag.*, **13**, 209 (1903).

From these data the indices for C and F light can be obtained by using the Hartmann dispersion net, with the following results:

Prism	*1*	*1a*	*2*	*3*	*Average*
B $-B_C=$	0.0125	0.0132	0.0128	0.0132	0.0128
$B/D=$	19.2	18.1	18.6	18.3	18.6

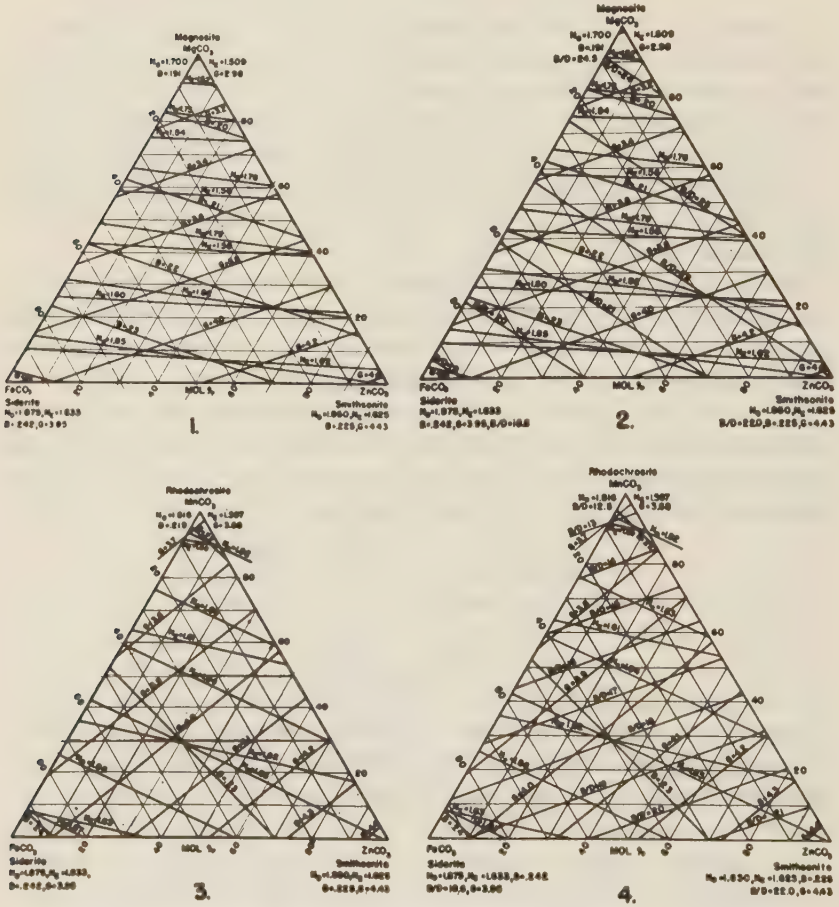

FIGS. 1, 2. Properties of $MgCO_3$–$FeCO_3$–$ZnCO_3$ without (1) and with (2) B/D lines.
FIGS. 3, 4. Properties of $MnCO_3$–$FeCO_3$–$ZnCO_3$ without (3) and with (4) B/D lines.

The only available data on the dispersion of rhodochrosite are derived from measurements[5] of the indices of a crystal[6] from Alma, Park County, Colorado, as follows:

[5] Made by W. B. Meek by the double variation method (with extrapolation for the O ray).

[6] Sundius, N. (*Geol. För. Förh. Stockholm*, **47**, 269 1925) gives the following analysis of crystals from the same locality: Mol. % $MnCO_3$ 97.83, $FeCO_3$ 1.60, $MgCO_3$ 0.58.

$\lambda = 656$(C)	589(D)	486(F)
$N_O = 1.7981$	1.8058	1.8245
$N_E = 1.5936$	1.5964	1.6032
$N_O - N_E = 0.2045$	0.2094	0.2213

Therefore $B_F - B_C = 0.0168$ and $B/D = 12.5$

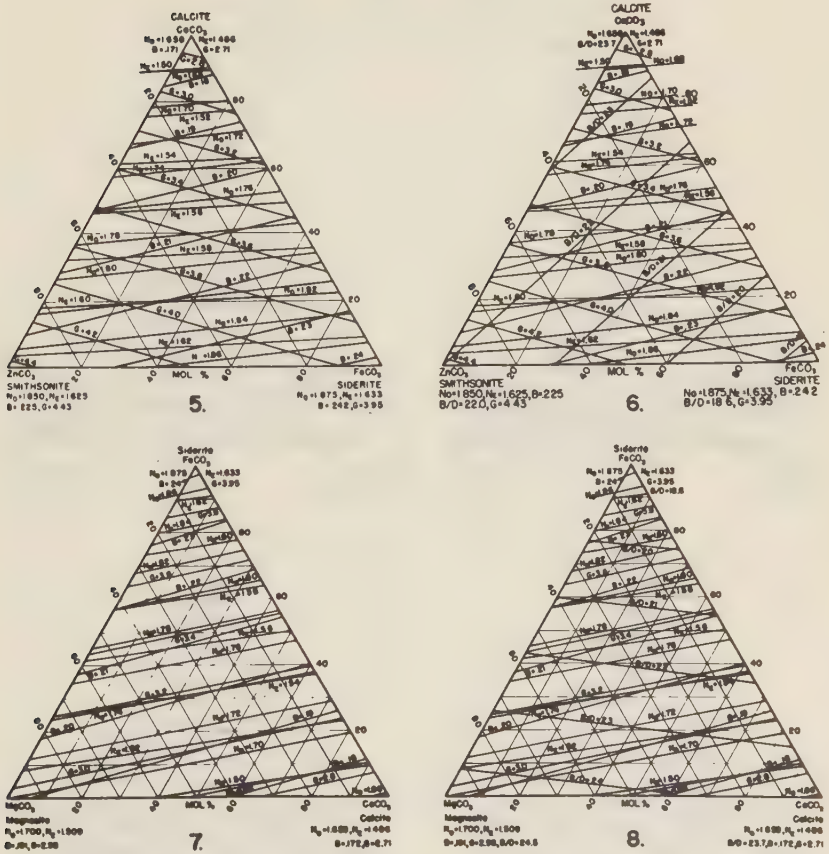

FIGS. 5, 6. Properties of $CaCO_3$–$ZnCO_3$–$FeCO_3$ without (5) and with (6) B/D lines.
FIGS. 7, 8. Properties of $FeCO_3$–$MgCO_3$–$CaCO_3$ without (7) and with (8) B/D lines.

A detailed study of smithsonite from Rhodesia containing 97.0 mol. per cent of $ZnCO_3$ and only 1.4 $MgCO_3$, 1.0 $FeCO_3$ and 0.6 $CaCO_3$ gave the following results:[7] G = 4.398.

$\lambda = 671$(Li)	656(C)	589(D)	535(Tl)	486(F)
$N_O = 1.8423$	1.8433	1.8485	1.8547	1.8621
$N_E = 1.6186$	1.6189	1.6212	1.6239	1.6274
$N_O - N_E = 0.2237$	0.2244	0.2273	0.2308	0.2347

Therefore $B_F - B_C = 0.0103$ and $B/D = 22.0$

[7] Mountain, E. D.: *Mineral. Mag.*, **21**, 51 (1926).

An unanalyzed sample of smithsonite studied by R. C. Emmons and E. F. Williams[8] gave the following data, as measured by W. B. Meek:

λ=656(C)	589(D)	486(F)
N_O=1.8418	1.8475	1.8614
N_E=1.6188	1.6213	1.6276
N_O-N_E=0.2230	0.2262	0.2338

Therefore B_F-B_C=0.0108 and B/D=20.94

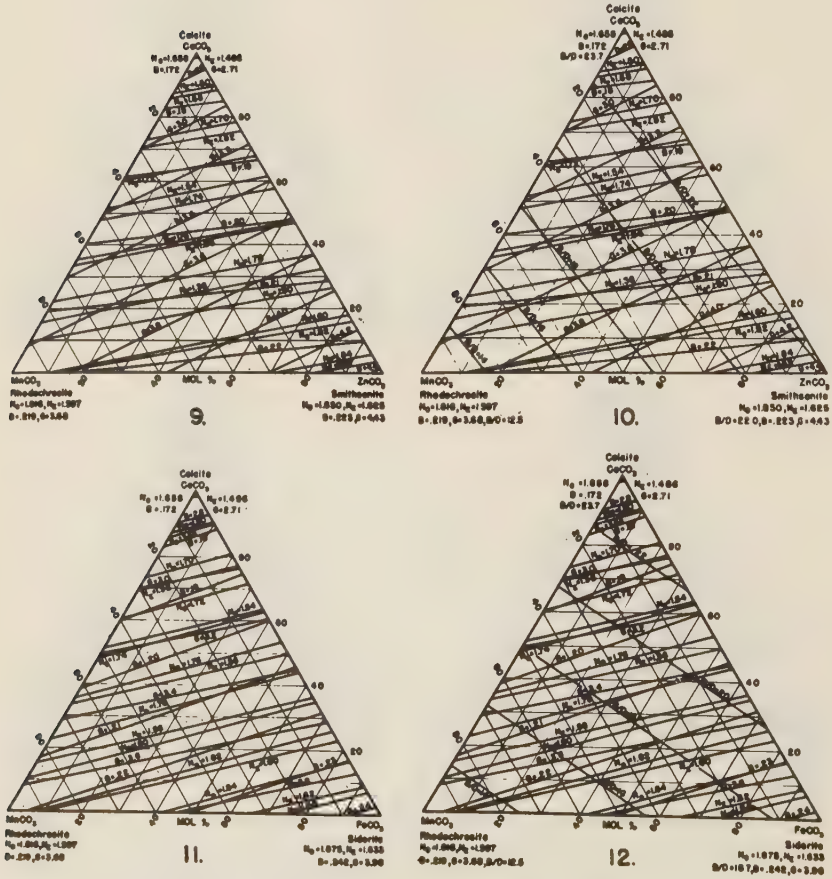

FIGS. 9, 10. Properties of $CaCO_3$–$MnCO_3$–$ZnCO_3$ without (9) and with (10) B/D lines.
FIGS. 11, 12. Properties of $CaCO_3$–$MnCO_3$–$FeCO_3$ without (11) and with (12) B/D lines.

Almost the only published data on the dispersion of magnesite are for a crystal from Greiner,[9] analysis of which gave 74.8 mol % $MgCO_3$, 13.4 $FeCO_3$, 10.6 $MnCO_3$, and 1.2 $CaCO_3$: its refractive indices were found to be:

[8] Emmons, R. C., and Williams, E. F.: *Jour. Sed. Petrol.*, **4**, 32 (1934).
[9] Eisenhut, K.: *Zeit. Kryst.*, **35**, 595 (1901).

$\lambda = 671$(Li)	589(D)	535(Tl)
$N_O = 1.7118$	1.7174	1.7215
$N_E = 1.5263$	1.5285	1.5304
$N_O - N_E = 0.1855$	0.1889	0.1911

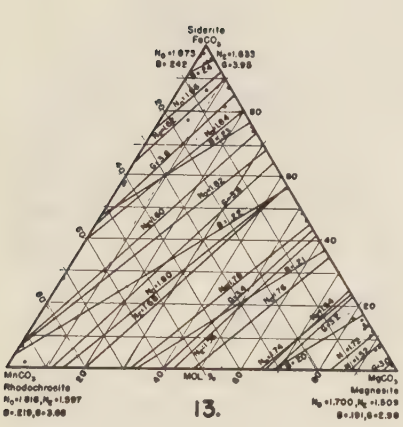

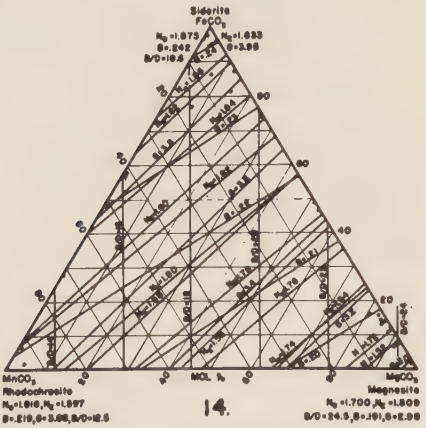

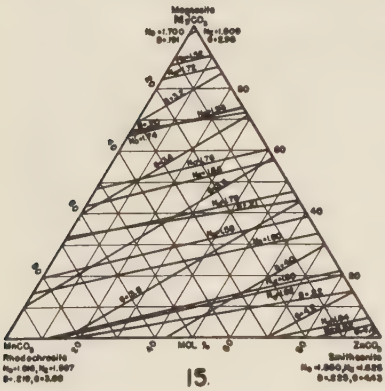

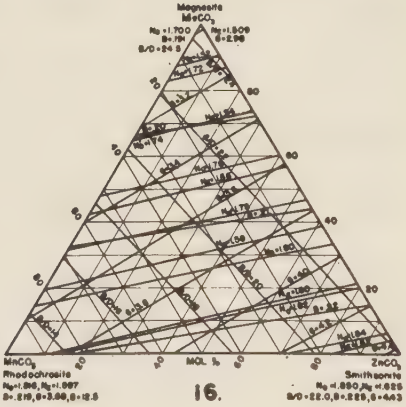

FIGS. 13, 14. Properties of $FeCO_3$–$MnCO_3$–$MgCO_3$ without (13) and with (14) B/D lines.

FIGS. 15, 16. Properties of $MgCO_3$–$MnCO_3$–$ZnCO_3$ without (15) and with (16) B/D lines.

These figures do not give straight lines on the Hartmann net, but, using Li and Tl to fix the straight lines, the indices for C and F are: $N_O = 1.7126$ C, 1.7272 F and $N_E = 1.5267$ C, 1.5329 F; therefore $B_F - B_C = 0.0084$ and $B/D = 22.5$. By making suitable allowance for the effects of Fe, Mn, and Ca, B/D for pure $MgCO_3$ is 24.5.

The following table summarizes the available data for the calcite group.

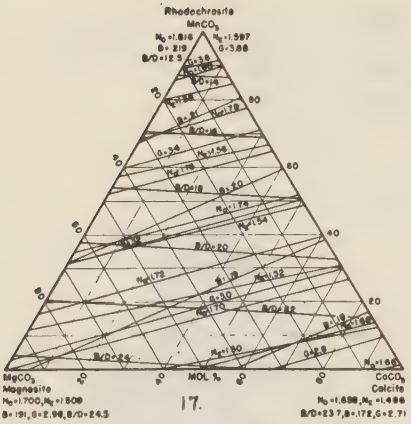

17.

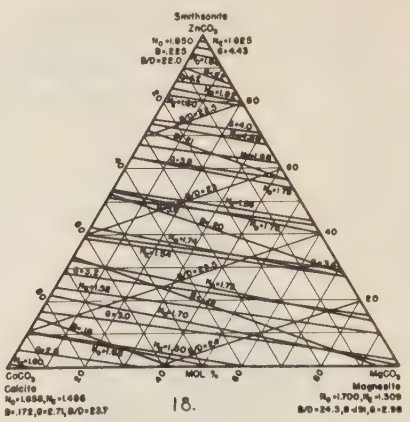

18.

FIG. 17. Properties of $MnCO_3$–$MgCO_3$–$CaCO_3$.
FIG. 18. Properties of $ZnCO_3$–$CaCO_3$–$MgCO_3$.

	$N_O(D)$	$N_E(D)$	B_D	B_F–B_C	B/D	G
Calcite	1.65835	1.48639	0.17196	0.00726	23.7	2.71 (5)
Dolomite	1.68005	1.50125	0.17880	0.00691	27.3	2.87
Magnesite meas.	1.7174	1.5285	0.1889	0.0084	22.5	
Magnesite pure $MgCO_3$	1.700	1.509	0.191		24.5	2.98
Siderite meas.	1.8734	1.6331	0.2403	0.0128	18.6	3.937
Siderite pure $FeCO_3$	1.875	1.633+	0.242		18.6	3.95
Rhodochrosite	1.8058	1.5964	0.2094	0.00168	12.5	3.68
Smithsonite meas.	1.8485	1.6212	0.2273	0.0103	22.0	4.398
Smithsonite pure $ZnCO_3$	1.850	0.625±	0.225±		22.0	4.43

These are the best data at present available, but unfortunately they are not very accurate, except in the case of calcite and dolomite. Of course dolomite is not strictly a member of the calcite group. The remaining five compounds yield ten ternary systems; the refringence, birefringence and density of eight of these are shown in Figures 1, 3, 5, 7, 9, 11, 13 and 15. It is easily seen that in most of these systems the ordinary properties give lines which are nearly parallel; in only two cases (Figs. 1 and 3) are the lines at an angle great enough to give the composition fairly well. The same eight ternary systems are shown in Figures 2, 4, 6, 8, 10, 12, 14, and 16 in which lines for the birefringence dispersion ratio (B/D) have

been added. It is obvious that these lines aid materially in the determination of the composition, especially in the case of $CaCO_3$–$ZnCO_3$–$FeCO_3$, $CaCO_3$–$MnCO_3$–$ZnCO_3$, $CaCO_3$–$MnCO_3$–$FeCO_3$, $FeCO_3$–$MnCO_3$–$MgCO_3$, and $MgCO_3$–$MnCO_3$–$ZnCO_3$. Figures 17 and 18 show that the same is true for the systems $MnCO_3$–$MgCO_3$–$CaCO_3$ and $ZnCO_3$–$CaCO_3$–$MgCO_3$. However, it is well known that six ternary systems of the calcite group which have $CaCO_3$ as one member are not continuous. Of the four others the composition of any mix-crystal can be determined rather well in two cases (Figs. 1 and 3) without using the new diagnostic. In the case of $FeCO_3$–$MnCO_3$–$MgCO_3$ and $MgCO_3$–$MnCO_3$–$ZnCO_3$, the use of the birefringence-dispersion ratio lines is very helpful, as shown in Figures 13–16.

PARASCHOEPITE AND EPIIANTHINITE, TWO NEW URANIUM MINERALS FROM SHINKOLOBWE (BELGIAN CONGO)

ALFRED SCHOEP AND SADI STRADIOT, *Baudeloostraat 97, Ghent, Belgium.*

ABSTRACT

Paraschoepite, a new mineral with a chemical composition corresponding to the formula $5UO_3 \cdot 9\frac{1}{2}H_2O$ has been found in the uranium mine of Shinkolobwe. Properties: color, yellow; habit, identical with tabular schoepite. $X=c$, $Y=b$, $Z=a$. $\alpha=1.705$, $\beta=1.760$, $\gamma=1.770$. $2V\pm46°$; $r>v$. H.=2–3. G.>3.3.

Epiianthinite, chemical composition is unknown but probably an uranium hydroxide. Color, yellow. Crystals are prismatic and elongated parallel to b. $X=c$, $Y=b$, $Z=a$. $\alpha=1.70$, $\beta=1.79$, $\gamma=1.793$. $2V$ very small. Pleochroism, yellow to deep yellow. G.>3.3; H.=2–3.

Paraschoepite and epiianthinite occur in the Shinkolobwe uranium mine (Katanga). They belong to the uranium hydroxide group of minerals whose inter-relationship Charles Palache rightly describes as peculiar. The name paraschoepite appeared to us as very suitable for the first mentioned mineral because it differs very little, both crystallographically and chemically, from schoepite.

In naming the second mineral epiianthinite we specially wished to emphasize the fact that it not only crystallizes on ianthinite, but also that its lattice is in continuity with that of ianthinite; at the same time the name designates its secondary character.

PARASCHOEPITE

Associations and crystallographic properties

Crystals of paraschoepite have been found directly on pitchblende or with secondary uranium minerals. They appear to be very closely associated with becquerelite and are frequently found as deposits on that mineral. The largest crystals observed reach a size of several millimeters. Their habit is tabular and they are orthorhombic in crystallization. Their color is yellow, less greenish than the yellow of schoepite and their transparency is less than that of the latter mineral. The mineral has a very perfect and easy cleavage, making it extremely brittle. The hardness ranges from 2 and 3 and the powder is yellow.

Paraschoepite resembles so closely certain tabular schoepite crystals that it is impossible to distinguish between them without determining their optical properties. Not having available at present any instrument for measuring crystals, we were able however to measure accurately the angles between the edges of crystals placed on the rotating stage of a microscope, and with these data we drew the crystal and showed that the drawings thus obtained (Fig. 1) could be exactly superimposed on drawings of similar schoepite crystals, drawn orthogonally from gnomonic projections. The paraschoepite crystals, which we have examined in this way, lie mostly on face $c(001)$, which is generally better developed than

the other forms and which is covered with fine striations running parallel to the b axis. As shown in Fig. 1, the forms include $c(001)$, $b(010)$, $a(100)$, $m(110)$, $n(120)$, $d(011)$, $f(021)$, $x(104)$ and $q(124)$. This crystal is relatively large; smaller crystals have fewer forms.

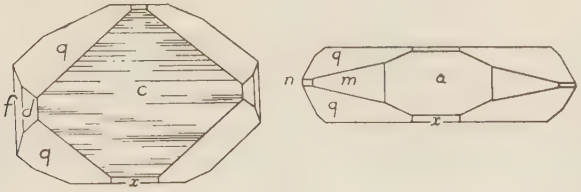

FIG. 1. Two views of a crystal of paraschoepite.

Optical properties

Under the microscope crystals of paraschoepite are yellow and translucent; they contain a considerable number of inclusions, apparently of a gaseous nature, which perhaps explains their limited transparency when examined with the naked eye. Zonal growth is nearly always discernible

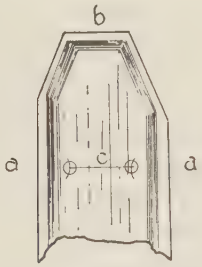

FIG. 2. Crystal of paraschoepite showing zonal growth. Axial plane is parallel to $b(010)$.

(Fig. 2). Between crossed nicols they react as orthorhombic crystals. The acute bisectrix is perpendicular to $c(001)$; the plane of the optic axes is parallel to $b(010)$; these axes are visible at the edge of the field with a No. 5 Leitz objective (numerical aperture 0.65). If the optic axes are observed on the natural face $c(001)$, it appears as if the axial plane is perpendicular to the striations which cover the face and this is a good characteristic which distinguishes paraschoepite from schoepite.

The indices of refraction as determined by the immersion method are given below.

Pleochroism: Z and Y, yellow; X colorless or nearly so.
Dispersion, $r>v$.

$\alpha=1.705$	$X=c$	$2V\pm40°$
$\beta=1.760$	$Y=b$	$B_x(-)$
$\gamma=1.770$	$Z=a$	$r>v$

Chemical properties and composition

Paraschoepite dissolves readily in hydrochloric, nitric and sulfuric acids and gives the uranium reaction; it also contains water but does not give a test for lead.

Analysis of Paraschoepite

	1.	2.	3.	4.
UO_3	89.26	0.312	1	89.31
H_2O	10.73	0.597	1.9	10.69

1. Analysis of paraschoepite of Shinkolobwe.
2. Molecular proportions.
3. Molecular ratios on the basis of $UO_3 = 1$.
4. Calculated analysis on the basis of the formula $5UO_3 \cdot 9\frac{1}{2}H_2O$.

Discussion of the formula

The chemical composition of paraschoepite places it in the group of uranium hydroxides, of which the following are already known: becquerelite, schoepite, mineral *X* (Palache), and fourmarierite. The last named is, it is true, a lead uranate if considered solely from the chemical point of view, but it is equally certain that its crystallographic characteristics place it next to schoepite.

We propose the following formula for paraschoepite: $5UO_3 \cdot 9\frac{1}{2}H_2O$. We should recall here that one of us, after one of the first analyses made of becquerelite and schoepite, gave, in a formula of the $y\ UO_3 \cdot x\ H_2O$ type assigned to these minerals, the value $\frac{1}{2}$ for the ratio $y:x$; the two minerals were at first given the same chemical formula. It must be admitted that these first analyses had been made on samples which could in no wise be claimed to be very pure; lead amongst others was always found to be present, whereas a number of analyses made on isolated and pure crystals of becquerelite and of schoepite had established the fact that these minerals contain no traces of lead.

Later we were able to obtain a sufficient quantity of pure crystals and we have re-analyzed these two minerals. It is in view of the results thus obtained that we realized that it was advisable to give to the coefficients y and x values which differed as little as possible from the molecular ratios found. The chemical composition of the two minerals was thus expressed as follows:

Becquerelite	$4UO_3 \cdot 7H_2O$
Schoepite	$3UO_3 \cdot 7H_2O$

The elementary cells of these minerals as well as of fourmarierite have since then been measured; the following results were obtained:

	Becquerelite	*Schoepite*	*Fourmarierite*
a_0	13.9 Å	14.40Å	14.07Å
b_0	12.55Å	16.89Å	16.72Å
c_0	14.9 Å	14.75Å	14.40Å

The formula suggested for fourmarierite, $PbO \cdot 4UO_3 \cdot 5H_2O$, corresponds to a molecular weight M, which introduced in the well known formula:

$$n = \frac{V \times d}{M \times 1.65}$$

gives a value for n which is quite acceptable, considering the specific gravity of the mineral. It was not the same for either becquerelite or schoepite; therefore, these minerals were, once more, analyzed and new determinations of specific gravity were made. Finally the following formulae were decided upon:

Becquerelite	$2UO_3 \cdot 3H_2O$
Schoepite	$4UO_3 \cdot 9H_2O$

for which the values of n were considered compatible with both the symmetry and specific gravity.

In the following table the known uranium hydroxides have been placed with some others which are theoretically possible; fourmarierite has been placed at the top of the list because in its formula:

$$y\ UO_3 \cdot z\ PbO \cdot x\ H_2O$$
$$y + z : x = 1$$

TABLE OF URANIUM HYDROXIDES

Name	Formula	x:y	UO_3%	H_2O%	α	β	γ
Fourmarierite	$4\ UO_3 \cdot PbO \cdot 5\ H_2O$	1.00	93.81	6.19	1.920	—	1.940
—	$4\ UO_3 \cdot 5\ H_2O$	1.25	92.70	7.30	—	—	—
Becquerelite	$2\ UO_3 \cdot 3\ H_2O$	1.50	91.37	8.63	1.725	1.825	1.83
Mineral x	$4\ UO_3 \cdot 7\ H_2O$	1.75	90.08	9.92	1.785	1.81	1.82
—	$5\ UO_3 \cdot 9\ H_2O$	1.80	89.82	10.18	—	—	—
Paraschoepite	$5\ UO_3 \cdot 9\frac{1}{2}\ H_2O$	1.90	89.31	10.69	1.705	1.76	1.77
—	$UO_3 \cdot 2\ H_2O$	2.00	88.81	11.19	—	—	—
Schoepite	$4\ UO_3 \cdot 9\ H_2O$	2.25	87.59	12.41	1.69	1.714	1.735

The position we have given to paraschoepite in this series of hydroxides will be noted from the above. It will be interesting to know its crystallo-

graphic constants and we hope that they will be published before long.

The position in the series which we have given to mineral x is based only on its chemical composition, after deduction of PbO and recalculation to 100%. Furthermore, we repeat that in formulating this table chemical considerations served as a guide.

It may be considered that the formula $5\,UO_3 \cdot 9\,H_2O$ might have served equally well to express the chemical composition of paraschoepite, but experience has shown that as far as these uranium hydroxides are concerned it is preferable not to round off the coefficients of either UO_3 or H_2O, given by an analysis of a superior type.

Differences between paraschoepite and schoepite

At first glance the differences between paraschoepite and schoepite are so slight that we take it for granted that one mineral must have been mistaken frequently for the other. Indeed, in so far as we are able to judge without goniometric measurements, the crystals of the two minerals are practically indistinguishable one from the other. An observation of the axial figure and the position of the axial plane is however sufficient; obviously, the determination of the indices of refraction is the infallible way to differentiate between the two minerals.

Epiianthinite

As we mentioned at the beginning of this paper, we assigned the name of epiianthinite to a mineral which occurs as an alteration product of ianthinite. Yet the homogeneity of the alteration product is perfect and its crystalline lattice is in continuity with that of ianthinite.

Herewith is given a brief summary of the history of ianthinite. This mineral is always found implanted directly upon uraninite and fills all its fissures and cavities. The acicular crystals (1–3 mm.) are of prismatic habit; they are black with a brownish violet tinge in reflected but violet in transmitted light. The pleochroism is intense, dark violet to colorless and the appearance of the crystals is shown in Fig. 3. When the orientation suggested by Charles Palache is adopted, the forms are:

$$c(001),\ g(101),\ m(103),\ d(011),\ f(130) \cdot (3)$$

Fig. 3. Crystal of ianthinite.

For some time one of us had observed that certain ianthinite crystals are edged by a zone that is homogeneous and translucent and yellow in color. It is known that ianthinite is a hydroxide of U^{IV} and that the compounds of U^{IV} oxidize easily to U^{VI}; at the same time the color changes from green or violet to yellow.

We have now been able to observe all the various stages of the change, passing from pure ianthinite to epiianthinite in which traces of the primary mineral are no longer perceived. Generally the traces of ianthinite inside epiianthinite occur as elongated patches of violet brown (Fig. 4).

FIG. 4. Remnants of unaltered ianthinite in crystal of epiianthinite and optical orientation of epiianthinite.

Optical properties

Epiianthinite crystals, examined under a microscope, are yellow in transmitted light; they have the same perfect cleavage as ianthinite and like the latter are orthorhombic in crystallization. A crystal observed in convergent light on face $c(001)$ exhibits a good interference figure; the acute bisectrix, perpendicular to $c(001)$, is negative; the optic angle is very small and the plane of the optic axes is perpendicular to the elongation, that is to the crystallographic b axis. The pleochroism is marked: $X = c$ pale yellow, $Y = b$ yellow, $Z = a$ deep yellow. The indices of refraction are: $\alpha = 1.70$, $\beta = 1.79$, $\gamma = 1.793$. The traces of ianthinite which one can see in many crystals appear as diffused and elongated shreds parallel to the b axis; they are violet in color and pleochroic; measured in the plane of $c(001)$, their indices of refraction are higher than those of epiianthinite.

Chemical composition

Up to the present we have not been able to determine the chemical composition of the mineral, which has proved practically impossible to purify. It is, of course, a product of the oxidation of ianthinite and its composition can very likely be expressed by $y\ UO_3 \cdot xH_2O$. We have, in the past, experimented with the oxidation of ianthinite by immersing the crystals for some minutes in a very dilute solution of hydrogen peroxide at a temperature around 50° C. The experiment was successful but the properties of the yellow crystals thus obtained bore no resemblance to those of epiianthinite; indeed their average index of refraction is only ± 1.60. Of course, the oxidation took place in water while epiianthinite probably formed under different conditions.

According to L. J. Spencer, ianthinite crystals do not keep their original color when exposed in the cases of the British Museum. He noted that when acquired (1922), the color was purple, but in 1927 it was greenish yellow but crystals that had been mounted in Canada balsam still retained their original color and intense pleochroism. He concluded that the change is evidently due to oxidation in the air of a hydrated uranous oxide to a hydrated uranic oxide (5).

References

(1) Billiet, V., en de Jong, W. F., Schoepiet en Becquereliet: *Natuurwetensch. Tijdschr*, **17**, 6 (1935).

(2) Brasseur, H., Contribution à la connaissance de la fourmarierite: *Bull. Soc. Roy. des Sc. de Liège*, **6**, (1941).

(3) Palache, C., and Berman, H., Oxidation products of pitchblende from Bear Lake: *Am. Mineral.*, **18**, 20 (1933).

(4) Schoep, A., Les minéraux du gîte uranifère du Katanga: *Ann. Musée du Congo Belge, Sér. I, T. I. Fasc. II.* (**1930**).

(5) Spencer, L. J., Mineralogical Chemistry (1926–27). Annual Reports of the *Chem. Soc.*, **24**, for 1927 (1928).

APPARATUS FOR OBTAINING POWDER-TYPE *X*-RAY DIFFRACTION PATTERNS FROM SINGLE CRYSTALS

GEORGE SWITZER, *Gemological Institute of America, Los Angeles, Calif.*,
AND
RALPH J. HOLMES, *Columbia University, New York, N. Y.*

ABSTRACT

An *x*-ray diffraction camera has been designed by means of which powder-type diffraction patterns are obtained from single crystals. Such patterns are obtained by imparting to the specimen a combination oscillatory and rotatory motion.

INTRODUCTION

There is a definite need for an instrument that will yield *x*-ray diffraction patterns useful for identification purposes (preferably, powder-type patterns) from large single crystals, or coarse crystalline aggregates. In cases where it is undesirable to remove and powder a fragment of the material to be tested, such an instrument would prove valuable. This need is felt especially in the field of gem identification, but also in many other types of work.

The instrument herein described was developed in the laboratories of the Gemological Institute of America, to be used in gem identification, especially for use with opaque materials or those having no plane surfaces, such as double cabochons or carved or irregular pieces. The instrument's design is based upon a suggestion made by Dr. Samuel G. Gordon, Associate Curator of the Academy of Natural Sciences of Philadelphia, and a member of the Educational Advisory Board of the Gemological Institute of America.

INSTRUMENT

To obtain a powder-type *x*-ray diffraction pattern of a crystalline substance, it is necessary to be able to bring a large group of atomic planes into a reflecting position. This is ordinarily accomplished by finely powdering the material, and by rotating the sample to bring about completely random orientation of the grains.

A pattern of this type from a single crystal may be obtained by imparting to the specimen a motion which will, during the course of the exposure, bring a much larger number of atomic planes into reflecting position than can be obtained by any simple rotary motion. When this is done, a powder-type pattern is obtained. The orientation of the single crystal at the time the sample is mounted in the camera is of no consequence.

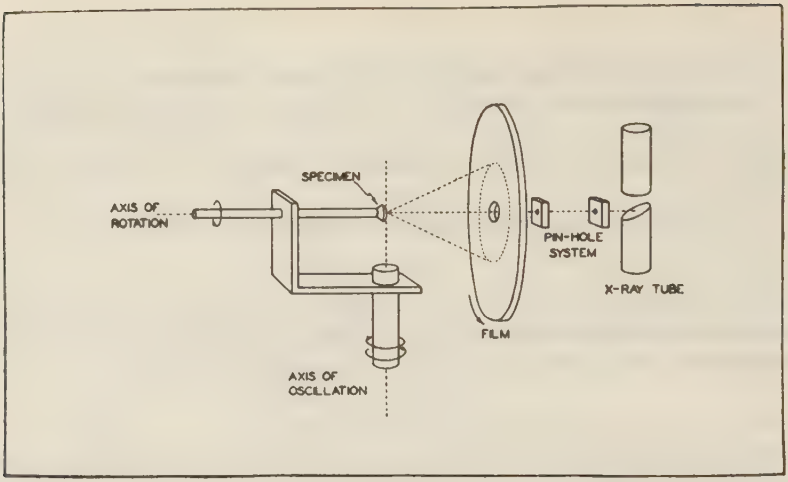

FIG. 1. Schematic representation of a camera designed to give powder-type x-ray diffraction patterns from single crystals.

The type of motion necessary to approximate the random-orientation condition of a powdered sample is produced by simultaneous rotation and oscillation of the specimen. The apparatus used to accomplish this is shown schematically in Fig. 1. The first model of the camera, now in use, employs an 80 degree oscillation of the sample at the rate of one degree per minute, and simultaneous rotation of the sample at one revolution per minute.

Because of the size of the samples ordinarily encountered, it was most desirable to utilize the back-reflection method. These are recorded on a flat film. A back-reflection type camera is also more feasible from the standpoint of mechanical design. In this respect, the camera resembles the standard back-reflection type commonly used in metallurgical work. In some cases, due to lack of completely random orientation, incomplete circles were recorded. This difficulty is easily overcome by rotating the film about the x-ray beam as an axis during exposure.

RESULTS

Typical results obtained with the instrument described are shown in Figs. 2 and 3. All of these patterns were obtained from single cut gems (single crystals) using filtered copper radiation, and a specimen to film distance of four centimeters. It will be noticed that there is a sharp separation of the K_{α_1} and K_{α_2} lines, as is to be expected from high angle reflections of this type.

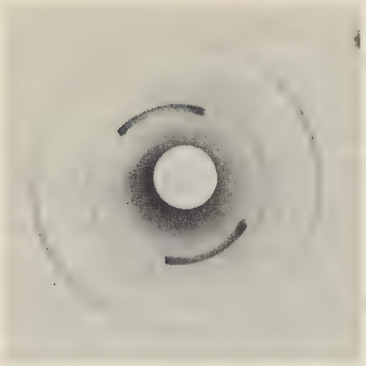

FIG. 2. Diffraction pattern of single crystal of corundum. Filtered copper radiation. Exposure 6 hours.

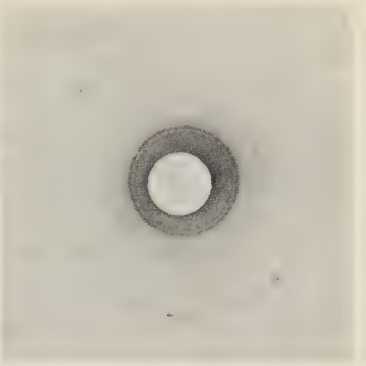

FIG. 3. Diffraction pattern of spinel. Filtered copper radiation. Exposure 6 hours.

CONCLUSIONS

The results herein described are the first obtained with an experimental model camera. An improved camera design is being worked on at the present time. The method could probably be adapted to an apparatus employing automatic recording of the x-ray spectra by means of a Geiger counter.

In practice, the advantages of a camera of this type for many kinds of work are manifold. The specimen may be a single crystal or a crystalline aggregate. In size it may vary from one millimeter or less up to any size that will be accommodated by the instrument. Specimens 10 centimeters in diameter can be handled in the present camera. A catalog can be readily built up similar to that published by the American Society of Testing Materials, using the spacings of the three strongest lines as a key. Such a catalog is now being prepared for gem materials, and will probably be expanded to other substances. Modification of the camera design to utilize forward reflections would make it possible to use the present A.S.T.M. cards.

THE PEÑA BLANCA SPRING METEORITE, BREWSTER COUNTY, TEXAS

JOHN T. LONSDALE, *University of Texas, Austin, Texas.*

ABSTRACT

The Peña Blanca Spring meteorite fell August 2, 1946, in the swimming pool at the headquarters of the Gage Ranch near Marathon in Brewster County, Texas. Twenty-four people were within a few hundred feet of the point of fall, and one person saw the meteorite in flight. Many interesting incidents were accurately reported.

Approximately 70 Kg. (155 lbs.) of the meteorite were recovered, consisting of one fragment of 47 Kg. (104 lbs.), one fragment of 13 Kg. (29 lbs.), and many smaller pieces down to mere grains. Reconstruction of the shape indicate that all but a few pounds of the stone have been recovered.

The meterorite is a white *aubrite* with a cream colored crust and remarkably coarse cataclastic-porphyritic texture. One phenocryst of pyroxene is 10×6×8 cm.; another, 6×3×1.5 cm.; and a number are larger than 3×3×3 cm. An approximate mode of the meteorite is iron free enstatite 93%, iron free diopside 5.0%, iron free forsterite 0.5%, oligoclase 0.5%, iron-nickel (iron rich) 0.5%, troilite 1.25%, and miscellaneous minerals 0.25%.

INTRODUCTION

As far as known, man has never constructed a device in which to trap a meteorite falling to the earth. Had he done so, possibly he could not have improved upon the swimming pool at the headquarters of the Gage ranch about 9.5 miles southeast of Marathon in Brewster County, Texas. This swimming pool received the Peña Blanca Spring meteorite with a violent splash at about 1:20 P.M. on August 2, 1946. The meteorite is named from the spring which forms the swimming pool and which is an historic landmark in the region. The exact location is longitude 103°7.1′ west longitude 30°7.5′ north latitude. The unusual location of the fall, the fact that the meteorite fell within a few hundred feet of twenty-four people, and its unusual petrographic character appear to warrant a fairly complete account.

PHENOMENA OF FALL

Peña Blanca (White Bluff) is formed by nearly vertical beds of white Caballos novaculite which outcrop as a ridge striking northeast-southwest. Springs issue at a point where a water gap has been eroded through the ridge and form a creek which flows southeast. About 400 feet below the springs, the creek is confined by a dam 4 feet high. At the head of the pool the water is about 10 feet in depth and 20 feet wide. A road parallels the northeast bank of the valley and the pool. Houses and other ranch installations are grouped around the body of water. The house of Mr. John Catto, Jr., is on the southeast flank of the novaculite ridge overlooking the downstream part of the pool. It is about 75 yards from

the upper part of the pool where the meteorite fell but that part of the pool is masked from the house by the steep slope. The house of Mr. D. E. Forker is about 150 yards southwest of the Catto house and from it only the lower part of the pool near the dam is visible. Corrals are located on the northeast side of the valley below the dam, and east of them about 150 yards is the house of the Mexican caretaker.

The meteorite was seen in the very final portion of its flight by one person. Two others had arrived in a motor truck opposite the point of impact almost at the instant of fall, and their truck was splashed with water. Horses grazing near the pool were startled by the noises of the fall, ran, and then stopped and all turned to look over their shoulders toward the point of impact. All of the twenty-four people nearby heard all or part of the noises accompanying the fall. The shock-wave explosion, the first phenomenon observed, was heard through the country generally at reported distances of 65, 35, 12, and 10 miles from the point of fall. However, the region is sparsely settled so that a relatively small number of people were in a position to hear noises or see anything unusual in the sky.

The first evidence of the fall was a loud explosion, the shock wave, likened to "a loud boom," "an explosion of fifteen sticks of dynamite," "a strong concussion," "heavy blasting some distance away," or "like a big shotgun at some distance." The explosion was followed by the flight noise generally likened to the noise of a falling airplane. Other descriptions included "more a movement of air than sound," "as though a blast had created a vacuum," and "there was a rush of air to fill the vacuum," "a sizzling sound," and "a sound like something burning awfully fast, not just like an airplane." The flight noise lasted an appreciable time, difficult to estimate but certainly several seconds and possibly as much as 20 seconds.

The families of Mr. D. E. Forker and Mr. John Catto, Jr., who were in residence at the ranch, were seated at lunch in their respective homes. Members of the Forker family heard the explosion, which sounded very close but which did not shake the floor. Some but not all heard the flight noise. All, however, realized that a heavy explosion had occurred nearby, but they did not sense its direction. Mrs. Forker heard excited voices from the house of the Mexican caretaker a few hundred feet east of the pool. She moved to the east door of the house and outside to a point from which she could see much of the ranch establishment. She saw a group of horses that had been grazing just below the Catto house rush down the creek until stopped by a fence just below the dam. They huddled there in great fright looking back up the creek. This was perhaps 30 seconds after the explosion and shows that something had oc-

curred near the head of the pool to frighten them. This undoubtedly was the noises connected with the flight and fall of the meteorite into the pool.

The cook at the Forker home was on the back porch of the house. She heard a loud noise but did not detect the direction. Then came a sizzling sound. She looked all around and her eye caught a falling object on a line in the direction of the swimming pool. "It looked," she said, "just like a black bag falling out of the sky. You know how you might hold a flour sack up and the bottom would drop out? It looked just like that. The bag was black and what was dropping out—the dust like—was kind of white." She stated also that it was "as big as that bucket."

The Catto house is only about 75 yards from the point of impact. The members of this family group were more impressed by the flight noise than the explosion. The flight noise sounded like an airplane and it seemed to be headed directly for their roof. Mrs. Catto heard not only the explosion and flight noise but also the sound produced by the impact. She illustrated this sound by striking her closed fist into the palm of her hand. Most of the members of this group sensed a westerly direction for the flight of the meteorite.

Two men, workers on the ranch, were in a truck traveling along the road which passes alongside the swimming pool within 25 feet of the point of impact. They heard the explosion, which did not frighten them, but the flight noise sounded almost on top of the cab of the truck. They must have been within 50 feet of the meteorite when it struck the water, and one of them stated that he actually saw a splash of black water very high in the air and reaching the road. Subsequent examination showed that water had been driven 100 feet from the edge of the pool. Wisps of moss from the pool were found on rocks and bushes at the edge of the pool and on the road. The water of the pool was not muddy but seemed to be darker than usual.

The meteorite fell about $2\frac{1}{2}$ feet from the bank of the pool in about 2 feet of water. After the pool was drained about 4 feet below normal level, it was seen that a hole about 2 feet in diameter and 1.5 feet deep had been driven into the silt and earth forming the shelving bank. Novaculite and chert rocks are present beneath the silt and earth and limited the penetration of the meteoritic material. One fragment of 13 kg. (29 lbs.) was recovered about 1 foot from alongside the hole (Fig. 1). Another of 47 kg. (104 lbs.) was recovered from the deeper water about 8 feet from the hole. Numerous fragments ranging from mere grains to one of 2162 grams weight were recovered from the hole and around it. One fragment of 444.2 grams weight was found outside the pool about 3 feet from the water. The total material recovered amounted to approximately 70.37

kg. (155 lbs.). It included 13 pieces larger than 2×2×2 inches and weighing more than 100 grams.

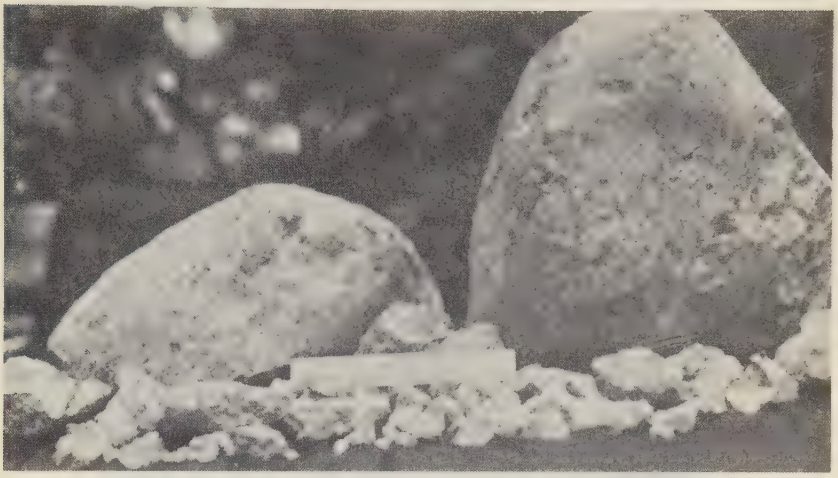

FIG. 1. Two largest fragments and other material, Peña Blanca Spring meteorite. Rounded surfaces and pits are shown on larger fragments.

There is evidence to suggest that the meteorite was broken by impact against a large boulder of novaculite. The boulder which was beneath the water was freshly broken. It appears probable, likewise, that upon impact and breaking, the two larger fragments rebounded, the smaller one a foot or so, the larger one several feet. In falling, the meteorite passed through the upper part of a willow tree on the bank of the pool. Smaller limbs were broken, and inconclusive evidence suggests that one about 2 inches in diameter was broken with a twisting motion and thrown upward about 4 feet, lodging in the upper part of the willow tree.

One additional feature of this remarkable fall deserves mention. The novaculite previously mentioned occurs as nearly vertical beds some 75 feet thick. At the point where the meteorite fell there is a virtual water gap through the novaculite, about 100 feet in depth, 100 feet wide at the top, and 50 feet wide at the bottom. The meteorite fell almost exactly in the middle of the gap and obviously at a high angle. A slightly different course would have resulted in impact on a bare novaculite surface and probably extensive fragmentation.

The major part of the recovery was made by Mr. O. E. Monnig, an ardent student and collector of meteorites, and Mr. Harrison H. Morse, both of Fort Worth, Texas. The residents of the ranch had recovered the

13 kg. and the 2162 gram fragment soon after the fall. Mr. Monnig and Mr. Morse arrived at the locality August 6 and made a very intensive search for material. It is believed that the combined efforts resulted in recovery of all except a few kilograms of the material. Mr. Monnig and Mr. Morse also made a very thorough investigation of observed astronomical phenomena of the fall. These along with a description of the general features of the meteorite were reported by Mr. Monnig before the Society for Research on Meteorites (now the Meteoritical Society) and will be published in its contributions.

Physical Properties and General Structure

Reconstruction of the shape of the meteorite shows that it was roughly one-half of an elongated spheroidal body bounded by undulating plane surfaces whose junctions are rounded (Fig. 1). The dimensions of the largest piece recovered are 15×13.5×11 inches and of the next largest

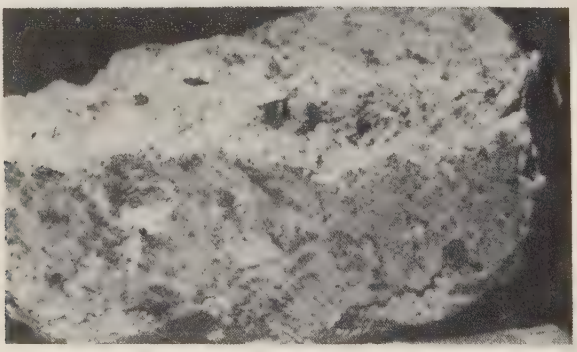

Fig. 2. Mottled light gray crust of the Peña Blanca Spring meteorite. Irregular line at lower right shows area from which crust has been flaked.

14.5×5.5×5.5 inches. One major external plane on the larger fragment is fresher than the others, only partly crusted and possibly is a separation plane recording a disruption of the mass prior to its fall at Peña Blanca.

Much of the original surface was covered by cream colored to mottled gray crust less than 1 mm. thick (Fig. 2). There is a distinct separation plane between the crust and the deeper material, and a good deal of the crust has been lost through flaking along this plane. Only a part of a flake which separates is isotropic, minute grains of crystalline materials forming the lower part of the flakes. Mottled gray areas of the crust have resulted from the diffusion of grains of opaque minerals in the crust melt. Minute sub-parallel flow lines are present in the crust, and with a hand lens the crust material appears vesicular or frothy.

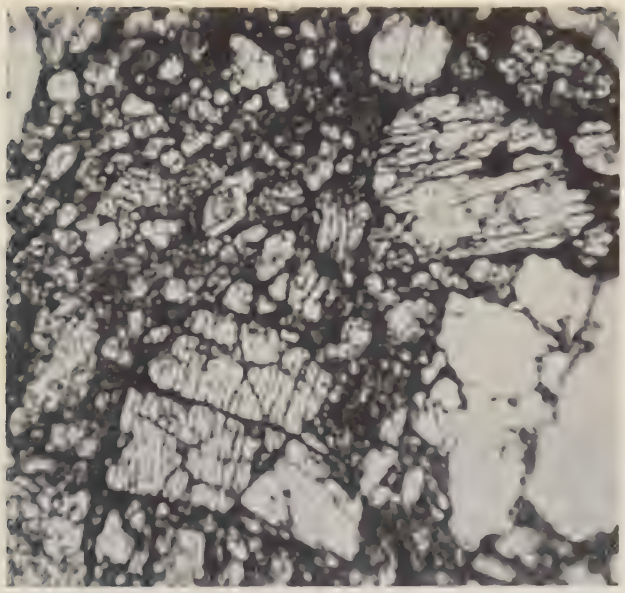

FIG. 3. Micro-section of the Peña Blanca Spring meteorite showing cataclastic texture.

FIG. 4. Fresh surface of Peña Blanca Spring meteorite. The large crystal, about 2.5 inches long is enstatite. The oval black spot at end of crystal is metal and sulfide.

Original surfaces of the meteorite are pitted with shallow pits up to 6.5 cm. in diameter (Fig. 1). These are irregularly spaced, and it is possible that they were the loci of larger crystals. A crack which appears to have been healed runs diagonally across nearly the complete external surface of the 13 kg. fragment.

Thin sections of the meteorite reveal a pronounced cataclastic texture (Fig. 3). However there are many subhedral crystals, and a few which are euhedral. In addition there are a few crystals so large that they are considered to be phenocrysts (Fig. 5). It seems probable that these crystals originally were larger than the others but that smaller original crystals may have been reduced in size during the development of the calaclastic texture.

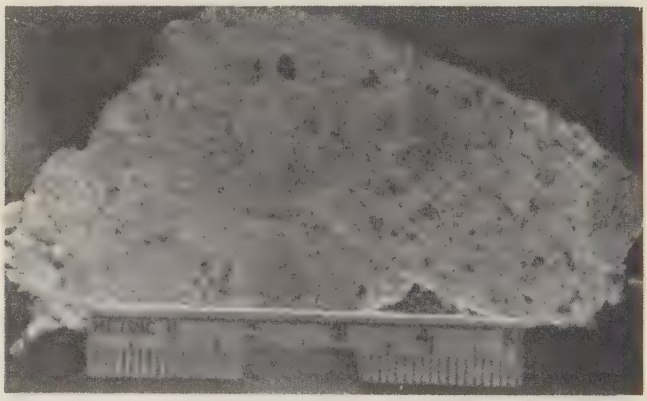

FIG. 5. Cut surface of Peña Blanca Spring meteorite showing darker enstatite grains and crystals in lighter matrix also mainly enstatite.

A freshly broken surface of the meteorite exhibits a light gray, nearly white, medium-grained groundmass in which are crystals of silicate minerals of various shades of color from light gray to dark gray and small grains of metal and brass colored sulfide (Figs. 4–5). Oxidation of the sufide was extremely rapid, producing brown areas of iron oxide within a few hours. The oxidation was accompanied by a distinct sulfur dioxide odor which still persists in the larger fragment five months after the fall. It is possible that the contact with water in the swimming pool promoted this rapid oxidation.

Except for the phenocrysts there is a great range in size of the crystals practically down to that of the grains of the groundmass which average a little more than 1 mm. The largest crystal observed is $10\times7.5\times6$ cm. Another is $6\times3\times1.5$ cm., another $2\times3\times3.8$ cm. Many of the crystals

are larger than 1 cm. Rare smaller crystals are euhedral. But a good many even of the larger ones show at least one well developed crystal face.

In general the phenocrysts are darker than the groundmass although there are exceptions (Fig. 5). Enstatite, the most abundant mineral, varies in color and luster in shades of gray. The cause of the variation has not been determined. The mineral exhibits fibrous to platy cleavage and rarely appears striated. Monoclinic pyroxene is white in color and not fibrous. However, these characters alone will not distinguish it from enstatite and generally it is necessary to confirm the identification with the microscope.

Olivine (forsterite) found in thin sections is so rare that it is not seen in hand specimens except in one area suggesting a chondrule. A circular area 7.5 cm. in diameter is composed mainly of stubby subhedral crystals of the mineral averaging 2 mm. in length (Fig. 6).

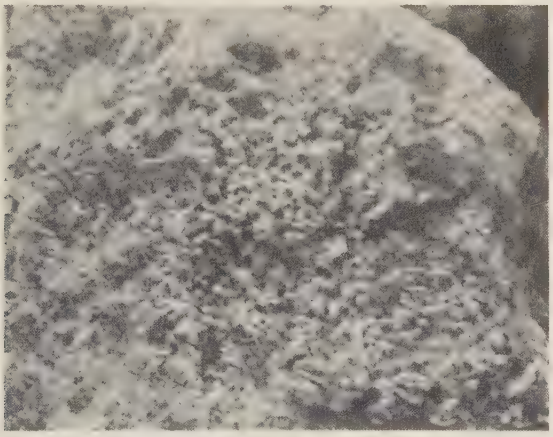

FIG. 6. Chondrule-like segregation of forsterite and enstatite. The forsterite crystals are subhedral, 1–2 mm. in size.

Metal and sulfide occur in irregular grains up to several millimeters with an occasional grain still larger in the groundmass and as inclusions in the pyroxenes. They are present together in many grains, and invariably those with sulfide are bordered by iron oxide.

The meteorite is exceedingly brittle but not friable. It does not appear to be brecciated. Fragments cannot be broken by the hands. However, numerous small cracks have developed, usually around larger crystals. Handling of larger fragments generally results in a certain amount of flaking and chipping along these cracks.

Petrography

The Peña Blanca Spring meteorite is an *aubrite* in Prior's classification. It is an achondrite in which the metal (Fe : Ni = 22 : 1) and sulfide are sparingly present and the bulk of the stone is composed of enstatite almost free from iron. The small amounts of monoclinic pyroxene and forsterite likewise are essentially iron-free .The feldspar, present in small amount, is oligoclase. The meteorite is not greatly different from the Shallowater aubrite described by Foshag,[1] having however still less metal and some monoclinic pyroxene not found in Shallowater. It differs in texture and probably contains the largest individual crystals yet found in meteorites.

Because of the exceedingly irregular texture a mode of the meteorite must be an estimate. The mode given below is based on a study of four thin sections, hand specimens and chemical analyses.

Mineral Composition of the Peña Blanca Spring Meteorite

Enstatite	93.0
Diopside	5.0
Forsterite	0.5
Oligoclase	0.5
Iron-nickel	0.5
Troilite	1.25
Others	0.25
	100

Enstatite occurs in the ground mass and as larger crystals including the largest observed. It varies in color from nearly white through light gray to dark gray vitreous material. As far as can be determined, no optical difference exists among the various types. A chemical analysis of material from a large crystal and optical properties are given below. It is essentially iron-free magnesian metasilicate. Optical determination checks closely with the analysis. *X*-ray diffraction patterns of two specimens of enstatite representing the range in outward appearance were very kindly made by Dr. J. W. Gruner[2] of The University of Minnesota. Dr. Gruner stated that "the patterns are very close to, if not identical with, enstatite." In thin sections many of the enstatite grains exhibit undulatory extinction, and in some, indistinct lamellar twinning appears. Some of the optical phenomena suggest intergrowths of monoclinic pyroxene but this could not be confirmed. Minute opaque inclusions are present in some grains.

[1] Foshag, William F., The Shallowater meterorite; a new aubrite: *Am. Mineral.*, **25**, 779–786 (1940).

[2] Gruner, J. W., Personal communication (1946).

ENSTATITE, PEÑA BLANCA SPRING METEORITE
F. A. GONYER, *Analyst*

SiO_2	59.24	
TiO_2	0.00	$\alpha = 1.650$
Al_2O_3	.27	β = n.d.
Fe_2O_3	.14	$\gamma = 1.658$
FeO	.45	2V = 30° approximately
CaO	0.00	Z ∥ to elongation
MgO	39.78	$(\gamma - \alpha) = .008$
MnO	0.00	
	99.88	

Thin sections show a small amount of monoclinic pyroxene, and grains or crystals also can be isolated from hand specimens. Some of the grains occur as inclusions in larger enstatite crystals. The mineral has been identified as iron-free diopside. It is optically positive with 2V about 60°; $\alpha = 1.660$, $\beta = 1.670$, $\gamma = 690$; $Z \wedge c = 38°$. The mineral shows irregular lamellar twinning.

Forsterite, except in the segregation previously mentioned, is very rare in the meteorite. Less than a dozen grains smaller than 0.5 mm. were observed in four thin sections. The mineral is colorless and anhedral. It is optically positive with 2V about 90°; $\alpha = 1.635$, $\beta = 1.650$, $\gamma = 1.670$; $(\gamma - \alpha) = .035$. These data indicate a forsterite essentially iron-free. This is confirmed by an analysis of the segregation which consists of about 60% forsterite and 40% pyroxene.

PEÑA BLANCA SPRING METEORITE, FORSTERITE SEGREGATION
F. A. GONYER, *Analyst*

SiO_2	50.84
TiO_2	.09
Al_2O_3	.23
Fe_2O_3	.38
CaO	.04
MgO	48.67
	100.25

Oligoclase is present in exceedingly small amounts. Only a few anhedral grains were found in the four thin sections studied. The mineral shows fine albite twinning and is Ab_{88} An_{12}.

A reddish-brown transparent mineral is present in sections in irregular grains of about the same size as the feldspar grains. The mineral is isotropic and has octahedral cleavage and a very high index of refraction. It is identified tentatively as spinel.

A chemical analysis of this meteorite presents a difficult sampling problem. It was not possible to sacrifice sufficient material for an unquestionably representative sample. Within these limitations, however, the analyses below generally confirm the mineralogical studies:

PEÑA BLANCA SPRING METEORITE
F. A GONYER, *Analyst*

METAL-FREE PORTION		METAL	
SiO_2	57.86	Fe	95.74
TiO_2	.06	Ni	4.22
Al_2O_3	.21	Co	.39
Fe_2O_3	0.00	Cu	0.00
FeO	2.00	P	0.00
CaO	1.08	Mn	.17
MgO	38.07		
NiO	0.00		100.52
Na_2O, K_2O	0.00		
P_2O_5	0.00		
FeS	1.21		
	100.49		

It will be noted that the alkalies were not detected. This is not surprising, because the feldspar is present in very small amount. On the other hand, the mineral or minerals in which the FeO is present have not been identified. It is possible that the minute inclusions in enstatite are responsible or that the sampling procedure produced a concentration of iron-bearing compounds.

ACKNOWLEDGMENTS

The writer is greatly indebted to the Catto and Forker families for permission to describe the meteorite and for specimens used in the thin sections and chemical analyses. Mrs. D. E. Forker made available the very detailed information which she collected concerning the interesting incidents which occurred in connection with the fall. Mr. Oscar E. Monnig very generously supplied details concerning his investigation of the fall and recovery of the meteorite. The chemical analyses were made possible through a grant from the Graduate Council of The University of Texas.

NOTES AND NEWS

RE-EXAMINATION OF BOKSPUTITE*

E. Wm. Heinrich, *Montana School of Mines, Butte, Montana.*

Introduction

Bokputite, $Bi_2Pb_6C_3O_{15}$, was described by E. D. Mountain (1935) from Boksput, Gordonia, Cape Province, South Africa. No other occurrences of bokputite have been recorded, but another new bismuth mineral, bismoclite, described in the same paper has since been found from several other localities (Schaller, 1941, and Frondel, 1943).

During the fall of 1945 the writer was concerned with the examination of a suite of secondary bismuth minerals from numerous pegmatites in Colorado and New Mexico. Most of the material proved to be bismutite by the *x*-ray powder method, but several of the specimens contained beyerite (Frondel, 1943; Heinrich, 1946), and a few *x*-ray patterns could not be matched. The only secondary bismuth mineral whose *x*-ray powder photograph was not in the film library of the Harvard Mineralogical Laboratory was bokputite. Accordingly the writer applied to Professor Mountain who generously sent a sample of "some of the original powder of bokputite from which the analysed material was obtained." The writer wishes to acknowledge the assistance of Professor Clifford Frondel both through discussions and a reading of the manuscript.

Examination

A powder *x*-ray photograph of the type material supplied by Professor Mountain is identical with that of bismutite (Frondel, 1943, pp. 524–525). Microscopic examination of the gray powder reveals the presence of three distinct minerals. The most abundant is nearly opaque, but near the edges of thin splinters a deep yellow brown color is apparent. It is attacked by the high index liquids ($n = 1.82$) with the evolution of bubbles of carbon dioxide. This substance is very likely the bismutite.

The second most abundant mineral occurs in minute plates marked by a wavy extinction and a pleochroism of light yellow to deep yellow. The birefringence is high. The indices of refraction are considerably above the highest liquid used (1.82). The plates show a negative Bx_a figure with 2V nearly 90°. The mineral is identified as massicot.

The third substance, which is very minor in amount, is colorless and isotropic. The index of refraction is close to that of the second mineral.

* Contribution from the Department of Mineralogy and Petrography, Harvard University, No. 283.

Conclusion

The writer believes that the substance described by Mountain under the name boksputite is a mixture essentially of bismutite and massicot. Other minor impurities may be present. The determination of the material as a new mineral species rested upon the chemical analysis and the x-ray photograph made by F. A. Bannister for Professor Mountain. The x-ray powder diffraction data obtained are not cited in the paper.

The analysis of boksputite approximates the ratio $6PbO \cdot Bi_2O_3 \cdot 3CO_2$ or $Bi_2Pb_6C_3O_{15}$, a rather complex formula for a supergene mineral, particularly for a secondary lead-bismuth mineral. Most supergene minerals are exceedingly simple in their chemical composition. Professor Mountain's analysis, recalculated to 100% for the three major constituents, is shown in Column 1. The composition of $Bi_2Pb_6C_3O_{15}$ is given in Column 2.

	1	2
PbO	69.23	69.13
Bi_2O_3	23.60	24.05
CO_2	7.17	6.82
	100.00	100.00

The approach of the analysis to a relatively simple atomic ratio must be regarded as fortuitous in the light of the rigid x-ray evidence and the presence of abundant microscopical impurities. It is difficult to explain the fact, however, unless the analysis is erroneous, that CO_2 is present in an amount greater than that required to combine with Bi_2O_3 to form Bi_2CO_5.

References

Frondel, Clifford, *Am. Mineral.*, **28**, 521–535 (1943).
———, *Am. Mineral.*, **28**, 536–540 (1943).
Heinrich, E. Wm., *Am. Mineral.*, **31**, 198 (1946).
Mountain, E. D., *Mineral. Mag.*, **24**, 59–64 (1935).
Schaller, W. T., *Am. Mineral.*, **26**, 651 (1941).

A MONOCHROMATIC LIGHT SOURCE FOR THE PETROGRAPHIC MICROSCOPE

R. C. Townsend and D. R. Townsend[1]

The writers have devised a low cost, compact, portable source of monochromatic light using 110 volt alternating current, by which it is possible to determine indices of refraction completely accurate to the third decimal place with liquids of high dispersion. Fairly reliable determinations may be made to the fourth decimal place.

The source of light consists essentially of a small transformer, a specially designed mercury vapor lamp on the Geissler tube principle, and a set of glass filters. The transformer is the type commonly used in neon display signs, converting 110 volt alternating current to approximately 2500 volts.

The lamp (Fig. 1) is a coil of capillary pyrex glass tubing with a bore of one mm., which is welded to electrode chambers about seven mm. in diameter.[2] The coil is 50 mm. in diameter and is coiled simply to increase the amount of light available to the microscope. The electrodes are tubular and are connected to copper leads which in turn are connected directly to the transformer (Fig. 2). Large electrode chambers not only assure adequate gas for the capillary tubing, but provide for electrodes having large surface area for proper discharge. A small amount of argon gas is present with the mercury in the tube to act as a carrier gas, but the brilliant mercury spectrum masks out the argon lines.

The filters are two-inch polished glass squares produced by Corning Glass Works. A combination of three filters (numbers 3486, 4303, and 5120) isolates the green line of 5460 Å.

The transformer, lamp, and filters are compactly arranged in a box with a lid, and with an aperture on one end slightly smaller than the filters (Fig. 2). The lamp is fastened to an asbestos-covered block of wood and the filters are supported in a metal bracket containing a spring, so that they may be easily removed yet fit closely over the aperture when in place. The box is $11'' \times 3'' \times 4''$ in size.

In making index of refraction determinations, the light may be used generally with as high as 400 magnifications, the brilliance of the image depending on the nature of the specimens and liquids. The 5460 Å line is close enough to the sodium reference line of 5890 Å. for routine use. For extremely accurate work, the light should be used in a dark room to eliminate extraneous light.

[1] Published by permission of the Director, United States Geological Survey, Washington, D. C.

[2] The lamp was made for the writers at the General Physical Laboratory, 509 Fifth Avenue, New York 17, New York.

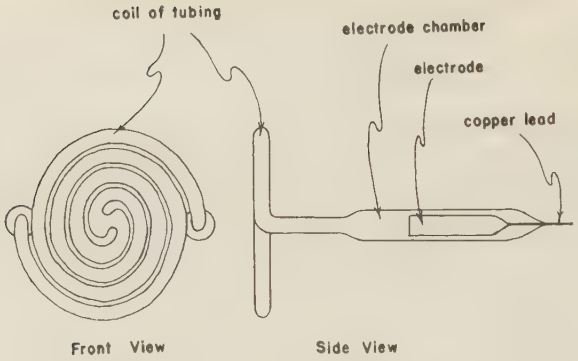

FIG. 1. Front and side views of mercury lamp.

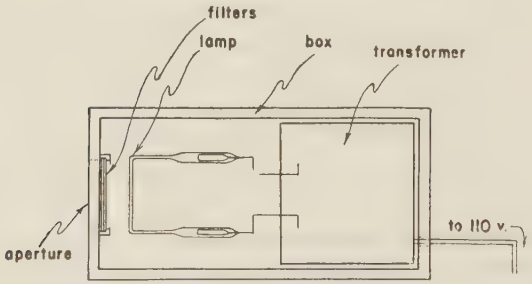

FIG. 2. Diagram of complete monochromatic light unit.

METHOD FOR POLISHING DIAMOND-DRILL CORE SPECIMENS

LOUIS MOYD[1]

Petrographic laboratories and museums occasionally find it necessary to polish large diamond-drill core specimens of rocks for study or display purposes. The writer is not familiar with any published procedure for accomplishing this and therefore considers that the method evolved at this laboratory may be of value to others confronted by the same problem.

Recently, a diamond-drill core, $2\frac{1}{8}$ inches in diameter and about four feet long, of a dark-colored, dolomitic limestone, containing clay seams and cut by numerous joint fissures healed with white coarsely crystalline dolomite, was received at this laboratory. Since this core exhibits numerous features in connection with the investigation of the suitability of rocks proposed for use as aggregates in concrete, it was decided that it be polished and retained as a display specimen in our museum.

[1] Geologist, Concrete Research Division, Waterways Experiment Station, Corps of Engineers, U. S. Army, Clinton, Mississippi.

Both ends of the core were cut square with a diamond saw. Shallow holes were drilled in the centers of the core at both ends, then the core was mounted in a wood-turning lathe.

The scoring made by the diamond-drill bit was removed by rubbing the core with strips of coarse emery paper as it revolved. Finer grades of emery paper were used, and the final polish was obtained with No. 304 emery in water, on a felt pad.

MEMORIAL OF BERNARD FISHER

ESPER S. LARSEN, JR., *Harvard University, Cambridge, Mass.*

Bernard Fisher was born in Boston, September 10, 1918. He was educated in the public schools of Boston and was graduated from Boston Latin School in 1935. He entered Harvard University, received his A.B. degree, *magna cum laude* in 1939, and continued graduate work in the Division of Geological Sciences at Harvard until the spring of 1942, when he joined the United States Geological Survey. In June 1942 he volunteered for the Army and in September of that year he went to England as a Second Lieutenant in the Army Engineers. He remained in England throughout the war, for a time with the Engineers and later with the Military Police. In 1944 he was promoted to Captain and, because of his training and ability, was assigned to a group of British and American Engineers who were stationed at Oxford, England, and engaged in preparing military maps and other important military data. He served with this group until the end of the war.

In November 1945 he was released from the Army and spent the following winter completing his thesis for the doctorate, which he received in June 1946. In March of 1946 he rejoined the United States Geological Survey and became a member of the group of geologists who were to study for the Army the active volcanoes of the Aleutian Islands.

In April he left for Umnak Island, Alaska. During the late spring he carried on his field investigations in the typically adverse Aleutian weather, with frequent high winds accompanied by rain, fog and sleet. On many evenings he returned from a day's field work completely drenched, but always with several pages of field notes and a happy disposition, much to the admiration of his colleagues.

As part of the study of the geology it was necessary to visit the small islands adjoining Umnak. On the afternoon of June 22, 1946, he and two Army officers left Umnak in a small boat to examine Ship Rock, a small but steep-sided island one mile offshore. The weather on that day was clear and calm and seemed ideal for the trip. The men in the boat were last seen as they went behind Ship Rock on the seaward side. It was thought that they had landed on the far side of the island. As they did

not return by dark, search was begun with plane and boat. After a prolonged and careful search the overturned boat was sighted, but no trace of the men was ever found.

Bernard was a loyal and constant friend, straightforward, generous, patriotic, yet critical and independent. He was dearly loved by his many friends at Harvard and elsewhere. We expected great things from him. He is one of the few geologists who have lost their lives while actually carrying on geologic work.

BIBLIOGRAPHY

(With W. T. Pecora), Drusy vugs in a monzonite dike, Bearpaw Mountains, Montana: *Am. Mineral.*, **31**, 370–385 (1946).

Igneous rocks of the northeastern Bearpaw Mountains, Montana. *Ph.D. Thesis*, Harvard, pp. 127, March 1946 (to be published).

(With F. M. Byers, Jr., D. M. Hopkins and K. L. Wier), Volcano investigations on Umnak Island, Alaska, 1946. Part 2 of *Alaskan Volcano Investigations* Report No. **2**: Progress of Investigations, 1946: *U. S. Geological Survey Special report*, **1947** (limited distribution).

Dr. Victor Moritz Goldschmidt, eminent Norwegian geochemist and one of the pioneers in the field of crystal chemistry, died in Oslo March 20, at the age of 59 years. When the Nazis conquered Norway he was arrested and sent to a concentration camp. He was rescued by the Norwegian underground and eventually reached England, where he became associated with the Macaulay Institute of Soil Research at Aberdeen, and also served as a consultant in the laboratories of the Rothamstead Agricultural Experiment Station. He returned to his position last year as Professor of Mineralogy and Geology and Director of the Geological Museum at the University of Oslo.

In 1929 Goldschmidt was called to the University of Göttingen as professor and as director of the University's Mineralogical and Petrographic Institute. He served until 1935 when conditions became intolerable and he returned to the University of Oslo. He was the Wollaston Medalist in 1944.

The tenth meeting of the Meteoritical Society will be held on Wednesday, June 18, and Thursday, June 19, 1947, in connection with the meeting of the Pacific Division of the American Association for the Advancement of Science in San Diego, California. The afternoon session of June 19 will be joint session with the Astronomical Society of the Pacific.

THE NEW YORK MINERALOGICAL CLUB, INC.

Abstract of meeting of Feb. 19, 1947

The principal speaker of the evening was Baron R. J. de Touche-Skadding who spoke on "The Agni Mani, Mystical Meteoric Gem of the Orient." The Agni Mani, or fire jewel, has been held in very high esteem in the Orient for at least 2500 years. It is a tektite, a highly siliceous glass of meteoric origin, found in several places in the East Indies and elsewhere. The material is amorphous and resembles obsidian but is found in places where

there are no volcanic rocks. The Agni Manis found in Biliton are strongly etched and bear no relation to the country rock. On Biliton the natives believe them to be "seeds of tin" and on finding one, bury it again so the tin mines will not become exhausted. Throughout the Orient, the Agni Mani is credited with bringing the wearer riches and a long line of descendants.

PURFIELD KENT, *Secretary*

NEW MINERAL NAMES

Falkenstenite

TOM. F. W. BARTH, Falkenstenite, a new zeolite in variolite from Horten, and the surface conditions during the effusion of the oldest Permian lavas. *Skrifter Norsk. Videnskaps—Akad. Oslo*, No. **8**, 13–22 (1945).

Varioles in basaltic lava near Falkensten, Oslo area, are described. The rock had the mode: pyroxene (diopsidic augite) 24.3, chlorite 23.3, zeolite 40.2, ore 10.2, apatite 1.6, calcite 0.4. A complete analysis of the rock is given from this, and assuming compositions for the pyroxene and chlorite that are in accord with the optical data, the composition of the zeolite is calculated to be $K_{2.5}Na_{2.5}Ca_{0.7}Mg_{2.9}Al_{12.6}Si_{27.4}O_{80} \cdot 16\frac{1}{2}\ H_2O$. The rock lost its water (6.49%) as follows: at 110° C. 2.76, at 500° 1.40, at 800° 2.33%.

Falkenstenite occurs intergrown with chlorite, or it is fibrous, thread-like with quadratic cross section and prismatic cleavage. It is uniaxial, negative, $n_o = 1.508$, birefringence about 0.003. The optical data are very close to those of gonnardite, but the latter contains no magnesium. The chemical composition, except for H_2O, is similar to that of ashcroftine, but the latter is optically positive, with $n_o = 1.536$. Hence falkenstenite does not seem to correspond with any known zeolite.

DISCUSSION: Further study is needed, including chemical, *x*-ray, and dehydration studies, before this mineral can be classified.

MICHAEL FLEISCHER

Courzite

ST. J. THUGUTT, Sur la courzite des environs de Symphéropol. *Archiwum Mineralogiczne* (Warsaw) **15**, 182–184 (in French), 185–187 (in Polish) (1945).

There are two analyses in the literature of wellsite, the original by Foote (1897), No. 1 below, and a second by Fersman (1909), No. 2 below. Each of these is the average of two analyses.

	SiO_2	Al_2O_3	Fe_2O_3	BaO	SrO	CaO	MgO
1.	43.86	24.96	–	5.07	1.15	5.80	0.62
2.	49.40	19.14	0.12	4.84	0.61	5.67	–

	K_2O	Na_2O	H_2O	*Sum*
1.	3.40	1.80	13.35	100.01
2.	3.50	0.12	16.78	100.18

Thugutt calculates these analyses in terms of molecules such as $CaO-Al_2O_3-3SiO_2$ and arrives at the conclusion that the first analysis represents largely trisilicates, the second largely hexasilicates ($RO-Al_2O_3-6SiO_2$). Hence the material studied by Fersman, despite its crystallographic similarity, must be different from wellsite, and the new name Courzite (modified version of the locality name Kurzy, Crimea) is proposed.

DISCUSSION: The method of calculation is invalid and the new name is a useless burden on mineralogy. If the same principle were to be applied to similar variations of Si and Al in all the zeolites, some dozens of new names would be required.

M.F.

Rooseveltite

ROBERT HERZENBERG, Nuevos minerales de Bolivia. *Bol. Técnico* No. **1**, *Fac. Nac. Ingeniera*, Univ. Técnica Oruro (1946).

CHEMICAL PROPERTIES: Composition $BiAsO_4$. Analysis Bi_2O_3 67.2, As_2O_5 33.2; sum 100.4%. Easily soluble in HCl, more slowly in HNO_3 and H_2SO_4. In closed tube, decrepitates slightly, turns yellow when hot, but gives original color on cooling. B.B. on charcoal, fuses to bead.

PHYSICAL PROPERTIES: Color gray, luster adamantine. No cleavage, fracture conchoidal; very brittle. H. = 4–4½, G. = 6.86 (pycnometer). Refraction very high, strongly anisotropic. Crystallographic system not determined. Synthetic $BiAsO_4$, prepared in 1903 by de Schulten, was reported to be monoclinic, with G. = 7.14.

OCCURRENCE: Found as a crystalline crust on wood tin veinlets in rhyolitic and dacitic lava flows at Santiaguillo, Macha, Potosi, Bolivia.

NAME: For Franklin Delano Roosevelt.

M.F.

Souxite

ROBERT HERZENBERG, Nuevos minerales de Bolivia. *Bol. Técnico* No. **1**, *Fac. Nac. Ingeniera*, Univ. Técnica Oruro (1946).

The name souxite is given to $SnO_2 \cdot xH_2O$, supposed to be the form in which tin soluble in HCl occurs in some Bolivian deposits. Analysis of a light yellow tin ore from the Utne veins, Cotamitos mine, Cerro de Potosi, gave: Sn total 25.8, Sn soluble in HCl 17.2, Sb 2.45, As 4.10, Bi 0.33, WO_3 0.19, S total 2.10, S as sulfide 1.04, SO_3 2.65, Fe 8.90, SiO_2 25.8, Al_2O_3 3.40, H_2O 11.89%. This is recalculated to give the following mineral composition of the ore: SnO_2 as cassiterite 10.95, SnO_2 as $SnO_2 \cdot xH_2O$ 21.85, wolframite 0.25, pyrite or marcasite 1.95, $Fe_2(SO_4)_3 \cdot xH_2O$ 4.41, $Fe_5As_3O_{15} \cdot xH_2O$ 13.60, $Fe_5Sb_3O_{15} \cdot xH_2O$ 5.07, Sb_2O_4 0.46, Bi_2O_3 0.37, Al_2O_3 3.40, SiO_2 25.80, H_2O 11.89; sum 100.00%.

NAME: For Mr. Luis Soux, a mine owner.

DISCUSSION: The only fact that emerges is that the material contains tin in some form soluble in HCl (and also in H_2SO_4). This may be a new mineral, but the evidence is certainly insufficient to justify a name or the assignment of a formula.

M.F.

Dunhamite

ERNEST E. FAIRBANKS, The punched card identification of ore minerals. *Econ. Geol.*, **41**, 761–768 (1946).

The name dunhamite is given to the oxidation product of altaite described by K. C. Dunham (*N. Mex. Bur. Mines, Bull.* **11**, 159–160 (1935)) from the Organ Mts., N. Mex., which is similar to material mentioned by Schneiderhöhn-Ramdohr. The statement is made, "Its mode of formation suggests the possible formula $PbO \cdot TeO_2$ (?)."

DISCUSSION: Fairbanks makes a plea for the naming of such material. He says, "If the determinative data are substantial, a name is certainly justified in spite of the inability to obtain a quantitative chemical analysis."

It is not clear whether Fairbanks re-examined this material or depended on the literature entirely. He reports the mineral to be anisotropic; Dunham says it is distinctly

isotropic (a misprint ?); Schneiderhölm-Ramdohr describe the oxidation product of altaite as strongly anisotropic. Fairbanks says the mineral contains Pb and Te; Dunham does not mention making any tests, but suggests that it may be a lead tellurite. Writing a formula under such circumstances has no justification.

If Dunham's judgment was that the data available were insufficient to justify a name, it seems inadvisable for a later worker to reverse the decision of the man who saw the material, unless new work had added further information.

M.F.

Fersmite

E. M. Bohnstedt-Kupletskaya and T. A. Burova, Fersmite, a new calcium niobate from the pegmatites of the Vishnevye Mts., the Central Urals. *Compt. rend.* (*Doklady*) *Acad. Sci. U.R.S.S.*, **52**, 69–71 (1946).

Crystallography: Orthorhombic. The crystals were imperfect, and the axial ratio found, $a:b:c=0.377:1:0.356$, is approximate. The main forms observed were: *b* (010), *m* (110) and *p* (111); *n* (130) is rather common; *r* (131) and *k* (021) have been observed.

Chemical Properties: Essentially a calcium columbate of the AB_2O_6 group, (Ca, Ce, Na) (Cb, Ti, Fe, Al)$_2$ (O, OH, F)$_6$. A complete and a partial analysis of material from two pegmatites gave (n.d.=not determined): SiO_2 0.715, n.d.; Cb_2O_5 70.12, 71.51; Ta_2O_5 traces, n.d.; TiO_2 3.21, 2.94; Fe_2O_3 1.71, 1.25; Al_2O_3 1.28, n.d.; rare earths 4.79, 3.98; CaO 14.49, 15.53; MgO 0.98, 0.97; MnO 0.48, n.d.; Na_2O 0.46, n.d.; H_2O 0.72, n.d.; F 1.87, n.d.; sum 100.86, —; less $O=F_2$ = 100.07%. *X*-ray chemical study by I. B. Borovsky showed the rare earth precipitate of #1 (4.79%) to consist of 80% Ce group, 10% Y group, 10% ThO_2. A qualitative *x*-ray chemical analysis is given.

Fersmite decrepitates before the blow-pipe. Brown and translucent on ignition. Sparingly attacked by H_2SO_4.

Physical and Optical Properties: Color black, powder grayish-brown. In thin section transparent to translucent. Luster resinous. No cleavage, fracture uneven to subconchoidal. H.=4½, G.=4.69. Radioactivity equivalent to 0.845% U_3O_8.

Optically, distinctly anisotropic, *n* about 2, birefringence medium; biaxial, probably positive, 2V large.

Occurrence: In two syenitic pegmatites, northern part of Vishnevye Mts., region of Lake Buldym. The rock of the veins is composed of microcline and plagioclase. Fersmite usually forms segregations with irregular outlines, up to 1–1.5 cm.; it is confined to oligoclase. Associated minerals include biotite, pyrochlore, hornblende, apatite, sphene, and quartz; accessories include pyrite, magnetite, muscovite, zircon, and xenotime.

Name: For A. E. Fersman. Not to be confused with fersmanite.

M.F.

Mansfieldite

Victor T. Allen and Joseph J. Fahey, *Am. Mineral.*, **31**, 189 (1946) (Abstract).

Bastinite

D. Jerome Fisher, *Am. Mineral.*, **31**, 192 (1946) (Abstract).

Tinticite

Bronson Stringham, *Am. Mineral.*, **31**, 395–400 (1946).

Montbrayite

M. A. Peacock and R. M. Thompson, *Am. Mineral.*, **31**, 515–526 (1946).

M.F.

DISCREDITED MINERALS

Antamokite

R. M. THOMPSON, Antamokite discredited. *Univ. Toronto Studies*, Geol. Series No. 50, 79 (1946).

X-ray and microscopic study of material from the type locality, Benguet mine, Antamok, Philippine Islands, indicate that the supposed new mineral was a mixture of petzite and calaverite.

M.F.

Klaprothite (=Wittichenite+Emplectite)

E. W. NUFFIELD, *Am. Mineral.*, **31**, 201 (1946) (abs.)

NEW DATA

Sauconite

CLARENCE S. ROSS, *Am. Mineral.*, **31**, 411–424 (1946).

M.F.